Some Investigations in Theoretical and Experimental Electrochemistry

Thesis by

James Brian Flanagan

In Partial Fulfillment of the Requirements

for the Degree of

Doctor of Philosophy

California Institute of Technology

Pasadena, California

1978

(Submitted December 15, 1977)

ACKNOWLEDGMENTS

I would like to acknowledge the direct contribution of data presented in this thesis by Drs. Katsuo Takahashi, Shlomo Margel and Akifumi Yamada. Many others have contributed helpful suggestions and discussion. In particular I would like to thank Carl Koval, Bruce Parkinson, Dr. John Turner and Professors W. R. Fawcett, Allen J. Bard and Robert Gagné.

My research director, Professor F. C. Anson, has contributed in many ways to the realization of this thesis. Much of the work presented here is based on his suggestions. I would also like to thank him for financial support as a research assistant provided through his grants.

Other financial support was provided by the ARCS Foundation, The Electrochemical Society (Colin Garfield Fink Summer Fellowship), and the California Institute of Technology through teaching assistantships.

ABSTRACT

This thesis is composed of three distinct topics. Chapters II, III and IV are concerned with the analytical consequences of adsorption of reactants at the electrode surface with d.c. polarography and normal and differential pulse polarography. Theoretical behavior was calculated by means of digital simulation and Laplace transform techniques. The effects of nonlinear adsorption isotherms and uncompensated resistance on current-potential response was calculated. The reaction $Cd^{+2}/Cd(Hg)$ with adsorption induced by the presence of iodide was used as a test system.

Chapters V and VI are concerned with the electrochemical behavior of molecules with more than one center for electron transfer. Classical statistical methods were used with computer calculation of results. Problems considered include concentration- and current-potential behavior of: (1) polymeric species with no interaction between centers; (2) dimers with interactions; and (3) asymmetric binuclear molecules.

Chapter VII discusses data analysis techniques for "large step" coulostatics in the study of electron transfer kinetics. The merits of the technique in electrochemistry are discussed. A method for the use of a numerically generated function as the basis function for nonlinear regression is discussed.

Chapter VIII presents a study of alternative methods of "small step" coulostatic data analysis. Strong cross-correlation was found between double layer capacitance, charge transfer parameters and diffusional parameters.

TABLE OF CONTENTS

CHAPTER I

Introduction

This thesis in electrochemistry is comprised of three distinct topics. Chapters II, III and IV are all concerned with the analytical consequences of adsorption of reactants at the electrode surface with d.c. and pulse polarographic techniques. Chapters V and VI are simple mathematical treatments of certain features of current-potential and concentration-potential behavior of molecules containing two or more electroactive centers. Chapters VII and VIII discuss some nuances of data analysis with the use of charge injection techniques to determine electrode kinetics.

The projects described herein illustrate some uses of numerical mathematics, statistics and mini-computer applications in electrochemistry. The PDP-11 computer was found to be indispensable to the projects since it allowed for several modes of use: as a "number cruncher", in large scale digital simulations, it saves the high costs involved with running programs on a large computer; as an interactive terminal, it allows rapid program correction and modification; and, of course, it is most valuable in control of customized experimental design and data analysis.

A brief summary of each Chapter and associated Appendices follows.

Chapter II[1] is a preliminary theoretical treatment of the effects of adsorbed product and reactant on pulse polarographic response. A closed-form solution for the current function was derived, and a computer was employed to generate differential pulse polarograms for comparison with theory. The computer programs for generating the theoretical curves are found in Appendix A.

Chapter III[2] is an extension of the ideas in Chapter II. Limitations of the mathematics are bypassed by means of digital simulation. The ways in which peak currents and wave shapes of differential pulse polarograms are affected by adsorption of reactants and products are examined with the additional complications of nonlinear adsorption isotherms and uncompensated resistance. Comparison of theoretical and experimental results is made for Cd(II) ion with adsorption induced by addition of iodide and bromide. Some additional material on the effects of adsorbed reactants on d.c. polarography is included in this chapter. The differential pulse computer programs are found in Appendix B, the d.c. programs in Appendix C.

Chapter IV[3] considers many of the same effects for normal pulse polarography as were discussed in Chapter III. Computer programs are found in Appendix D.

Chapter V[4] is concerned with the statistical treatment of molecules with many centers for electron transfer. It is shown that when negligible coulombic or other physical or chemical interaction occurs between centers, the shape (but not the magnitude) of the resulting current-potential curves in voltammetry or polarography are identical for polymer or monomer species.

Chapter VI is an extension of the work in Chapter V with emphasis on two frequently encountered perturbations: interaction between centers, and non-symmetry of centers. For simplicity the derivations were restricted to dimers although extension to any particular case should be trivial. Some cases from the literature are discussed.

Chapter VII is concerned with the analysis of large step coulostatics data. Nonlinear regression is employed to determine standard rate constants and transfer coefficients, assuming that the formal potential and double layer capacitances are known to high accuracy. The method of computation which allows highly accelerated convergence for the theoretical calculations is developed. Error analysis of the method is discussed.

Chapter VIII reports the results of a study of the use of small step coulostatics in the analysis of electrode kinetics. The use of nonlinear regression analysis of the coulostatic data is critically discussed with regard to the cross correlation of unknowns and the analysis of errors. Several experimental systems are discussed.

REFERENCES

(1) F. C. Anson, J. B. Flanagan, K. Takashi, and A. Yamada, J. Electroanal. Chem., 67, 253 (1976).

(2) J. B. Flanagan, K. Takahashi and F. C. Anson, J. Electroanal. Chem., 81, 261 (1977).

(3) J. B. Flanagan, K. Takahashi, and F. C. Anson, J. Electroanal. Chem., 85, 257(1977).

(4) J. B. Flanagan, S. Margel, A. J. Bard and F. C. Anson, J. Am. Chem. Soc., submitted for publication.

CHAPTER II

A Preliminary Analysis of the Effects of Adsorbed Reactants on Differential Pulse Response

INTRODUCTION

Experimentally it was observed that a remarkable enhancement of differential pulse polarographic currents[1] can be seen when adsorption-inducing anions are added to solutions of certain metal cations. For example, Fig. 2.1 compares the differential pulse polarogram for a 10 μM solution of Cd(II) in 0.1 M KNO_3 where no adsorption of Cd(II) occurs, with that in 0.1 M KI where extensive adsorption of Cd(II) is induced.[2] The peak current in the iodide electrolyte is almost twice as large as that in the nitrate electrolyte and even greater current enhancements (3 to 5-fold) have been obtained by decreasing the time at which the differential pulse polarographic current is sampled after the application of each potential pulse. While the likely utility of this phenomenon in increasing the analytical sensitivity of differential pulse polarography seems evident and well worth exploiting, in this hapter I wish to emphasize the particular virtues of this phenomenon in studies directed at measuring and characterizing reactant and product adsorption at electrode surfaces.

FIGURE 2.1

Differential pulse polarograms for 10 μM Cd(II) in 0.1 M KNO_3 and 0.1 M KI. Pulse amplitude: 25 mV; potential scan rate: 1 mV s^{-1}; drop age: 2 s; drop area: 0.0161 cm^2. A - 0.1 M KNO_3. B - 0.1 M KI. Potential measured vs. SCE.

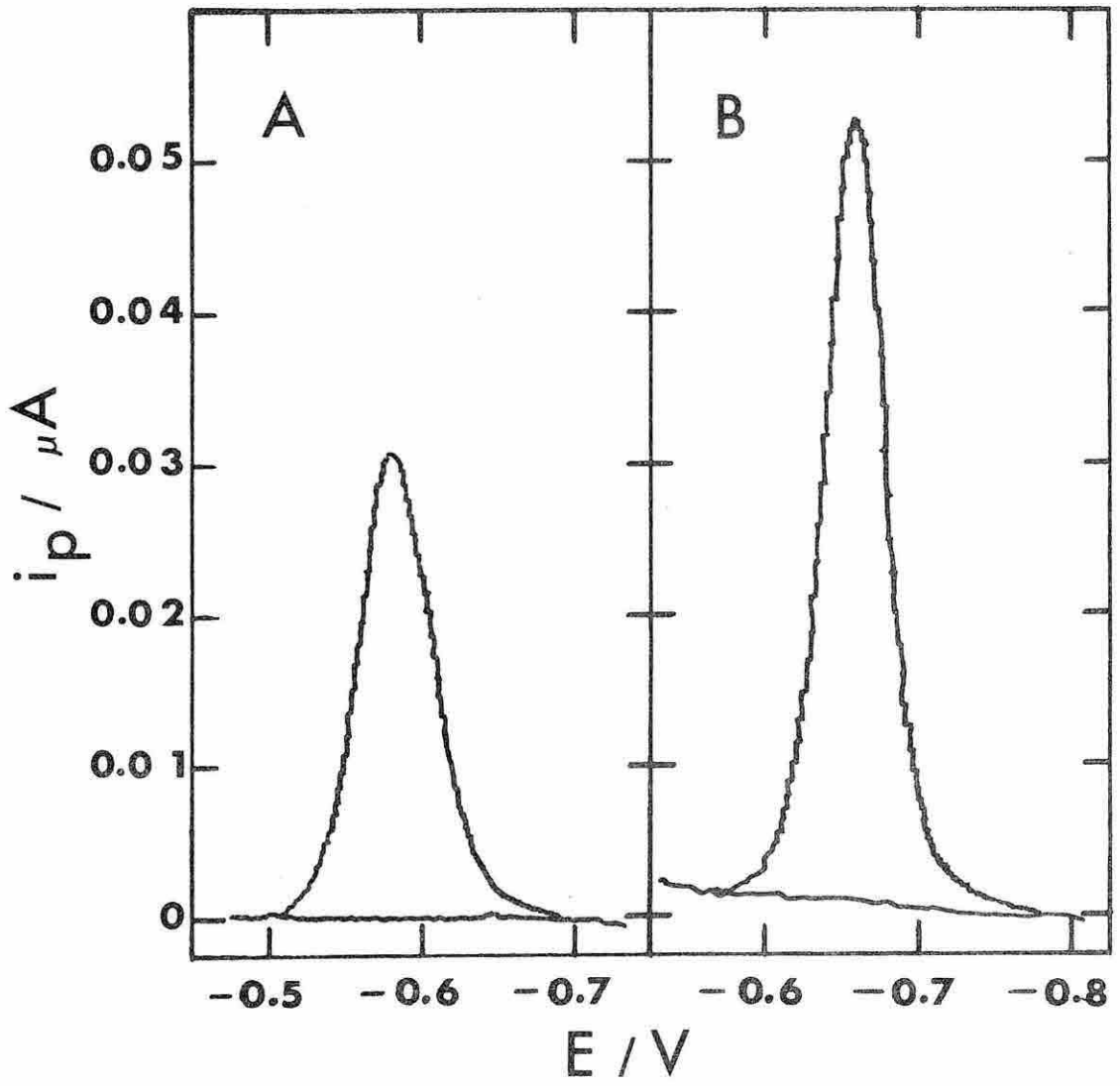

FIGURE 2.1

EXPERIMENTAL

The differential pulse polarograms were obtained with a Princeton Applied Research Model 174 "Polarographic Analyzer" including the electro-mechanical dropping electrode dislodger supplied with this instrument. A Houston Omnigraph XY Recorder was used to record the polarograms. Electrolysis cells, oxygen removal and the operating procedure were all conventional. Measurments were made at 25 ± 1° C.

Solutions were prepared from triply distilled water and reagent grade chemicals. With concentrations of reactants greater than ca 100 μM the peak currents were evaluated with the d.c. potential held constant in order to compensate for the slow response of the instrument.[3] With smaller concentrations the d.c. potential was usually scanned at the rate of 0.1–2 mV s^{-1}.

THEORY

The adsorption-induced enhancements of the differential pulse polarographic peak currents were measured at reactant concentrations in the micromolar range where the total amount of reactant adsorbed was so small that Henry's law was assumed to hold (i.e., the adsorption was assumed to obey a linear isotherm):

$$\Gamma_R = K_R c_R(x=0) \tag{2.1}$$

$$\Gamma_P = K_P c_P(x=0) \tag{2.2}$$

where Γ is the concentration (mol cm^{-2}) of the adsorbed species, $c(x=0)$ is the concentration (mol cm^{-3}) of the corresponding species in the solution at the electrode surface, K is the Henry's law adsorption coefficient (cm), and the subscripts R and P refer to the reactant and product, respectively.

The values of $c_R(x=0)$ and $c_P(x=0)$ were assumed to be given by the Nernst equation

$$\frac{c_P(x=0)}{c_R(x=0)} = \exp\left[-\frac{nF}{RT}(E-E^\circ)\right] \equiv \theta \tag{2.3}$$

Initially, only the reactant is present in the solution at concentration c*.

The d.c. Faradaic currents which flow before each potential step is applied when E is in the vicinity of E° were neglected in calculating the pulse polarographic current responses. This approximation, which amounts to the assumption that the composition of the layer of solution at the electrode surface matches that of the bulk of the solution, has been shown by Christie[4] to lead to negligible error in the calculated peak currents under most typical experimental conditions. The approximation

will become better and better as the drop time is increased and the time after each pulse when the current is sampled is decreased.

The solution of Fick's diffusion equations for this set of boundary and initial conditions has been previously discussed by several authors[5-10]. Equations (2.1) through (2.6) in the paper of Reinmuth and Balasubramanian[9] can be combined with eqns (2.1) and (2.2) above to obtain the following expression for the current density as a function of the time, t, after the application of each potential step of magnitude $(E_2 - E_1)$:

$$I = \frac{nF\gamma\theta_2}{K_R\theta_2 + K_P}\left\{\frac{D_R^{\frac{1}{2}}K_P + D_P^{\frac{1}{2}}K_R - \beta K_R K_P}{(\pi t)^{\frac{1}{2}}} + \left[K_R K_P \beta^2 - \beta(D_R^{\frac{1}{2}}K_P + D_P^{\frac{1}{2}}K_R) + D_R^{\frac{1}{2}}D_P^{\frac{1}{2}}\right]\exp(\beta^2 t)\,\mathrm{erfc}(\beta t^{\frac{1}{2}}) + K_R K_P \delta(t)\right\} \qquad (2.4)$$

where: $\gamma = c_R/\theta_2 - c_p$

at $t = 0$: $c_R = \xi\theta_1 c^*/(\xi\theta_1+1)$; $c_p = \xi c^*/(\xi\theta_1+1)$; $\xi \equiv (D_R/D_p)^{\frac{1}{2}}$

and $\beta = (D_R^{\frac{1}{2}}\theta_2 + D_P^{\frac{1}{2}})/(K_R\theta_2+K_P)$

$$\delta(t) = 0 \text{ for } t > 0; \int_{o-}^{o+} \delta(t)\,dt = 1$$

$$\theta_i = \exp[-(nF/RT)(E_i - E^\circ)]$$

No capacitive charging current is included in eqn (2.4) because the differential pulse polarographic current read-out eliminates most of this current. Except for this feature, eqn (2.4) is not restricted to differential pulse polarography. It is a general expression for current vs. time when the potential is stepped between any two potentials in a polarographic wave for adsorbing reactants or products which obey linear isotherms.

Equation (2.4) reduces to the equation given by Parry and Osteryoung[1] when K_R and K_P are equal to each other or approach zero, except for the small difference arising from our neglect of the current flowing just before each potential step. (Reinmuth[9] has presented a good account of the reasons for the disappearance of the effects of adsorption when $K_R = K_P$.)

RESULTS AND DISCUSSION

Equation (2.4) was used with the aid of a computer to calculate complete pulse polarograms by varying E_1 while keeping $(E_2 - E_1)$ constant. The resulting peak currents were evaluated for various values of K_R, K_P and the current sampling time, t. Some results are shown in Fig. 2.2 in which the ratio of the calculated peak currents in the presence and absence of adsorption are presented as a function of the adsorption coefficients

FIGURE 2.2

Calculated peak currents for adsorbed reactants divided by those that would result in the absence of adsorption. The parameters used in eqn (2.4) were: $D_R = D_P = 10^{-5}$ cm^2 s^{-1}; $(E_2 - E_1) = 10$ mV. (——) Reactant adsorption, $K_P = 0$; (-----) product adsorption, $K_R = 0$; current sampling times: (1,4) 1 ms; (2, 5) 10 ms; (3, 6) 50 ms.

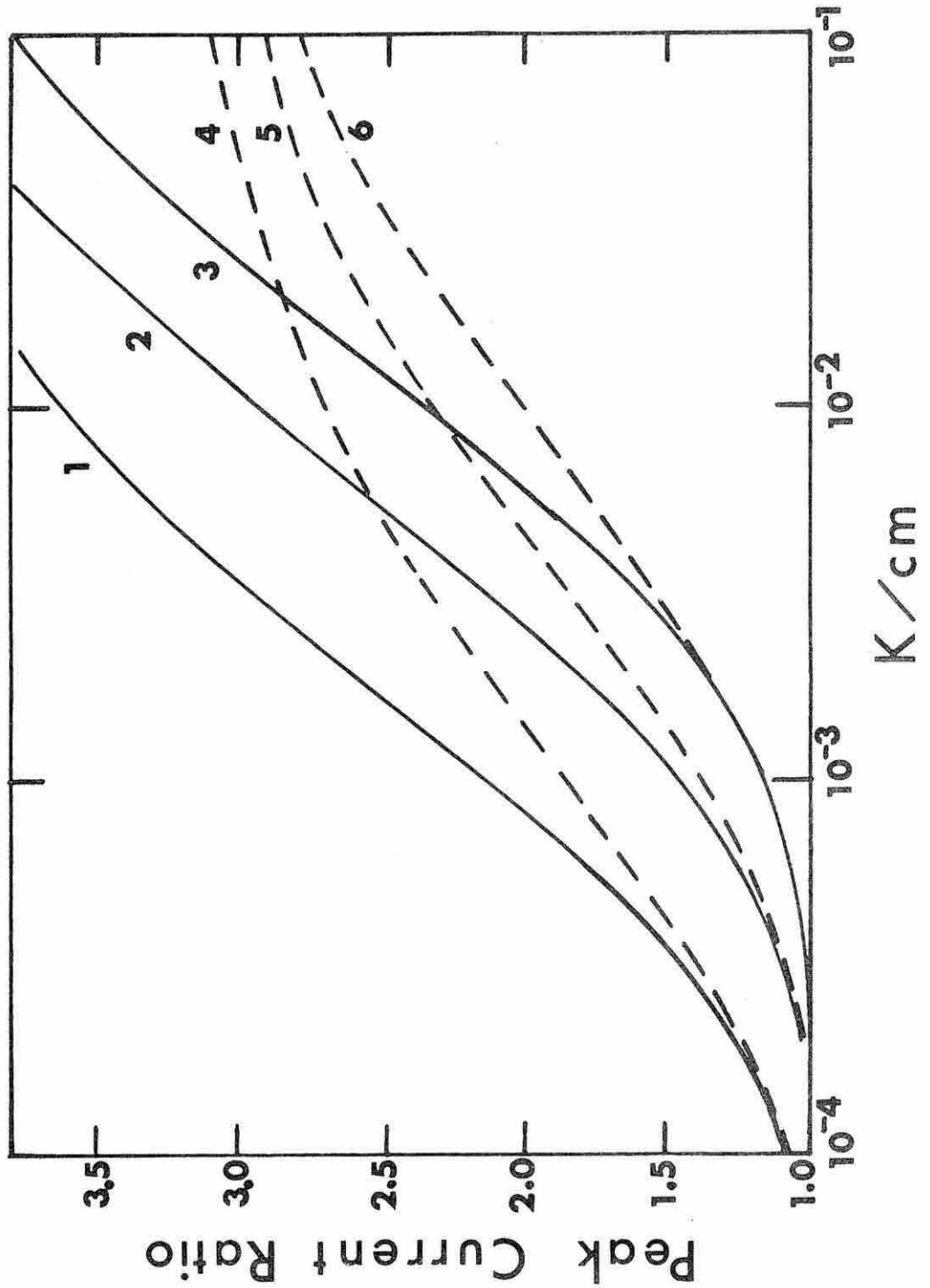

FIGURE 2.2

and of the time following the application of the potential pulse that the current is sampled. Note that the calculated peak currents can exceed the values obtained in the absence of adsorption by factors of three or more for sufficiently large values of the adsorption coefficients or sufficiently short sampling times.

The PAR 174 instrument has an effective sampling time of ca. 48 ms. With this value of t, $D_R = 5.3 \times 10^{-6}$ cm^{-2} s^{-1}, $D_P = 1.7 \times 10^{-5}$ cm^{-2} s^{-1}, $K_P = 0$ and the measured ratio of 1.7 for the two peak currents in Fig. 2.1 a value of K_R of 2×10^{-3} cm was obtained by manipulation of eqn (2.4). This value of K_R leads to a calculated adsorption of 2×10^{-11} mol cm^{-2} of Cd(II) from a 10 μM solution of Cd(II) in 0.1 M KI. At a potential of -550 mV the adsorption amounted to 1.9 to 2.1×10^{-11} mol cm^2. This good agreement between the measured adsorption and that calculated from the pulse polarographic peak current ratios supports the theoretical analysis which lead to eqn (2.4).

The curves in Fig. (2.2) remain independent of the bulk concentration of the reactant only in the range where the adsorption isotherm remains linear. As the concentration of the reactant is increased the adsorption isotherm must eventually become non-linear when the finite capacity of the electrode surface to accept

additional adsorbing species limits the adsorption. At this point the diffusive contribution to the peak currents will continue to grow as the bulk concentration of reactant increases while the adsorptive contribution does not and the peak currents will tend toward their values in the absence of adsorption. This behavior is shown in Fig. 2.3 where the normalized peak currents for Cd(II) in the iodide electrolyte (i.e., the peak current divided by the bulk concentration of Cd(II) and the (drop age)$^{2/3}$ to account for changes in area) are plotted versus the concentration of Cd(II). There are two level portions of the curve. At the lowest concentrations the adsorption follows a linear isotherm and the relative current enhancement due to adsorption is constant. At the highest concentrations the surface is saturated, the adsorption becomes independent of bulk concentration and the ratio of peak current to concentration falls to the constant value representative of the absence of adsorption. The range of concentrations over which the peak current-to-bulk concentration ratio varies is the range within which the adsorption isotherm is non-linear.

At dropping mercury electrodes the concentration of adsorbing reactants may be depleted near the electrode surface early in drop life even in the absence of a

FIGURE 2.3

Concentration dependence of normalized peak currents for Cd(II) in 0.1 M KI. Pulse amplitude: 25 mV; drop age: (×) 0.5 s; (□) 1 s; (○) 2 s; (△) 5 s; the effective sampling time of the PAR 174 instrument is ca. 48 ms.

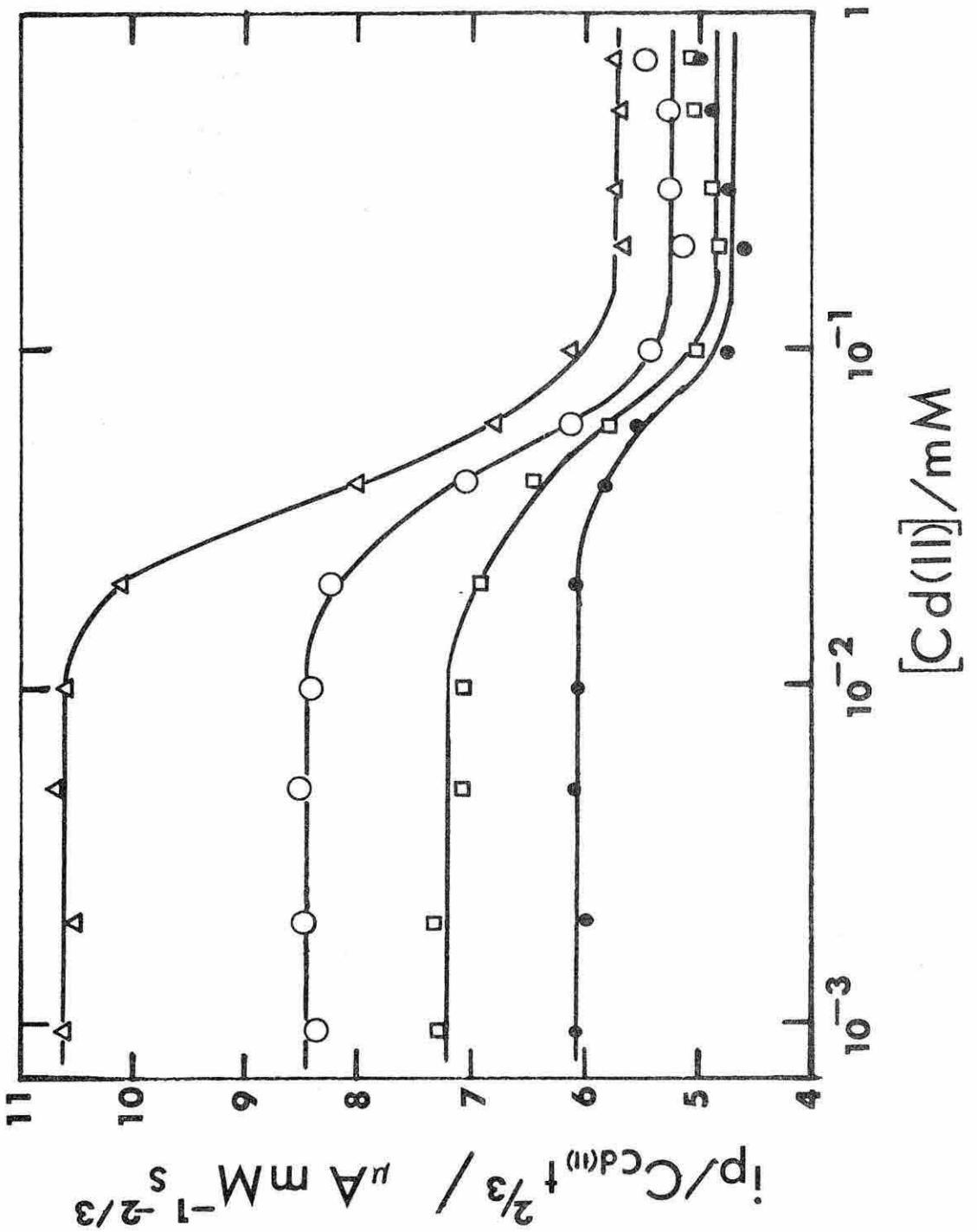

FIGURE 2.3

faradaic reaction. In the derivation of eqn (2.4) it was assumed that the concentrations of reactant and product were uniform before the application of each pulse so that any depletion of the reactant concentration at the electrode surface because of its adsorption would result in smaller measured currents than those calculated according to eqn (2.4). This additional complication will be independent of the bulk concentration of reactants which obey linear isotherms but it will be influenced by the age of the dropping electrode t_d. The systematic decrease in the normalized peak currents for Cd(II) in iodide (Fig. 2.3) as the drop times are decreased from 5 to 0.5s is very likely a manifestation of such reactant depletion. Adsorptive depletion of the reactant can be overcome by replacing the DME with a hanging mercury drop electrode which can be equilibrated with the solution for as long a time as necessary prior to measurement of the peak current. However, currents which increase with time at constant potential are obtained with reactants (both adsorbed and unadsorbed) which are reduced to amalgams at the HMDE. This phenomenon results because the amalgam concentration within the drop increases as the electrolysis proceeds which leads to a corresponding increase in the concentration of the reactant in the solution at the drop surface.

The lack of coincidence of the four curves in Fig. 2.3 at the highest concentrations of Cd(II) is believed to result from a different effect: The adsorption of a reactant introduces a large faradaic pseudocapacitance into the cell impedance faced by the pulse polarograph. The magnitude of the pseudocapacitance can be estimated as $\frac{n^2F^2\Gamma}{RT}$. This amounts to ca. 2800 $\mu F\ cm^{-2}$ for the amount of Cd(II) present on the saturated surfaces at the higher Cd(II) concentrations in Fig. (2.3). The presence of this large capacitance prolongs the effective time constant for decay of the "charging current" (both faradaic and non-faradaic) to the point that it contributes to the net currents sampled by the PAR 174 instrument despite the 48 ms delay between pulse application and current measurement. The charging current contribution will be larger the longer the drop time because the electrode area and, therefore, the faradaic pseudocapacitance will be greater.

The effect is not confined to adsorbing reactants which are reduced to amalgams. The same behavior is also observed with anthraquinone monosulfonate which is reduced to a hydroquinone soluble in the solution phase.[11]

The explanation of the drop time dependence in terms of a large pseudocapacitance is supported by the

fact that with nitrate electrolytes, where there is no adsorption of Cd(II), plots such as those in Fig. 2.3 are much more nearly coincident at all drop times and concentrations of Cd(II). Tests of the PAR 174 instrument with dummy cells also confirmed that the instrument fails to discriminate completely against charging currents in the differential pulse mode when capacitances as large as those produced by extensive reactant adsorption are introduced in the circuit.

The ways in which reactant (and product) adsorption alter conventional differential pulse polarograms suggest that this technique may prove to be valuable in studies of adsorption: (i) Sensitivity is high. Easily measured peak current enhancements result from the adsorption of quantities of reactant much smaller than could be determined (or, in most cases, even detected) with chronocoulometric or interfacial tension measurements. However, reasonably large adsorption coefficients ($>10^{-4}$ cm) are still essential to produce measurable peak current enhancements at the small reactant concentrations needed to obtain a linear adsorption isotherm (Fig. 2.2). (ii) The differential pulse polarograms allow adsorption coefficients to be evaluated at the potentials where the absorbate is reacting at the electrode. This may be an important

advantage in kinetic investigations of adsorbed reactants because direct chronocoulometric measurements of adsorption coefficients are necessarily restricted to initial potentials where no electrode process is occurring. (iii) Although the possible potential dependence of adsorption coefficients was not considered in the derivation of eqn (2.4), the shapes of the differential pulse polarograms should be analyzable to determine whether a significant potential dependence is present.

The large enhancement of differential pulse polarographic peak currents resulting from reactant adsorption is entirely analogous to the well known and large effects that reactant adsorption produces in faradaic impedance measurements.[12] However, because of its higher sensitivity, the differential pulse polarographic technique can be used to examine adsorption in much more dilute solutions, thus ensuring that a linear adsorption isotherm is obeyed. In addition, the quantitative analysis of faradaic impedance data to determine adsorption coefficients is considerably more complex and requires the knowledge of more parameters than is true for differential pulse polarography.

REFERENCES

(1) E. P. Parry and R. A. Osteryoung, Anal. Chem., 37, 1634 (1965).

(2) F. C. Anson and D. J. Barclay, Anal. Chem., 40, 1791 (1968).

(3) J. H. Christie, J. Osteryoung and R. A. Osteryoung, Anal. Chem., 45, 210 (1973).

(4) J. H. Christie, Ph. D. Thesis, Colorado State University, 1974; J. H. Christie and R. A. Osteryoung, J. Electroanal. Chem., 49, 301 (1974).

(5) K. Holub and J. Koryta, Collect. Czech. Chem. Commun., 30, 3785 (1965).

(6) G. C. Barker and J. A. Bolzan, Z. Anal. Chem., 216, 215 (1966).

(7) K. Holub, Collect. Czech. Chem. Commun., 31, 1461 (1966).

(8) R. Guidelli, J. Electroanal. Chem., 19, 5 (1968).

(9) W. H. Reinmuth and K. Balasubramanian, J. Electroanal. Chem., 38, 79 (1972).

(10) W. H. Reinmuth and K. Balasubramanian, J. Electroanal. Chem., 38, 271 (1972).

(11) F. C. Anson and B. Epstein, J. Electrochem. Soc., 115, 1155 (1968).

(12) M. Sluyters-Rehbach and J. H. Sluyters in A. J. Bard (ed.), Electroanalytical Chemistry, Vol. 4, Marcel Dekker, New York, 1970.

CHAPTER III

Effects of Adsorptive Depletion of Reactant, Nonlinear Adsorption Isotherms and Uncompensated Resistance on Differential Pulse and D.C. Polarographic Response

INTRODUCTION

The previous chapter described and analyzed some conditions under which adsorption of the reactants or products can lead to enhanced peak currents in differential pulse polarography. The equation which was derived to account for the current enhancement involved several simplifying assumptions: (a) depletion of a reactant from solution near the electrode surface due to its adsorption was neglected; (b) the cell was assumed to be free of uncompensated resistance; (c) the adsorption was assumed to obey a linear isotherm (Henry's law). The same assumptions were also made by Barker and Bolzan[1] who clearly recognized and described the effects of reactant adsorption in pulse polarography. These assumptions severely limit the quantitative applicability of the previous equation because all three assumptions are frequently not justified in studies of dilute solutions of strongly adsorbing species. It has proved possible to calculate the expected differential pulse polarographic

currents without the use of these simplifying assumptions for nernstian reactions involving adsorbing reactants or products by means of digital simulation techniques.[2] The calculational approach employed and a comparison of calculated currents with experimental results for the iodide-induced adsorption of Cd(II) are described in this report.

The results are relevant to analytical applications of differential pulse polarography in the presence of adsorption inasmuch as the calculations show that significant effects are to be expected on peak currents, peak potentials and wave shapes.

EXPERIMENTAL

The differential pulse polarograms were obtained with the PAR (Princeton Applied Research) Model 174 "Polarographic Analyzer" which had been modified to permit measurements at variable pulse widths and sample times, following a scheme suggested by Abel et al.[3] The resulting sampling time and pulse widths were calibrated by means of a Systron Donner Counter, Model 1033.

The polarograms were recorded with an XY recorder. Most polarograms were recorded with 25 mV pulse amplitudes and potential scan rates of 0.2 to 2 mV s^{-1}. External

uncompensated resistance was introduced into the circuit by means of a decade resistance box inserted between the working electrode terminal of the PAR 174 and the DME.

The additional adsorption data used to establish an isotherm for the iodide-induced adsorption of Cd(II) were obtained by means of double potential step chronocoulometry.[4] Since rather low concentrations of Cd(II) were necessarily employed, each hanging mercury drop electrode was exposed to the solution for 60 s at the initial potential (-500 mV) to ensure that adsorption equilibrium had been obtained. (The solution was unstirred, but increased exposure times produced no changes in the resulting polarograms.) Initial data points obtained during the reverse potential step were discarded until no further changes in the measured adsorptions resulted. This occurred at times following the second potential step that were shorter than required for establishing adsorption equilibrium[5] because of the small dependence of the double layer capacitance on the amount of Cd(II) adsorbed.[6] Solutions were prepared from triply distilled water and reagent grade chemicals. Dissolved oxygen was removed by bubbling pre-purified nitrogen through the solutions. Measurements were made at room temperature: 25 ± 2° C.

RESULTS AND DISCUSSION

Digital simulation. The digital simulation of differential pulse polarograms was described recently by Dillard and Hanck.[7] Portions of the procedure employed in this work were similar to those described in ref. 7 but there were also substantial differences resulting from the more complex boundary conditions which were required in order to allow for the adsorption of reactant product according to non-linear isotherms, and for the presence of uncompensated resistance. In the present analysis the electrode reactions were assumed to be reversible and nernstian with both the reactant and product soluble in either the solution or mercury electrode. Adsorption equilibrium was assumed to be established instantaneously and the adsorption was assumed to produce no effect on the electrode reaction rates of either reactant or product.

A difference between the present procedure and that used by Dillard and Hanck[7] was the choice of time intervals in the simulation. The discrete time units utilized by these authors were of the same magnitude during the periods before and after the application of each potential step, while the simulation used in the present work involved different time intervals for the two periods.

This tactic was adopted in order to optimize the calculation of the current after application of the potential step without committing an unreasonable amount of time to the calculation during the less critical period prior to the potential step. For example, a 5 s period prior to the potential step was typically divided into 100 intervals of 50 ms, while the 50 ms period following the potential step was divided into 100 intervals of 500 μs. Of course, when the discrete time unit is changed, a corresponding change must be made in the discrete distance unit in order to satisfy the stability criterion for the explicit difference method[8] which was used to simulate the diffusion of reactant and products. In recalculating the concentration profile following the changes in time intervals, a simple linear interpolation method was used.

The presence of uncompensated resistance in the cell made it necessary to carry out an iterative calculation for the current and the true electrode potential until self-consistent values were obtained. It was also necessary to determine the quantity of adsorbed reactant and its surface concentration which satisfied simultaneously the adsorption isotherm, the Nernst equation, and conservation of mass at the electrode surface at each time interval. For a general non-linear isotherm, several

iterations of a Newton-Raphson procedure[9] were required to obtain self-consistent values. Since this calculation was nested within the one used to calculate the current and true electrode potential, this portion of the program consumed about the same amount of computer time as did that devoted to the mass transfer calculations.

Ohmic potential drops through the uncompensated resistance were neglected during the period before each potential step but adsorption equilibrium was included in the calculation. The mass transfer calculation during this period consisted of diffusion to an expanding plane calculated according to standard procedures. Following the potential step, further expansion of the electrode area was neglected, but the ohmic drop through the uncompensated resistance and double layer charging were included in the calculation.

The values for diffusion coefficients, double layer capacitance, uncompensated resistance and adsorption isotherm parameters which were required in order to compare the simulated and experimental results were evaluated in independent experiments. The digital simulation utilized in this work gave calculated currents which matched those predicted by the Parry and Osteryoung equation[10] within a few percent when the adsorption

coefficients for both reactant and product were set equal to zero. The simulation converged smoothly to constant calculated current values as the number of calculational intervals was increased. The calculational accuracy of most of the simulated results given in the figures is estimated to be better than ±5%. Listings of the complete differential pulse simulation programs are shown in Appendix B.

The Adsorption Isotherm. A previous chronocoulometric study of iodide-induced adsorption of Cd(II) on mercury[6] did not extend to concentrations of Cd(II) below 0.2 mM and contained insufficient data to establish a reliable adsorption isotherm. Therefore additional chronocoulometric measurements of Cd(II) adsorption were conducted in the range between 5 and 100 μM Cd(II) from a supporting electrolyte containing 0.9 m KNO_3 and 0.1 M KI. The resulting values of $\Gamma_{Cd(II)}$, the surface concentration of adsorbed Cd(II), were then fitted to a Frumkin adsorption isotherm[11] by means of the plot shown in Fig. 3.1. The Frumkin isotherm can be written as in eqn (3.1)

$$\ln c - \ln[\theta/(1-\theta)] = \ln(\Gamma_m/K) + A\theta \qquad (3.1)$$

where c is the concentration of the adsorbate, Cd(II), at the surface of the electrode, $\theta = \Gamma/\Gamma_m$ is the coverage,

FIGURE 3.1

Plot of adsorption data for Cd(II) in 0.9 M KNO_3 - 0.1 M KI according to eqn (3.1). Coverages, θ, were obtained from double potential step chronocoulometry. Γ_m was taken to be 2.2×10^{-10} mol cm^{-2}. (●) Data from this work; (○) data from ref. 6.

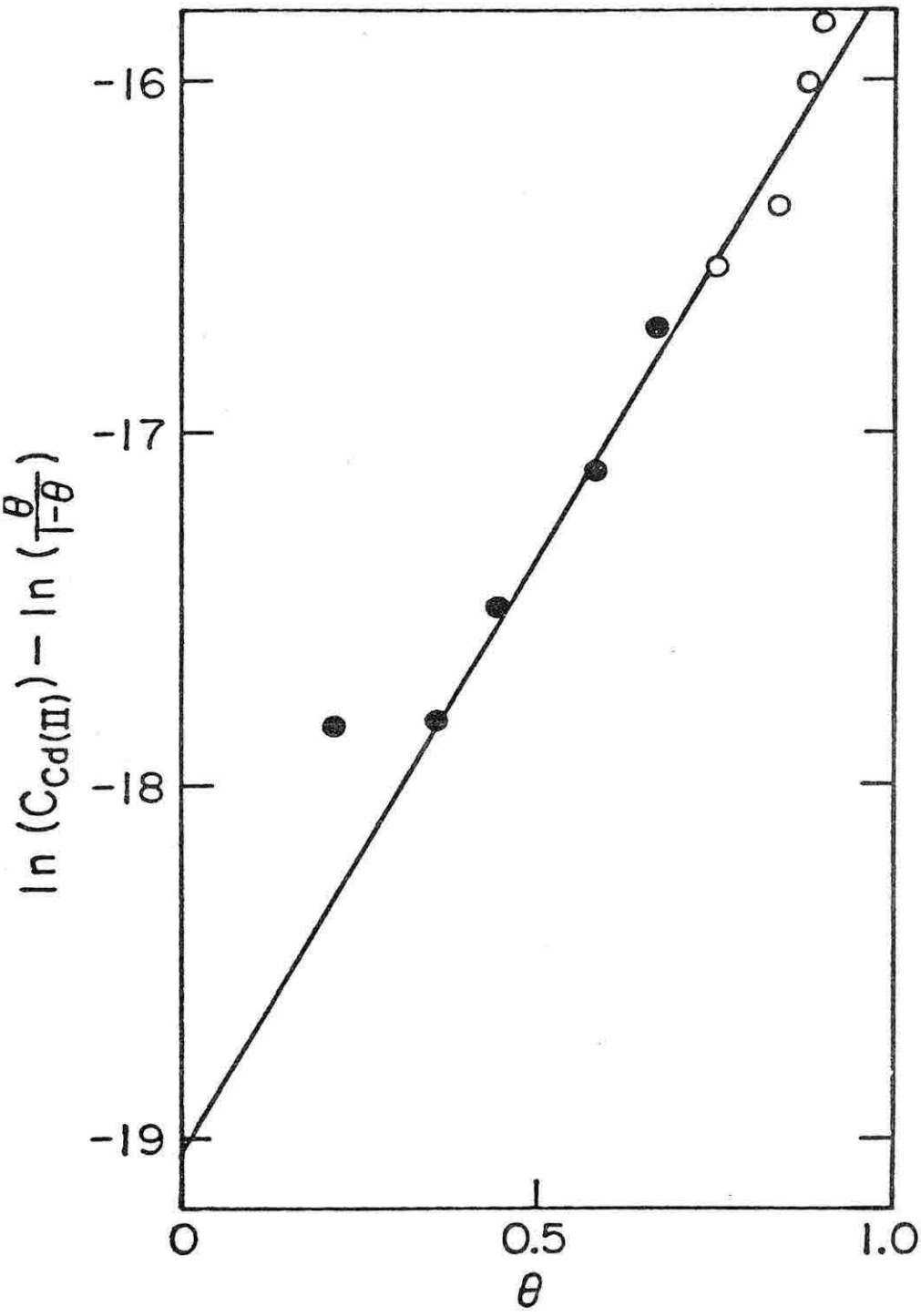

FIGURE 3.1

Γ and Γ_m are the concentrations of the adsorbate on a partially and fully covered surface, respectively, K is the Henry's Law adsorption coefficient (Γ = Kc at low coverages) and A is the Frumkin parameter which measures the strength of the intermolecular interactions between adsorbate molecules on the surface. Figure 3.1 is a plot of the l.h.s. of eqn (3.1) versus θ for the iodide-induced adsorption of Cd(II). The best fit of the data to a straight line resulted when Γ_m was taken as 2.2×10^{-10} mol cm^{-2} instead of 1.9×10^{-10} mol cm^{-2} which was the value measured previously[6] at the largest concentration of Cd(II) studied (1.2 mM). The slope of the line in Fig. 3.1 corresponds to A = 3.6 which implies strong repulsive interaction between the adsorbed Cd(II) species.

The value of K resulting from the intercept of the line in Fig. 3.1 is 0.04 cm. These values of the isotherm parameters were used in the digital simulation calculations despite the fact that the most negative potential at which the chronocoulometric data could be obtained (-500 mV) differed from the pulse polarographic peak potentials (~625 mV). A preferable approach might be to evaluate the isotherm parameters at several potentials and attempt to extrapolate to the pulse polarographic peak potential.

Effect of Adsorption on Peak Currents. Figure 3.2 presents plots of normalized differential pulse polarographic peak currents as a function of the bulk concentration of Cd(II). The plotted data points are experimental measurements and the solid lines are the result of the digital simulation.

In general the simulation is reasonably successful in accounting for the concentration and drop age dependences of the data. As was noted in the previous chapter, the largest normalized currents are obtained at the smallest bulk concentrations where the adsorption isotherm is approaching linearity and the coupling of adsorption, mass transfer and the Nernst equation leads to maximum enhancement of the current. The drop age dependence of the normalized currents arises from the adsorptive depletion of reactant from the solution at the electrode surface which the digital simulation manages to map fairly successfully. In our earlier chapter a similar drop age dependence was attributed to reactant depletion at the lower bulk concentrations but no quantitative assessment was possible. The present simulation results show that the effects of depletion persist up to concentrations as high as 1 mM. Moreover, the simulation shows that under some conditions the normalized peak currents can fall

FIGURE 3.2

Concentration and drop time dependence of normalized differential pulse polarographic peak current densities for Cd(II) in 0.1 M KI -0.9 M KNO_3. The plotted points are experimental values for drop times of 0.5 s (●) and 5.0 s (○) and curves 1 and 2 are the corresponding digital simulation results using the Frumkin isotherm parameters determined in Fig. 3.1. Curve 3 corresponds to a Langmuir isotherm having the same values of K_R and Γ_m as in curves 1 and 2 and drop time of 5 s. The dashed line corresponds to no adsorption for both drop times. Parameters used in the simulation: $D_R = 10^{-5}$ cm^2 s^{-1}, $D_P = 1.5 \times 10^{-5}$ cm^2 s^{-1}, mercury flow rate = 1.04 mg s^{-1}; double layer capacitance = 65 μF cm^{-2}; uncompensated resistance - 130 Ω (actual measured values were 100 and 175 Ω with 5 and 0.5 s drop times).

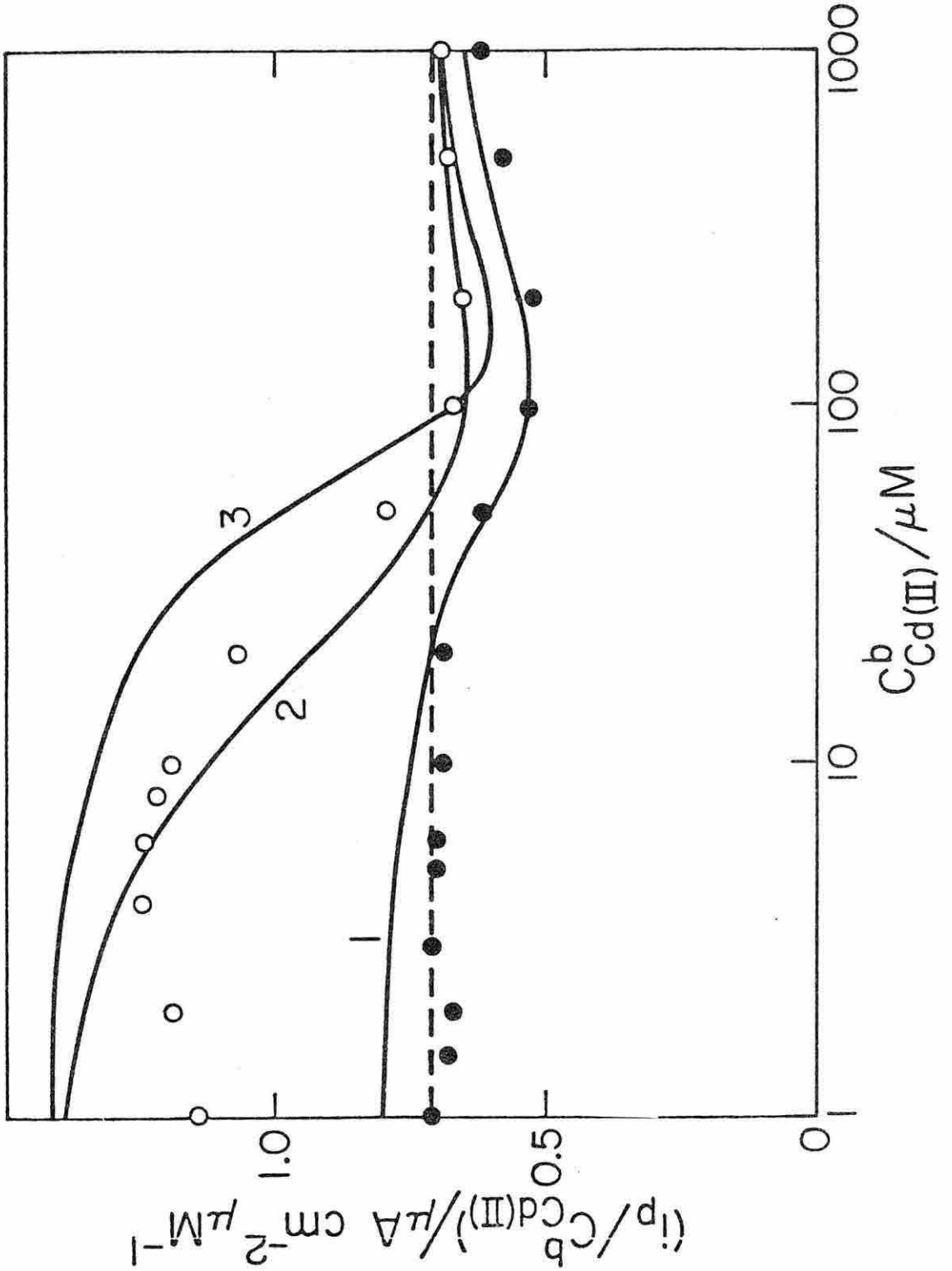

FIGURE 3.2

below the values corresponding to no perturbation by reactant adsorption. This behavior results when the depletion of the concentrations of the reactant because of its adsorption depresses the current more than the nernstian coupling of mass transfer and adsorption enhances it. The Cd(II) adsorption exhibits this feature quite prominently at the shorter drop time shown in Fig. 3.2 (curve 1).

In order to compare the response obtained with an adsorbed reactant obeying a Frumkin isotherm with that expected when the adsorption is langmuirian, curve 3 of Fig. 3.2 was simulated by employing the same values of K_R, Γ_m and drop time as were used for curves 1 and 2 but setting A = 0 in eqn (3.1). The larger predicted current enhancements at the lower concentrations under these conditions are the result of the stronger adsorption to which the chosen value of K_R corresponds in a Langmuir isotherm. The more rapid decrease of curve 3 at higher concentrations is a reflection of the more rapid rise to saturation coverage of Langmuir than of repulsive Frumkin isotherms.

For analytical applications where reactant adsorption might be induced (by selection of the proper supporting electrolyte) to enhance sensitivity it is clearly desirable

to minimize adsorptive depletion of the reactant. This can sometimes be achieved by utilizing dropping electrodes with longer natural drop times or hanging mercury drop electrodes. However complications resulting from spherical diffusion within the finite electrode may be encountered at longer-lived drops with amalgam-forming reactions.

Effects of Adsorption on Peak Potentials and Wave Shapes. Strong reactant (or product) adsorption produces shifts of differential pulse polarographic peak potentials. Examples of such shifts are shown in the differential pulse polarograms in Fig. 3.3 which were simulated for conditions corresponding to very strong adsorption with a linear adsorption isotherm. The pronounced drop time dependence evident in these polarograms results from the differences in the extent of adsorptive depletion of the reactant at long and short drop times. Note that the breadth as well as the peak potentials of the polarograms are affected by the depletion. Adsorption of the product instead of the reactant causes greater broadening of the polarogram (Fig. 3.3) and smaller enhancement of the peak current.[1] However, with equivalent adsorption coefficients, the peak potential is shifted from the value obtained without adsorption[10] by the same amount (but in opposite directions) by the adsorption of the reactant or the product.

FIGURE 3.3

Simulated differential pulse polarograms for strongly adsorbed reactant or product obeying a linear adsorption isotherm. $\Gamma_i = K_i c_{x=o}$; K_R and K_P are the adsorption coefficients for reactant and product, respectively and $c_{x=o}$ is the concentration of adsorbate at the electrode surface. The potential is referenced to the standard potential, E°. The ratio of the current density to the concentration of Cd(II) is plotted as ordinate.

Curve	K_R/cm	K_P/cm	Drop time/s
1	0	0	1 or 100 (superimposed curves)
2	0.1	0	1
3	0.1	0.0	100
4	0	0.1	1
5	0	0.1	100

Other parameters: $D_R = D_P = 10^{-5}$ cm^2 s^{-1}; n = 2; c_R = 100 μM; pulse amplitude = 25 mV; current sampling time = 25 ms; uncompensated resistance and double layer capacitance were assumed to be negligibly small; mercury flow rate = 1 mg s^{-1}.

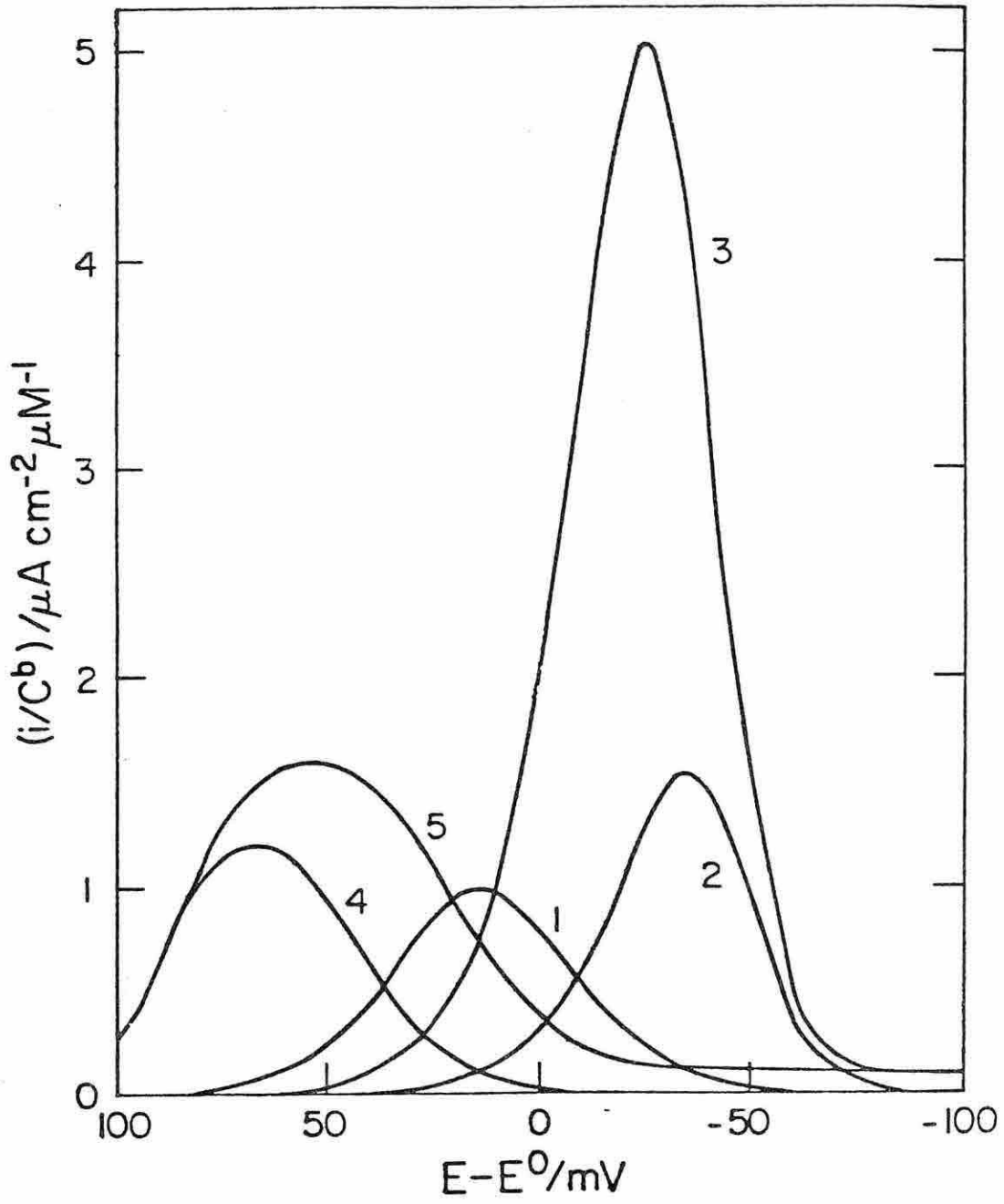

FIGURE 3.3

When non-linear adsorption isotherms are involved, doubly-peaked differential pulse polarograms can sometimes result just as reactant adsorption can lead to doubly-peaked cyclic voltammograms.[12] Figure 3.4 shows some examples of simulated polarograms for very strongly adsorbed reactants which obey Langmuir isotherms. The peak appearing near $(E-E^\circ) = 0$ represents the diffusion-controlled wave that would be present in the absence of adsorption. The peak currents for this wave were evaluated at such long drop times that they suffered no diminishment from adsorptive depletion of the reactant. These polarograms, therefore, correspond to those that would be obtained at a stationary electrode of the same area. The peak appearing at more negative potentials arises from the reaction of the adsorbed reactant. Its position is close to that corresponding to the maximum in the faradaic pseudocapacitance of a nernstian reactant obeying a Langmuir isotherm, namely

$$E_p = E^\circ - (RT/nF) \ln [(\Gamma_m + KC^b/\Gamma_m)] \qquad (3.2)$$

The magnitude of the adsorbed reactant peak decreases more rapidly with increasing sampling time than does the diffusion-controlled peak. This difference results

FIGURE 3.4

Simulated differential pulse polarograms for a strongly adsorbed reactant obeying a Langmuir isotherm. $\Gamma/(1-\theta) = K_R c_{x=o}$; $\theta = \Gamma/\Gamma_m$; Γ_m = concentration of adsorbate on a saturated surface. Ordinate as in Fig. 3.3.

Isotherm parameters:

Curve	K_R/cm	$10^{10}\ \Gamma_m$/mol cm^{-2}
1	0.5	3
2	0.1	2
3	0.1	1
4	0.3	1
5	0.6	1

Other parameters utilized in the simulation: $D_R = D_P = 10^{-5}$ cm^2 s^{-1}; n = 2; pulse amplitude = 10 mV; current sampling time = 50 ms; electrode area = 0.0627 cm^2; uncompensated resistance = 100 Ω; double layer capacitance = 20 μF cm^{-2}; bulk concentration of reactant = 50 μM.

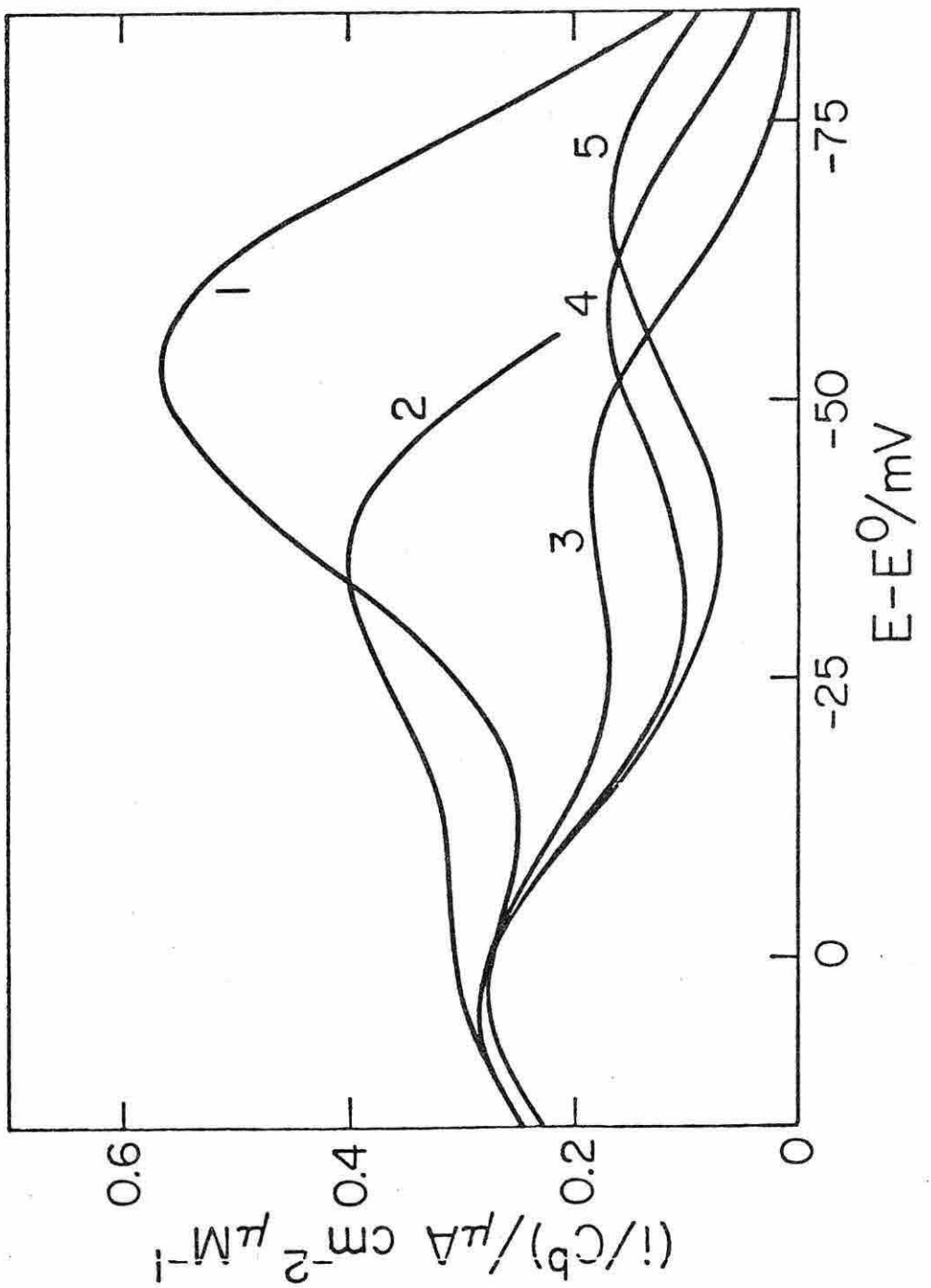

FIGURE 3.4

from the approximately exponential time dependence of the former peak compared with the square-root of time dependence of the latter peak.

In Fig. 3.5 are shown the effects of increasing bulk concentration of an adsorbate which obeys a Langmuir isotherm. Adsorptive depletion of the reactant has been included in the simulation of these polarograms which is the reason that the first wave essentially disappears at low reactant concentrations: the adsorption removes almost all of the reactant from the solution at the electrode surface under these conditions. At higher reactant concentrations (curves 3 and 4) the adsorptive depletion becomes less severe, the height of the first wave approaches the value that would result in the absence of adsorption, and the second wave diminishes relative to the first as the current arising from the diffusing reactant overtakes that corresponding to the reduction of the adsorbed reactant.

Figure 3.6 shows some simulated polarograms for adsorbed reactants which obey Frumkin isotherms. The double peaks found with Langmuirian adsorbates (curve 3) become less pronounced (curve 2) and eventually disappear (curve 1) as progressively more repulsive interaction parameters are introduced into the isotherm. By contrast, double peaking becomes more prominent in the presence of

FIGURE 3.5

Concentration dependence of simulated differential pulse polarograms for a strongly adsorbed reactant obeying a Langmuir adsorption isotherm. Adsorptive depletion of the reactant was included in the simulation. Ordinate as in Fig. 3.3. Parameters utilized in the simulation: K_R = 0.5 cm; Γ_m = 3×10^{-10} mol cm^{-2}; $D_R = D_P = 10^{-5}$ cm^2 s^{-1}; n = 2; pulse amplitude = 10 mV; current sampling time = 50 ms; uncompensated resistance = 100 Ω; mercury flow rate = 1.5 mg s^{-1}; drop time = 5 s; double layer capacitance was neglected; bulk concentration of reactant/ M: (1) 1; (2) 50; (3) 100; (4) 200.

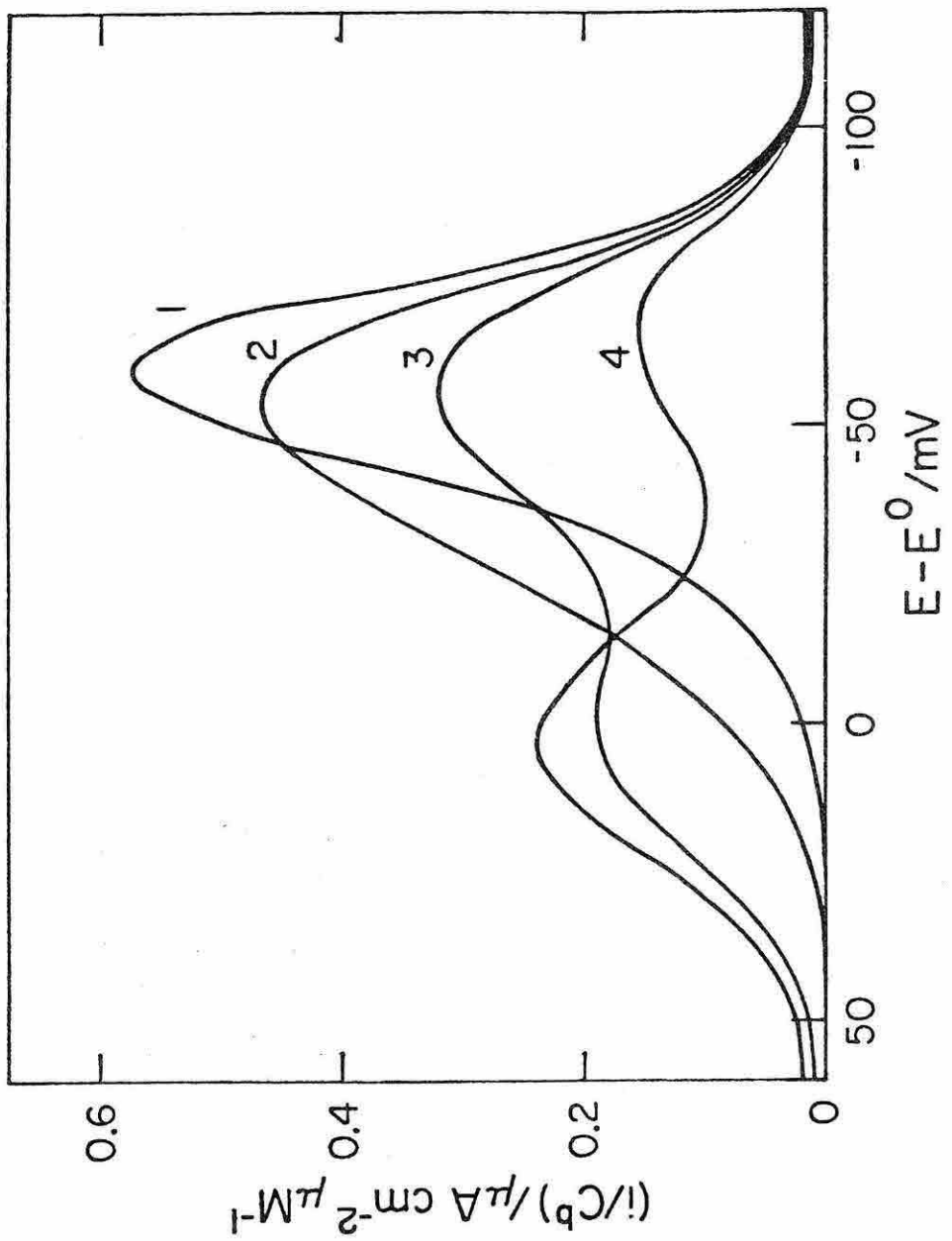

FIGURE 3.5

FIGURE 3.6

Simulated differential pulse polarograms for a strongly adsorbed reactant obeying a Frumkin isotherm, eqn (3.1). Values of the interaction parameters, A, were (1) 5; (2) 1; (3) 0 (Langmuir isotherm); (4) -1. Other parameters were the same as those for Fig. 3.5. Ordinate as in Fig. 3.3.

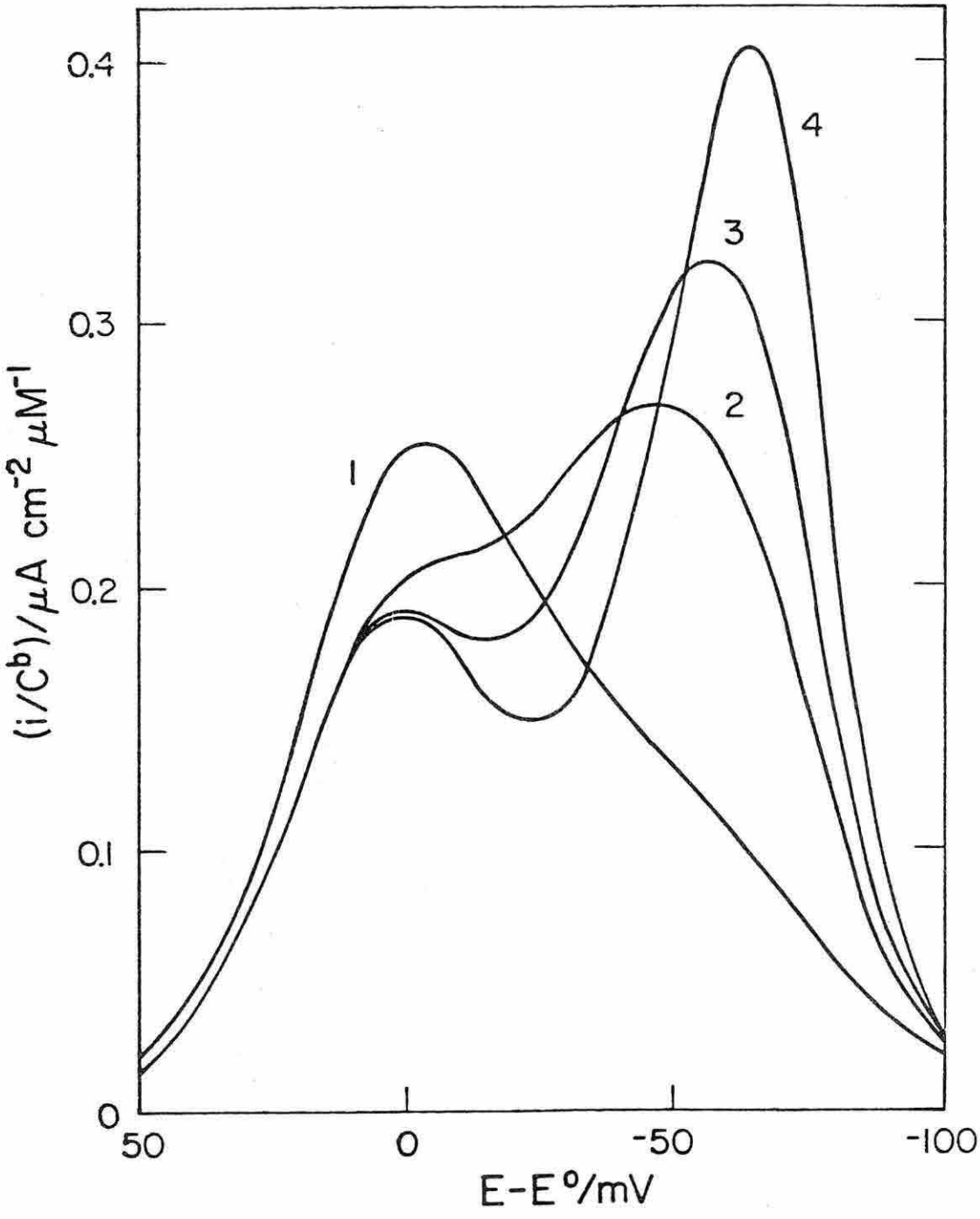

FIGURE 3.6

attractive interactions among the adsorbed species (curve 4).

The adsorption of Cd(II) from iodide electrolytes appears to correspond to a Frumkin isotherm with a repulsive interaction parameter (Fig. 3.1). Polarograms simulated using the isotherm parameters evaluated in Fig. 3.1 contain only a single peak as do the experimental polarograms (Fig. 3.8). Detailed comparisons of simulated and experimental polarograms were not attempted because the isotherm parameters evaluated chronocoulometrically corresponded to more positive potentials than those at which the pulse polarograms occur. However, comparisons between the peak potentials and widths of simulated and experimental polarograms at several bulk concentrations of Cd(II) are shown in Table 3.1. There is fair agreement between the calculated and measured peak potentials and the observed maximum in half-peak width as the bulk concentration increases is matched at least qualitatively, by the simulated results.

Effects of Uncompensated Resistance. The presence of uncompensated resistance can produce large changes in differential pulse polarographic current. Figure 3.7 shows a set of differential pulse polarograms recorded for solutions of Cd(II) in nitrate supporting electrolytes

TABLE 3.1

Peak Potentials and Half-peak Widths for Differential Pulse Polarograms of Cd(II) in 0.9 M KNO_3 - 0.1 M KI

Concn. of Cd(II)/ M	$-E_p$(experiment)[a]/mV	$-E_p$(simulation)[b]/mV	Half-peak width(experiment)/mV	Half-peak width(simulation)/mV
10	630	634[c]	40[d]	47
100	620	614[c]	60	65
1000	609	---	55	53

[a] Experimental parameters: drop time, 5 s; current sampling time, 11.3 ms; pulse magnitude, 25 mV. Frumkin isotherm parameters from Fig. 3.1.

[b] Simulation parameters: $D_R = 1 \times 10^{-5}$ cm^2 s^{-1}, $D_p = 1.5 \times 10^{-5}$ cm^2 s^{-1}; double layer capacitance and uncompensated resistance assumed negligible.

[c] Calculated by setting the simulated and experimental peak potentials equal to each other at 1000 μM. In the absence of adsorption the peak potentials are independent of concentration.[10]

[d] The half-peak width is calculated[10] to be 54 mV at all concentrations in the absence of adsorption.

FIGURE 3.7

Effect of uncompensated resistance on experimental differential pulse polarograms for a 19.6 μM solution of Cd(II) in 0.1 M KNO_3. Pulse magnitude = 25 mV; current sampling time = 5.83 ms; drop time = 2 s; drop area = 0.0141 cm^2. Residual uncompensated resistance in cell = 410 Ω. Added uncompensated resistance/kΩ: (1) -0; (2) 0.5; (3) 1.0; (4) 2.0; (5) 5.0; (6) 10; (7) 20. Each polarogram commences at -450 mV.

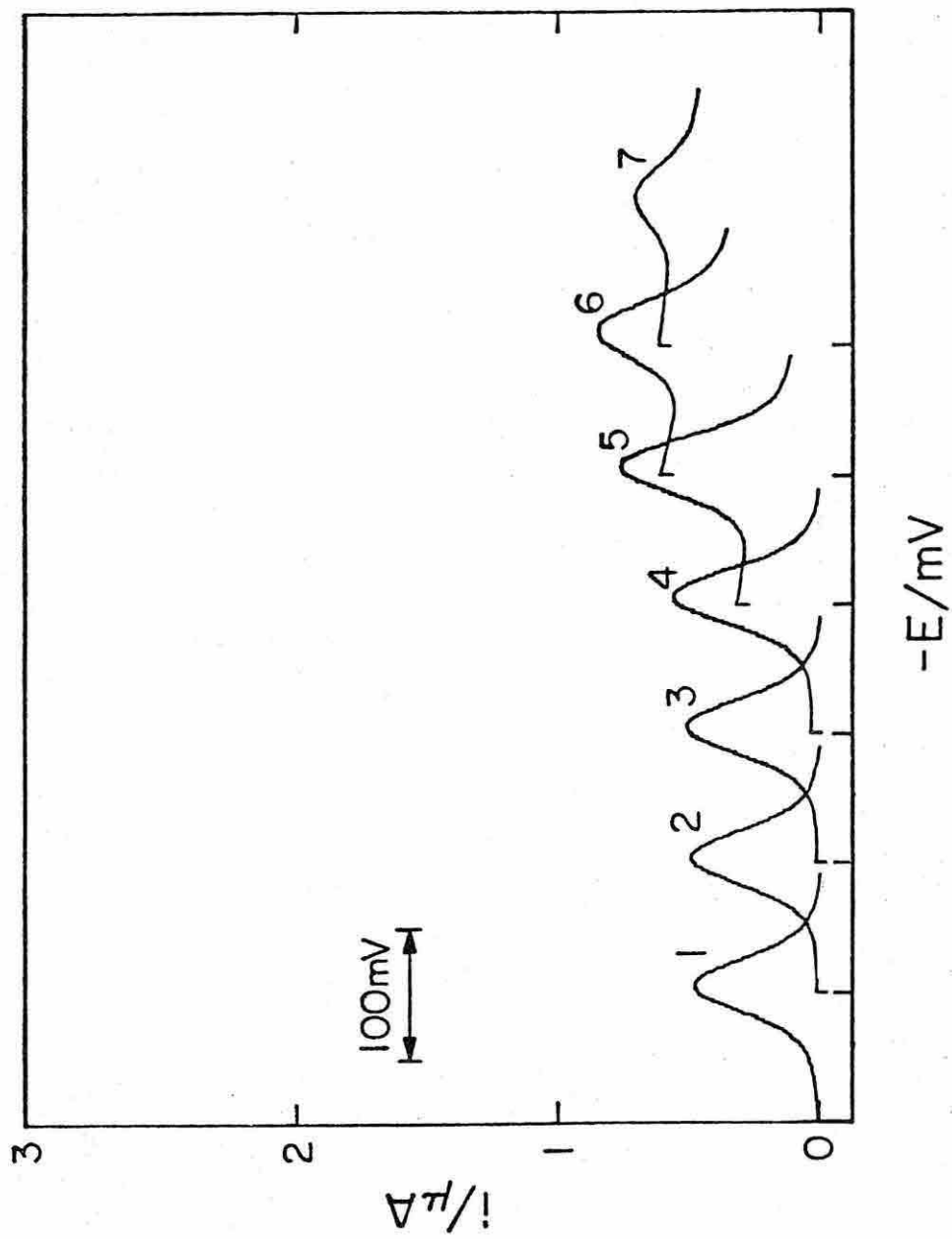

FIGURE 3.7

where no adsorption of Cd(II) is detectable and Fig. 3.8 shows a corresponding set in an iodide electrolyte where strong adsorption of Cd(II) is induced. Note that the addition of uncompensated resistance increases the background currents as well as the peak currents. Figures 3.9 and 3.10 show how the peak currents (measured with respect to the absolute zero current line, not from the extrapolated background current line) depend on the magnitude of the uncompensated resistance in the cell circuit. The maxima in the plots of peak current versus uncompensated resistance result because the circuit consisting of the uncompensated resistance in series with the double layer capacitance leads to a current-time response given by eqn (3.3).

$$i = (\Delta E/R_u)\exp\ (-t/R_u C_{dl}) \qquad (3.3)$$

where ΔE is the magnitude of the potential pulse applied across the circuit, R_u is uncompensated resistance, t is the time at which the current is measured, and C_{dl} is the double layer capacitance. This equation predicts a maximum current when $R_u C_{dl} = t$. In Fig. 3.9 the current was sampled 5.83 ms after the pulse and the double layer capacitance of the dropping mercury electrode at the peak potential determined in the absence of a faradaic

FIGURE 3.8

Effect of uncompensated resistance on experimental differential pulse polarograms for a 19.6 μM Cd(II) solution in 0.1 M KI. Curve numbers and experimental parameters are the same as in Fig. 3.7 except that the residual uncompensated resistance was 370 Ω. Each polarogram commences at -550 mV.

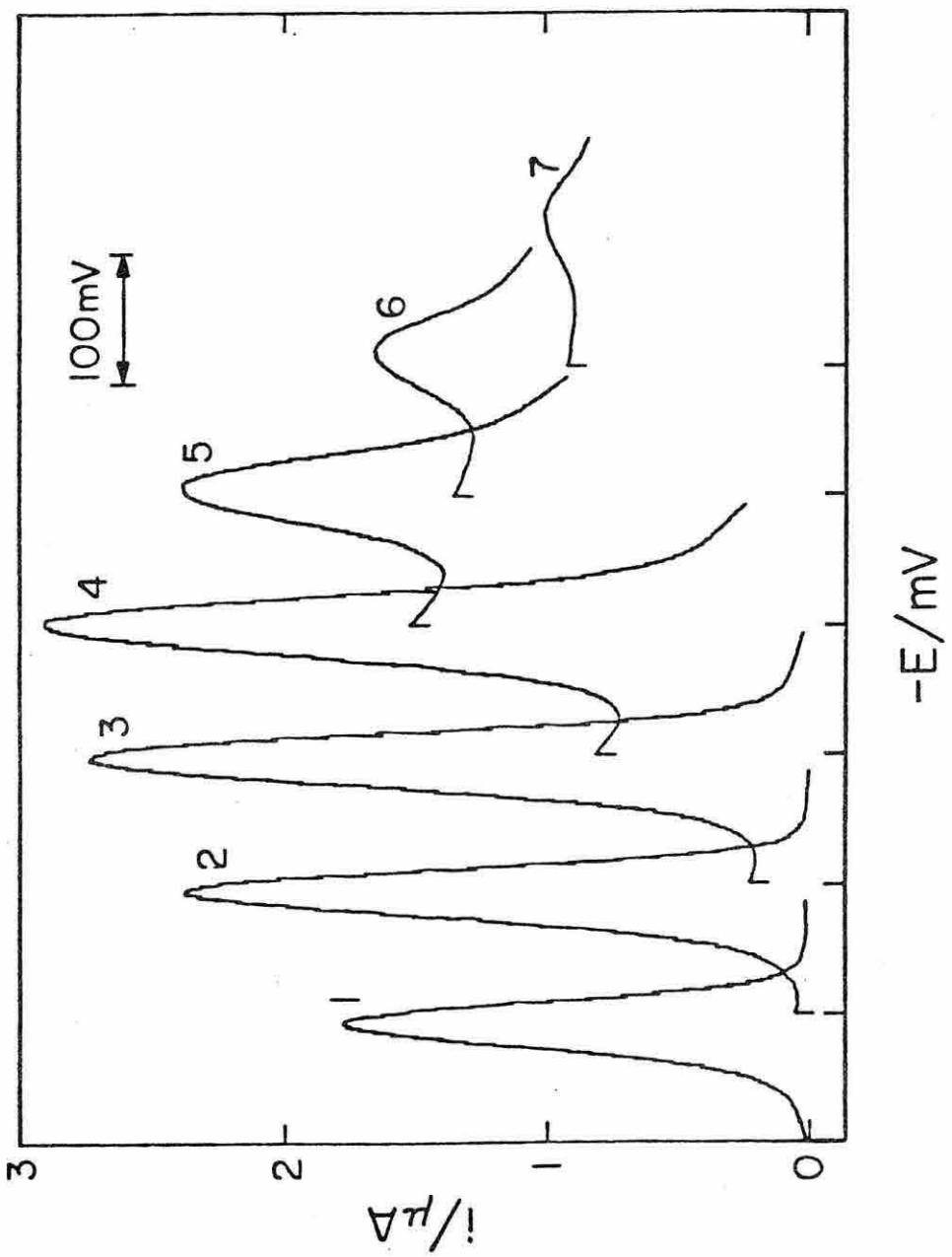

FIGURE 3.8

FIGURE 3.9

Differential pulse polarographic peak current vs. uncompensated resistance for Cd(II) in 0.1 M KNO_3. Peak currents were measured with respect to the zero current line. Experimental parameters as in Fig. 3.7. Concentration of Cd(II)/μM: (1) 0; (2) 5.0; (3) 9.9; (4) 19.6.

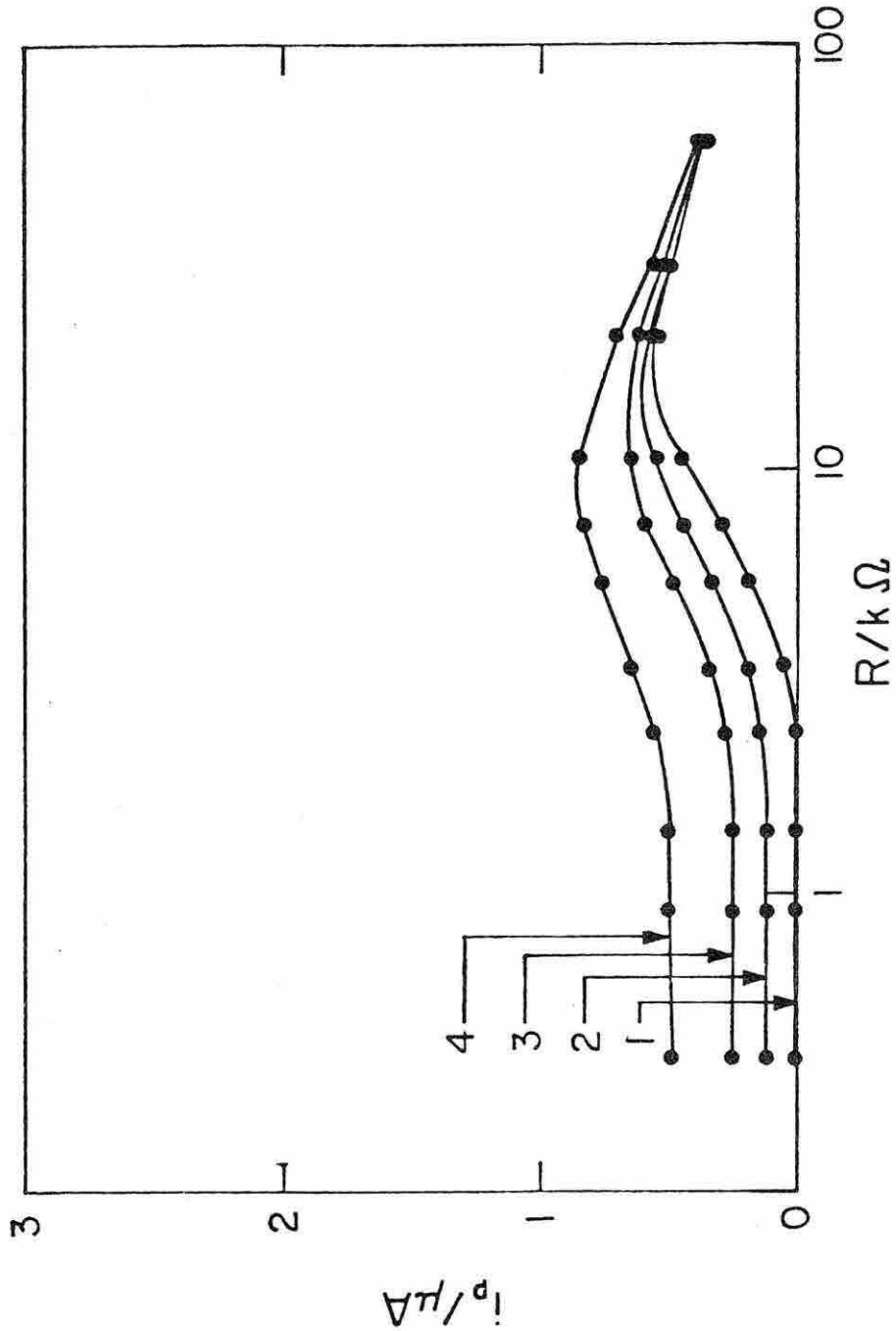

FIGURE 3.9

FIGURE 3.10

Differential pulse polarographic peak currents vs. uncompensated resistance for Cd(II) in 0.1 M KI. Peak currents were measured with respect to the zero current line. Experimental parameters as in Fig. 3.7. Concentration of Cd(II)/μM: (1) 0; (2) 5.0; (3) 9.9; (4) 19.6.

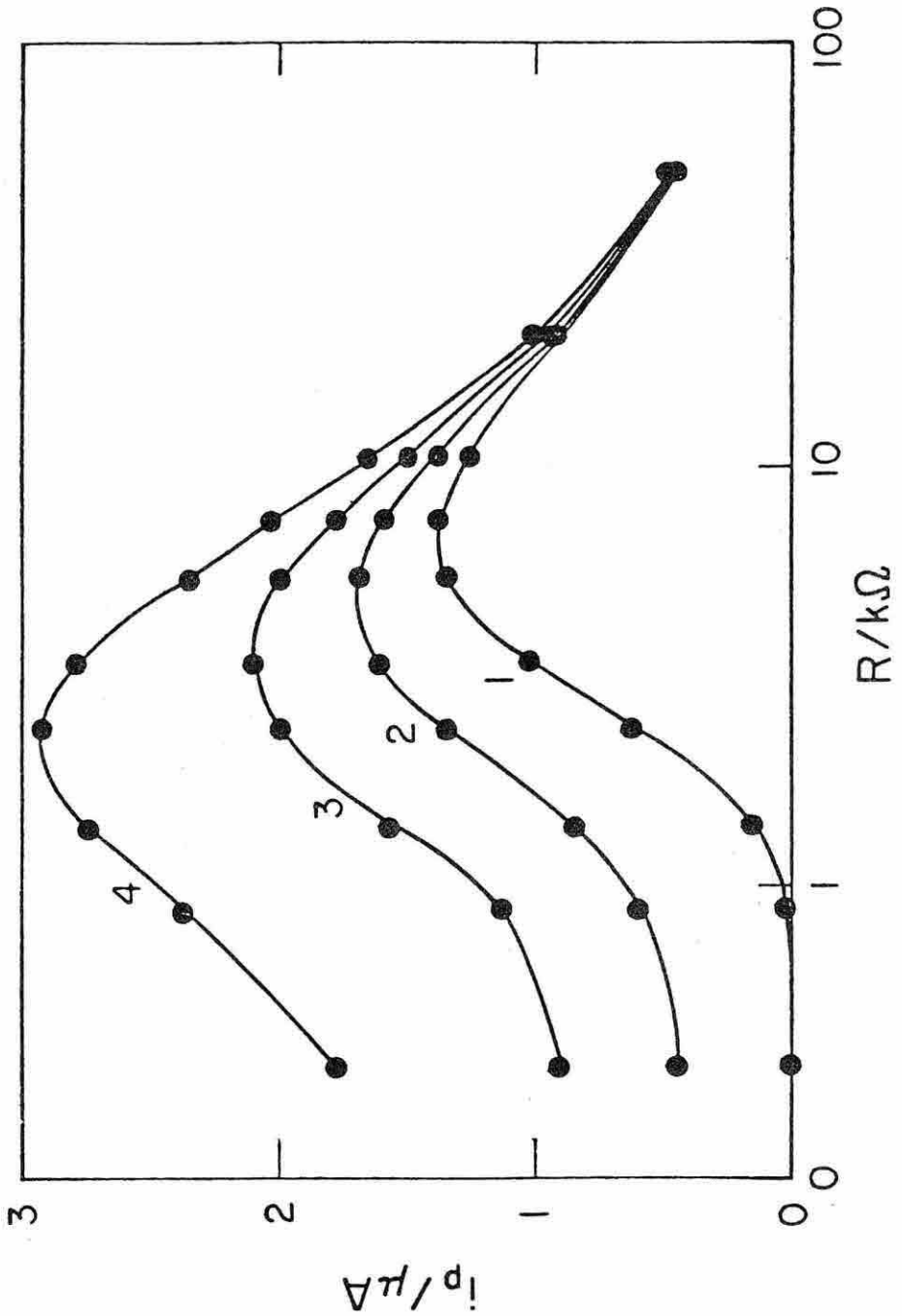

FIGURE 3.10

reaction by a.c. impedance measurements was 0.33 μF. The calculated value of R_u which corresponds to the maximum peak current is 17.7 kΩ which is in reasonable agreement with the value shown in Fig. 3.9 in the absence of Cd(II). The maxima remain as Cd(II) is added but they shift to smaller values of R_u as increasing faradaic contributions to the total current make eqn (3.3) (which neglects faradaic current arising from diffusing reactants) a poorer and poorer approximation.

The presence of reactant adsorption introduces a large pseudocapacitance, C_a, in parallel with the double layer capacitance and the maximum peak current is to be expected when $t = R_u(C_{dl} + C_a)$ at reactant concentrations small enough for contributions to the current from diffusing reactant to be neglected. Figure 3.10 shows data for Cd(II) in an iodide supporting electrolyte where strong adsorption occurs. The current maxima are much more pronounced and appear at smaller values of R_u as expected. The double layer capacitance in the iodide electrolyte was 0.87 μF at the peak potential which leads to a predicted value of 6.7 kΩ for R_u at the peak current maximum. This value matches well the maximum in curve 1 of Fig. 3.10.

We have explored the possibility of utilizing the effects of added uncompensated resistance on differential

pulse polarographic current responses to evaluate C_a and, thereby, the extent of adsorption of weakly adsorbing reactants which are beyond the capabilities of chronocoulometry. However, we do not believe that this approach offers significant promise because the double layer capacitance dominates the current response when adsorption is weak and accurate evaluation of the small, additional capacitance arising from the adsorbed reactant is difficult.

The overall shape of the curves in Figs. 3.9 and 3.10 are understandable on the basis of eqn (3.3) at sufficiently large values of R_u the current is dominated by the pre-exponential term which does not depend on the reactant concentration so that at sufficiently large values of R_u all of the curves approach a current equal to $\Delta E/R_u$ whether or not there is reactant adsorption. At lower values of R_u the curves become nearly parallel and the currents approach the values that would be obtained in the absence of uncompensated resistance.

A point of some importance to analytical applications of differential pulse polarography under conditions where significant uncompensated resistance may be unavoidable is the lack of a linear relation between peak currents and reactant concentrations when the peak currents are measured, as is usual in analytical applications, with

respect to the extrapolation of the background current. Figure 3.11 shows the degree of non-linearity introduced by a modest amount of uncompensated resistance with and without reactant adsorption. Electroanalysts would have to be especially wary in attempting to execute analyses in circumstances such as these.

D. C. Polarography. Because in differential pulse the initial potential is varied within the wave, information is available from the simulation about the d.c. polarographic response. Since this work was completed, two papers have appeared on this subject, both utilizing the diffusion layer approach.[14,15] Comparison of these results with the results of digital simulation reveals good qualitative agreement about the effects of adsorbed reactant and product under conditions of linear and Langmuir isotherms. Virtually all the questions treated by this simulation were treated in the two papers, the most important of these being the relationship between isotherm parameters and experimental conditions with wave shapes[14] and current-time response at the growing drop[15] (current may sometimes go through a maximum then decrease rather than the ordinary behavior, $i \propto t^{1/6}$). The one thing which the diffusion layer treatment was not able to demonstrate is concentration-distance profile such as

FIGURE 3.11

Differential pulse polarographic peak current vs. concentration of Cd(II) in the presence of uncompensated resistance. Supporting electrolyte: (A) 0.1 M KNO_3; (B) 0.1 M KI. Total uncompensated resistance present/kΩ: (1) 0.41; (2) 1.41; (3) 2.41; (4) 5.41; (5) 0.37; (6) 1.37; (7) 2.37; (8) 5.37. Other experimental parameters as in Fig. 3.7.

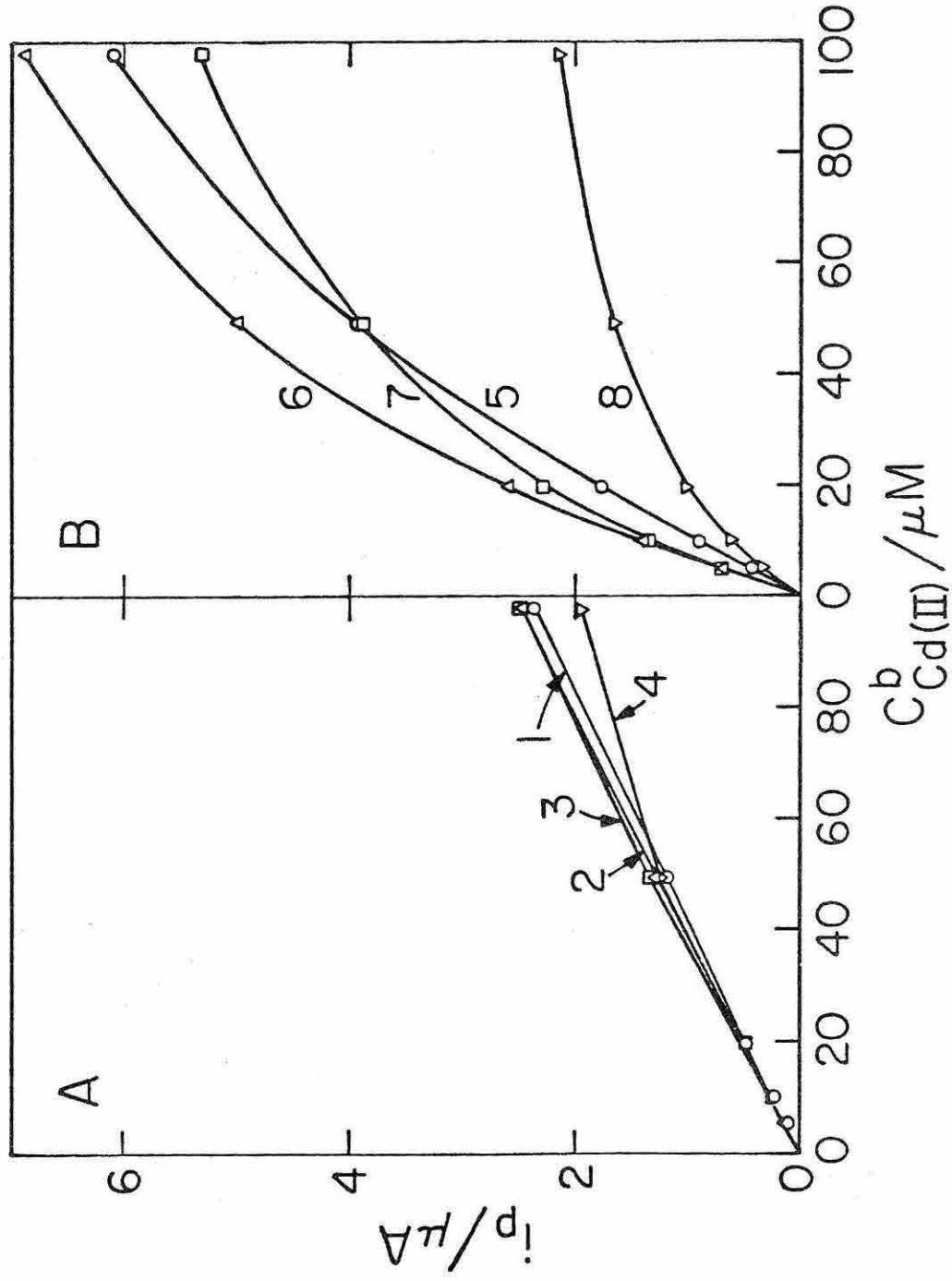

FIGURE 3.11

shown in Fig. 3.12. This figure is illustrative of the "depletion effect" noted earlier in connection with Fig. 3.2. The concentration profiles calculated by digital simulation show that with short drop time and strong adsorption, the surface concentrations of both product and reactant are strongly depleted. The ratios of product to reactant are equal in both cases, since even in the presence of adsorption, surface concentrations must obey the nernst equation. Extrapolation of the slope $(\frac{dc}{dx})_{x=0}$ until it intersects the bulk value can be used as a measure of the "diffusion layer" thickness. Figure 3.12 shows that the diffusion layer thicknesses for reactant with and without adsorption do not differ markedly. Thus the diffusion layer approximation used in refs. 14 and 15 is probably adequate under these circumstances. There might be occasions when the diffusion layer approximation would not hold; for example, when isotherms with large positive or negative interaction parameters are involved.

Figure 3.13 treats a situation not considered in the paper of Sluyters-Rehbach, et.al.,[14] the case of interaction between adsorbed molecules on the surface. The figure shows the effect of attractive and repulsive interaction parameters in a Frumkin isotherm. As was

FIGURE 3.12

Simulated concentration profiles with and without adsorption. $D_{ox} = 7.8 \times 10^{-6}$ cm^2/sec, $D_R = 1.52 \times 10^{-5}$ cm^2/sec, n = 2, $C_{ox}^b = 1$ μM, m = 1.129 mg/sec, $t_d = 0.5$ sec., E = E° + 10 mV. (a) C_{ox} (x), no adsorption; (b) C_R (x), no adsorption; (c) C_{ox} (x), K_{ox} = 0.036 cm, $K_R = 0$; (d) C_R (x), $K_{ox} = 0.036$ cm, $K_R = 0$. Dotted lines: extrapolations of $\left(\frac{dC_{ox}}{dx}\right)_{x=o}$.

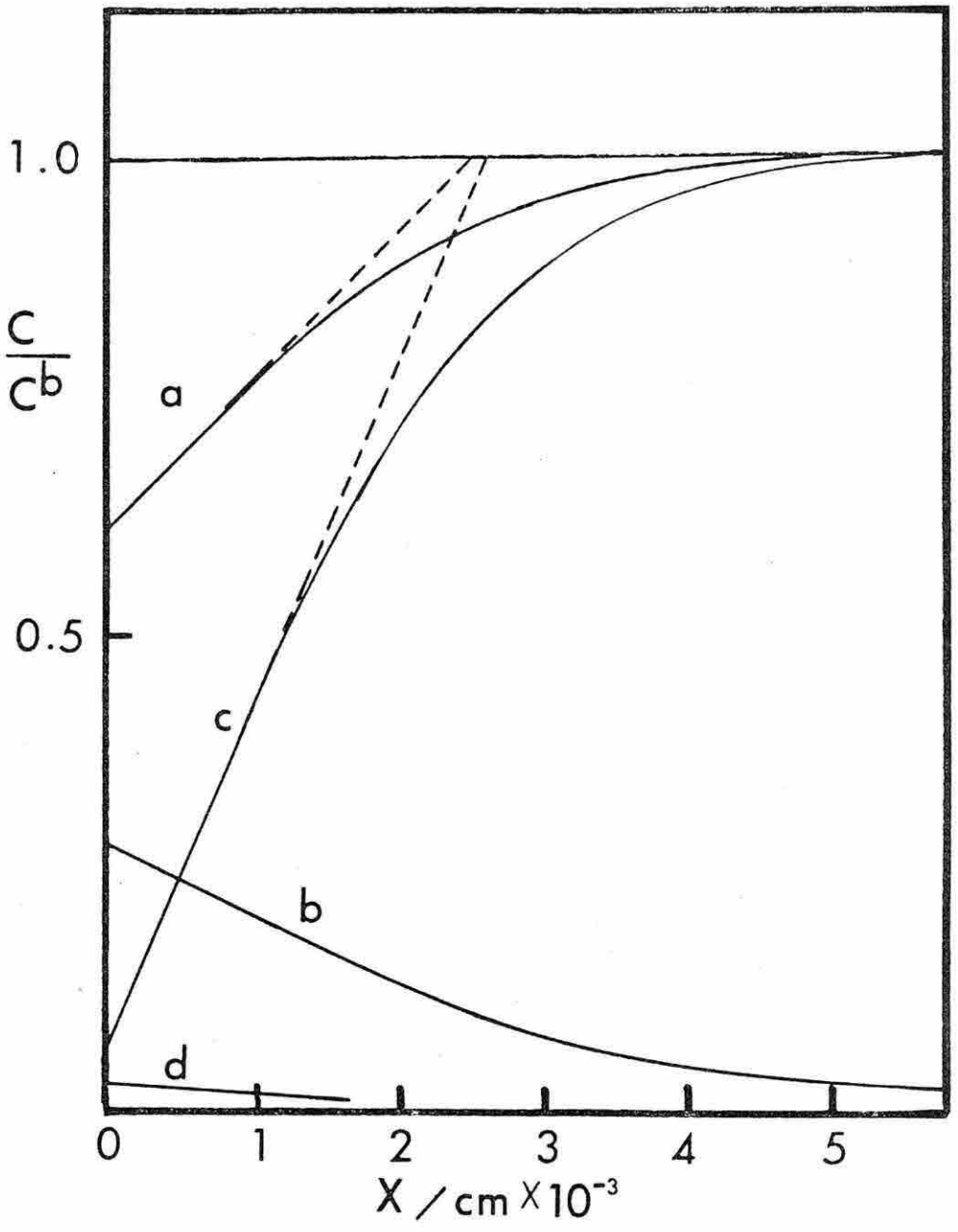

FIGURE 3.12

FIGURE 3.13

Simulated d.c. polarograms, Frumkin isotherm. $D_{ox} = D_R = 10^{-5}$ cm^2/sec, n = 2, C_{ox} = 100 μM, m = 1.5 mg/sec., t_d = 5 sec., K_{ox} = 0.5 cm, $\Gamma^m = 3 \times 10^{-10}$ moles/cm^2. A refers to the Frumkin isotherm interaction parameter.

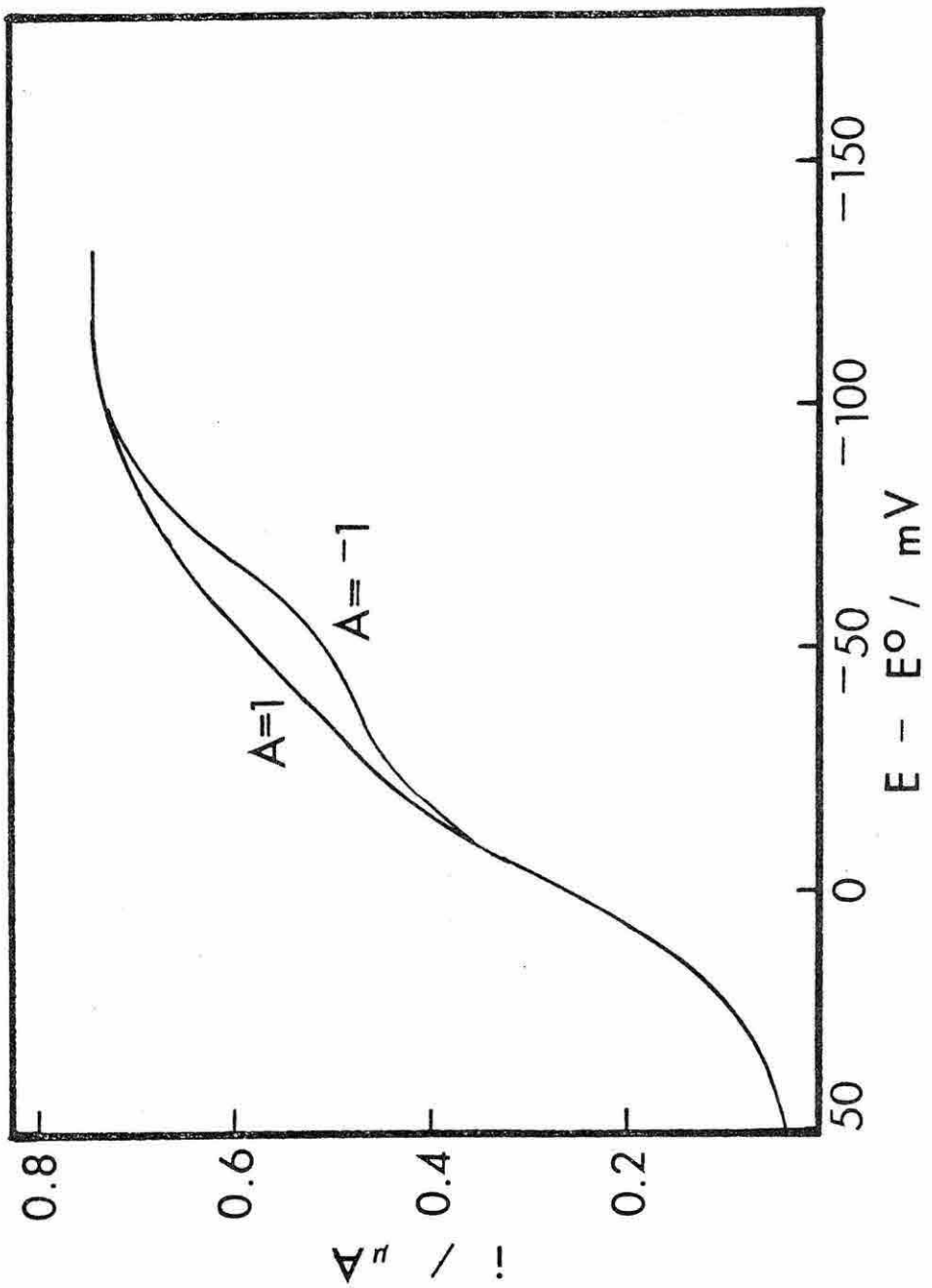

FIGURE 3.13

noted for differential pulse and will be seen in the next chapter for normal pulse, attractive interactions tend to "sharpen" the current-voltage responses, whereas repulsive interactions tend to smear them out.

The computer programs used to generate the d.c. polarograms are shown in Appendix C.

REFERENCES

(1) G. C. Barker and J. A. Bolzan, Z. Anal. Chem., 216, 215 (1966).

(2) S. W. Feldberg in A. J. Bard (Ed.), Electroanalytical Chemistry. A Series of Advances, Vol. III, Marcel Dekker, New York, 1969.

(3) R. H. Abel, J. H. Christie, L. L. Jackson, J. G. Osteryoung and R. A. Osteryoung, Chem. Instrum., in press.

(4) F. C. Anson, Anal. Chem., 38, 54 (1966).

(5) C. M. Elliott and R. W. Murray, Anal. Chem., 47, 908 (1975).

(6) F. D. Anson and D. J. Barclay, Anal. Chem., 40, 1791 (1968).

(7) J. W. Dillard and K. W. Hanck, Anal. Chem., 48, 218 (1976).

(8) Ref. 2, p. 206.

(9) S. S. Kuo, Numerical Methods and Computers, Addison-Wesley, Reading, Mass., 1965, p. 90.

(10) E. P. Parry and R. A. Osteryoung, Anal. Chem., 37, 1634 (1965).

(11) A. N. Frumkin, Z. Phys., 35, 792 (1926).

(12) R. N. Wopschall and I. Shain, Anal. Chem., 39, 1514 (1967).

(13) R. Parsons, Trans. Faraday Soc., 55, 999 (1959).

(14) M. Sluyters-Rehbach, C. A. Wijnhorst, and J. H. Sluyters, J. Electroanal. Chem., 74, 3 (1976).

(15) R. Guidelli and F. Pergola, unpublished manuscript.

CHAPTER IV

Effects of Reactant and Product Adsorption in Normal Pulse Polarography

INTRODUCTION

Perturbations in the shapes of normal pulse polarograms due to reactant adsorption were first reported by Barker and Bolzan[1] who correctly interpreted the origin of the peaked "maxima". An additional result of reactant adsorption is a depression of the limiting current below the value that would be obtained in the absence of adsorption. Barker and Bolzan[1] also mentioned this effect but discussed it only cursorily. In fact, this feature turns out to be a general consequence of reactant adsorption. It results whenever the adsorption is strong enough to lead to a "Barker-Bolzan peak" in the normal pulse polarograms and is of obvious importance in analytical applications of the technique.

The depletion of adsorbing reactants near the electrode surface which is the origin of the depression in the limiting current and the pre- and post-waves which result from non-linear adsorption isotherms is examined in this chapter, both experimentally and by means of digital simulation. The normal pulse polarograms were

obtained with the modified pulse polarograph (Princeton Applied Research Model 174) by procedures essentially the same as those described in the previous chapter on differential pulse polarography.

RESULTS AND DISCUSSION

Digital Simulation. The digital simulation program employed was a straightforward extension of that described previously for differential pulse polarography (Appendix D). The electrode reaction was assumed to be nernstian and reversible at all coverages with both reactant and product soluble in either the solution or the mercury electrode. Initial and boundary conditions were identical to those given previously (Chapters II and III), except for the constant initial potential and increasing pulse amplitude characteristic of normal pulse polarography.[1]

Experimental Observations. Figure 4.1 compares the normal pulse polarograms for Cd(II) in nitrate and iodide supporting electrolytes. The iodide-induced adsorption of Cd(II) produces both a current peak of the type described by Barker and Bolzan[1] and a depression of the limiting current on the plateau of the wave. The adsorption-induced peaking of the current originates from the same phenomenon that produces enhancement of peak

FIGURE 4.1

Normal pulse polarograms for 20 μM Cd(II). Supporting electrolyte: (1) 1 M KNO_3; (2, 3) 0.9 M KNO_3 - 0.1 M KI. Current sampling time: (1, 2) 48.5 ms (current averaged between 39.7 and 57.3 ms); (3) 22.7 ms (current averaged between 19.9 and 25.5 ms). Drop time: 2 s. Mercury flow rate: 1.04 mg s^{-1}. Initial potential: -450 mV vs. SCE.

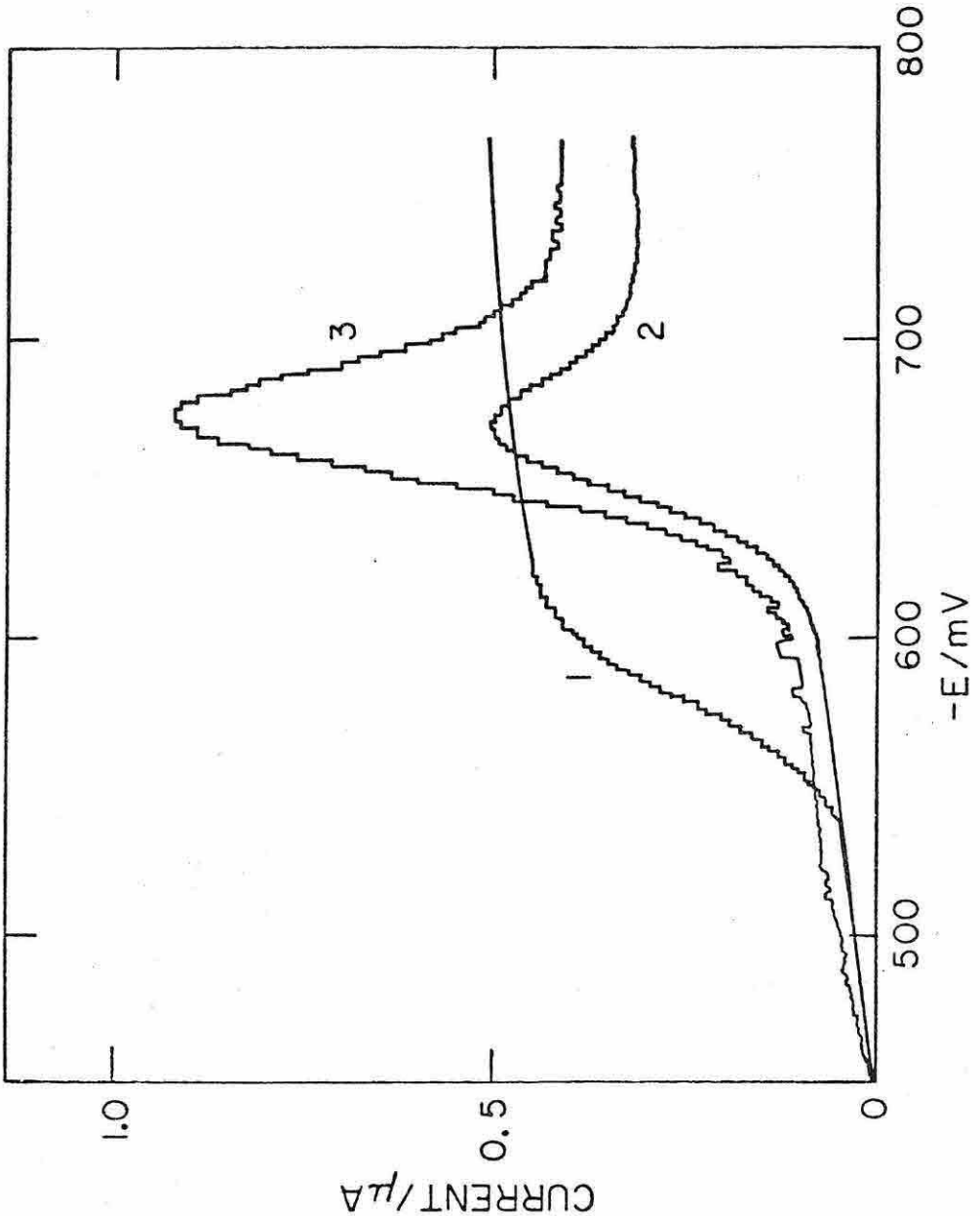

FIGURE 4.1

currents in differential pulse polarography: For nernstian reactions the rate of reduction of adsorbed reactant at potentials in the vicinity of the standard potential is limited by the rate at which the reaction product can diffuse away from the electrode surface. As a result, the additional current corresponding to reduction of the adsorbed reactant continues to be a significant component of the total current when it is sampled by the pulse polarograph. For this reason the prominence of the current peak is enhanced by decreases in the current-sampling time (Fig. 4.1, curve 3).

Depletion of the Cd(II) concentration in the solution at the surface of the dropping electrode because of its adsorption is responsible for the depression in the limiting current of the pulse polarogram recorded in the iodide electrolyte (Fig. 4.1). At potentials on the limiting current plateau all of the adsorbed reactant is reduced instantaneously upon application of the potential step so that when the current is sampled it contains contributions only from the diffusing reactant whose concentration has been depleted by the prior adsorption and reduction of a portion of the reactant initially present at the electrode surface.

If the normal pulse polarograms for Cd(II) in iodide electrolytes are recorded in the anodic direction from

initial potentials on the reduction current plateau, no current maximum nor limiting current depression result (Fig. 4.2). In this case the electrode reaction involves the conversion of an unadsorbed reactant (Cd(Hg)) to an adsorbed product but the pulse polarogram contains no clue of the presence of product adsorption. The limiting current is somewhat larger in the electrolyte containing iodide because the diffusion coefficients of Cd(II)-iodide complexes are larger. (Even though a net anodic limiting current is measured its magnitude should be determined by the diffusion coefficient of Cd(II) in the solution phase, not in the mercury electrode according to eqn. 4 in reference 2.)

The iodide-induced adsorption of Cd(II) obeys a (non-linear) Frumkin isotherm. Before comparing the observed experimental behavior with that calculated by digital simulation for this more complex case, the calculated behavior of adsorbates which obey linear isotherms will be exposed.

Simulated Polarograms with a Linear Adsorption Isotherm. Figure 4.3 contains a set of normal pulse polarograms simulated for the case that the adsorption of reactant and product obey a linear (Henry's law) isotherm. The initial potential lies outside the range of faradaic

FIGURE 4.2

Reverse scan normal pulse polarograms for 20 μM Cd(II). Initial potential: -800 mV vs. SCE. Supporting electrolyte: (1) 1 M KNO_3; (2) 0.9 M KNO_3 - 0.1 M KI. Current sampling time: 48.5 ms. Other conditions as in Fig. 4.1.

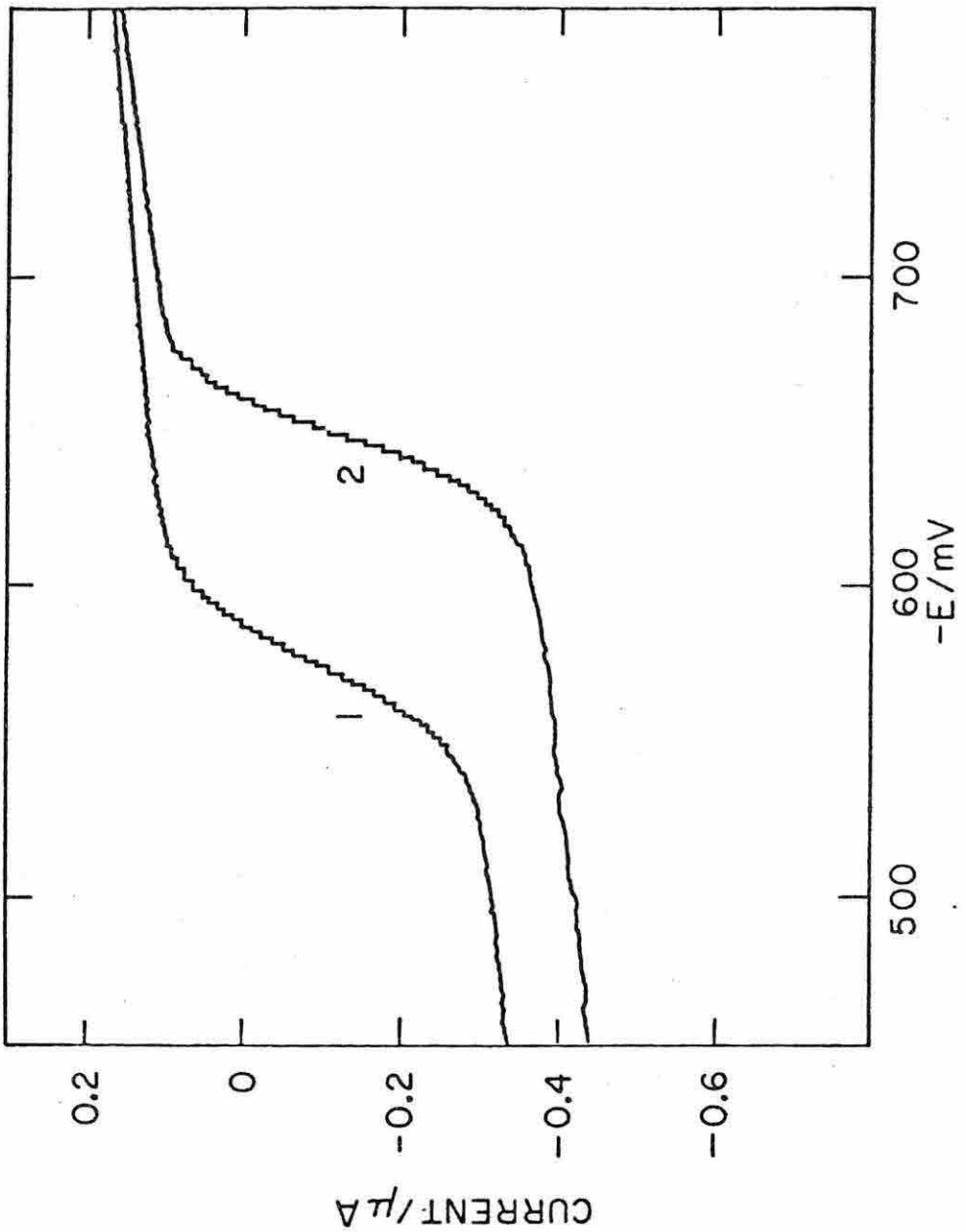

FIGURE 4.2

FIGURE 4.3

Simulated polarograms for adsorbed reactants and products obeying linear adsorption isotherms. Potential scanned in the forward direction. Adsorption coefficients (cm) for reactant and product, respectively: (1) 0,0 (i.e., no adsorption); (2) 0.05, 0; (3) 0, 0.05; (4) 0.05, 0.05; (5) 0.05, 0.001. Simulation parameters: Reactant concentration: 100 μM; initial potential: +150 mV vs. E°, the standard potential of the reactant/product couple; n = 2 electrons; diffusion coefficient: 10^{-5} cm^{-2} s^{-1} (for both reactant and product); drop time: 5 s; current sampling time: 50 ms; DME mercury flow rate: 1 mg s^{-1}.

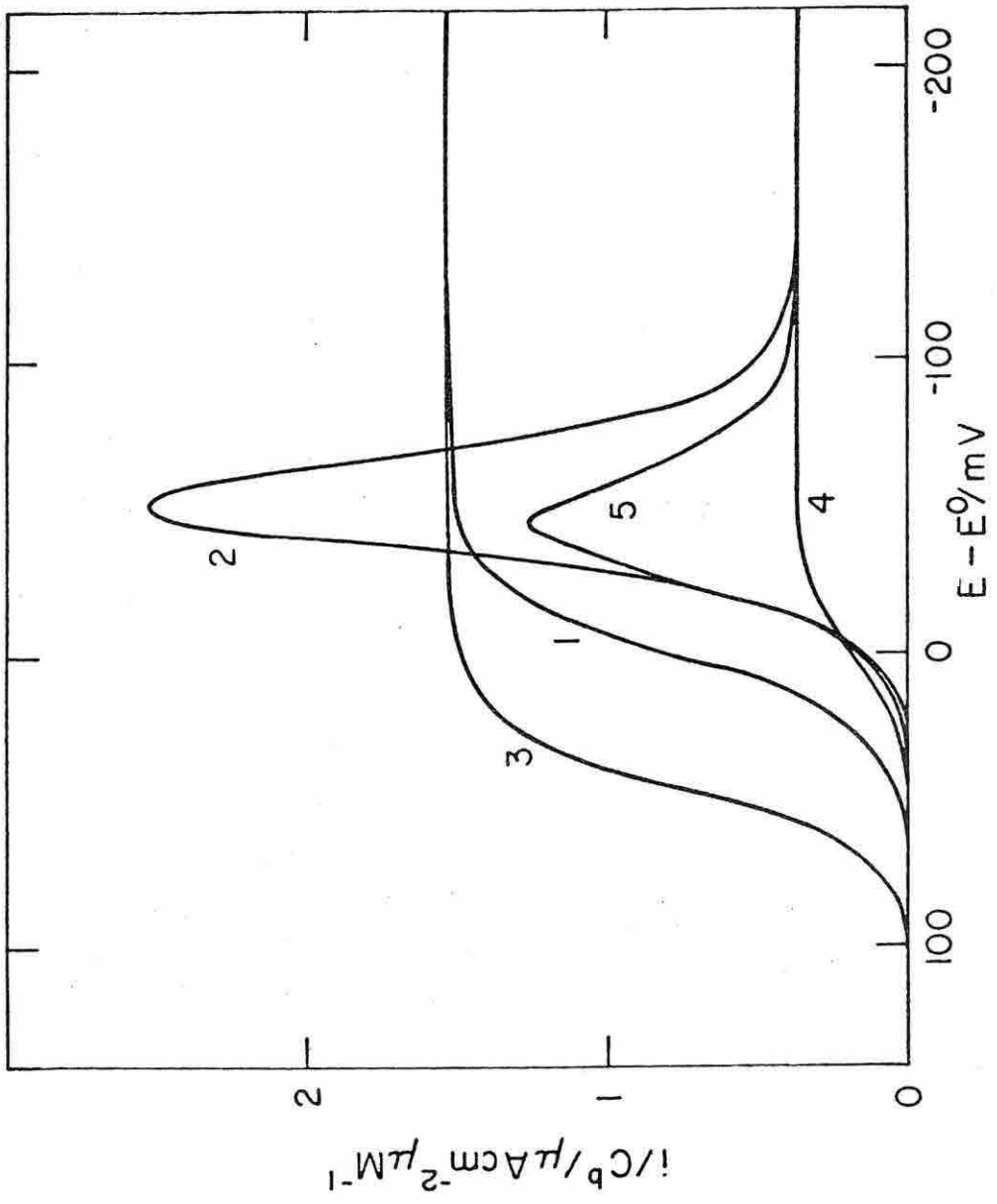

FIGURE 4.3

activity and the potential is scanned into the region where the faradaic reactions proceeds ("forward scan", e.g., a cathodic scan with a solution of a reducible reactant). Figure 4.4 contains a similar set of simulated polarograms for which a faradaic reaction is proceeding at the initial potential which is chosen to lie on the limiting current plateau. The potential is scanned in the direction of decreasing faradaic activity ("reverse scan", e.g., an anodic scan with a solution of a reducible reactant).

Curve 1 in both Figures corresponds to no adsorption of either reactant or product. Curve 2 in Fig. 4.3 corresponds to a strongly adsorbed reactant being converted to a non-adsorbed product. Note the large current maximum and the severely depressed limiting current. Curve 2 in Fig. 4.4 is the result of a reverse scan with the same system. The shape of this polarogram is identical to that of curve 1 because all of the dissolved reactant which diffuses to the electrode before the application of each potential step is immediately converted to unadsorbed product just as is true when the initial reactant is not adsorbed. Note, however, that the position of the wave on the potential axis is shifted because of the adsorption. The magnitude of this shift is determined by the magnitude

FIGURE 4.4

Simulated polarograms for adsorbed reactants and products obeying linear adsorption isotherms. Potential scanned in the reverse direction. Adsorption coefficients and simulation parameters as in Fig. 4.3 except the initial potential was -150 mV vs. E°. Residual (cathodic) current flowing at the initial potential was substrated from each polarogram.

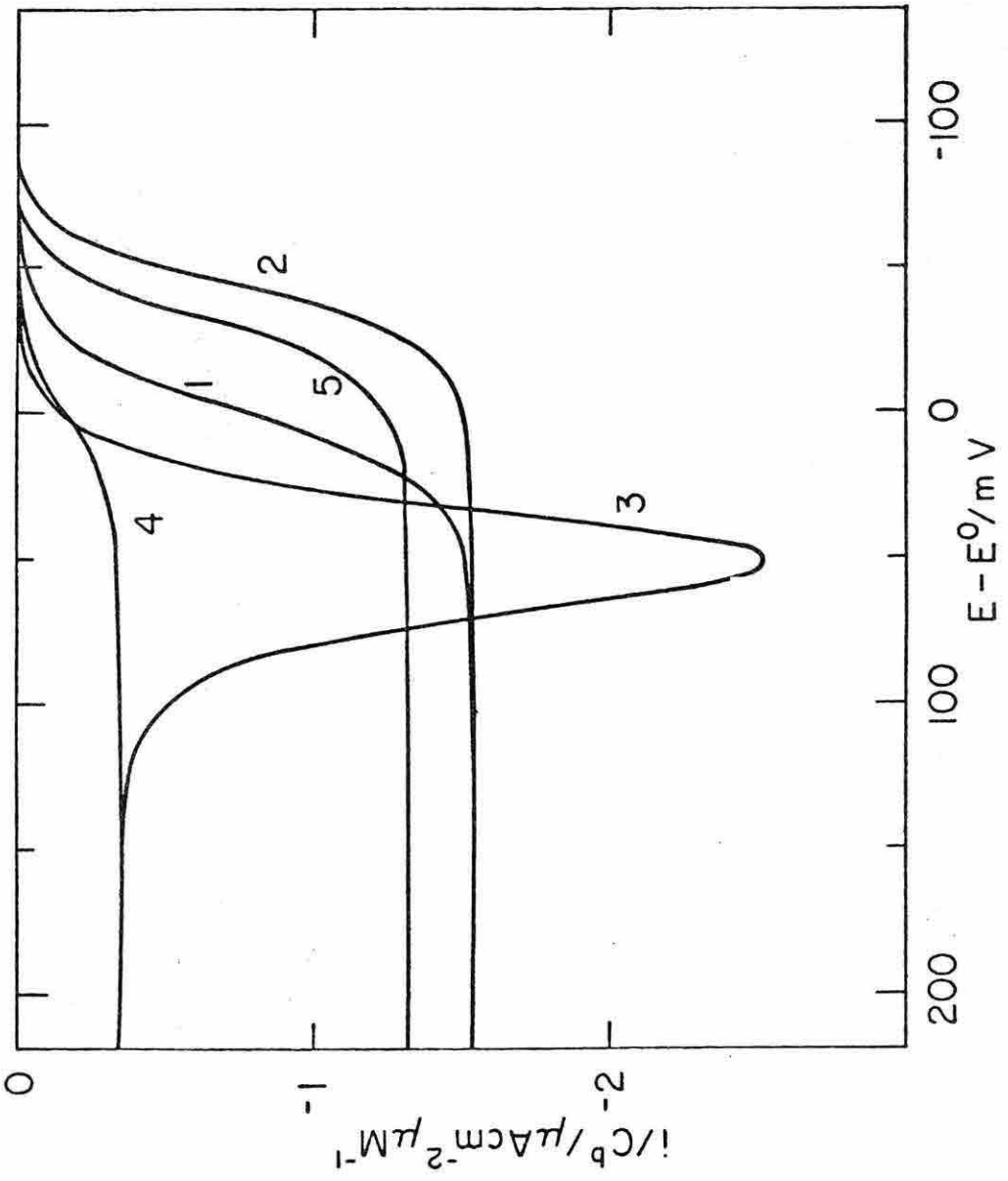

FIGURE 4.4

of the linear adsorption coefficient but it is not influenced by the bulk concentration of the reactant.

The polarograms labeled 3 in Figs. 4.3 and 4.4 are just the converse of those labeled 2 and their properties can be understood on the basis of the discussion in the preceding paragraph.

Note that normal pulse polarograms corresponding to an electrode process which converts an unadsorbed reactant into an adsorbed product are distinguished from the polarograms corresponding to no adsorption of the reactant or the product only by a difference in half-wave potential for the two cases. In the absence of an independent determination of the standard potential of the system involved there is no way to deduce the presence of product adsorption from the normal pulse polarogram. This contrasts with the behavior obtained with differential pulse polarography where enhanced peak currents result from the adsorption of the product as well as the reactant. However, for reversible electrode reactions, the presence of adsorption can easily be verified in normal pulse polarography by recording the polarogram in the opposite scan direction, thus interchanging the effective reactant and product.

If both the reactant and product are adsorbed with equal adsorption coefficients (curve 4 in Figs. 4.3 and 4.4)

there is no current maximum nor shift in half-wave potential but the limiting current is depressed identically in both the forward and the reverse scan directions.

Finally, the polarograms labeled 5 in Figs. 4.3 and 4.4 correspond to adsorption of both product and reactant but with much stronger adsorption of the latter. During the forward scan (Fig. 4.3) a current maximum appears but its magnitude is considerably smaller than is true in the absence of product adsorption (compare curves 2 and 5 in Fig. 4.3) despite the fact that the same reactant adsorption coefficient is involved. Reactant depletion resulting from the adsorption produces a depressed limiting current with a magnitude that is independent of the strength of product adsorption (compare curves 2, 4, and 5).

The polarogram obtained during the reverse scan (Fig. 4.4, curve 5) shows no current maximum when the reactant adsorption coefficient exceeds that of the product but the limiting current is nevertheless depressed by adsorptive depletion.

Figure 4.5 shows how the shape of the polarogram changes as the adsorption coefficient of the reactant is increased in the absence of product adsorption. These polarograms resemble those given by Barker and Bolzan (Fig. 6 of reference 1) except that adsorptive depletion

FIGURE 4.5

Simulated polarograms for adsorption of reactant but not product. Potential scanned in the forward direction. Adsorption coefficient (cm): (1) 0; (2) 0.001; (3) 0.002; (4) 0.005; (5) 0.01. Other simulation parameters as in Fig. 4.3.

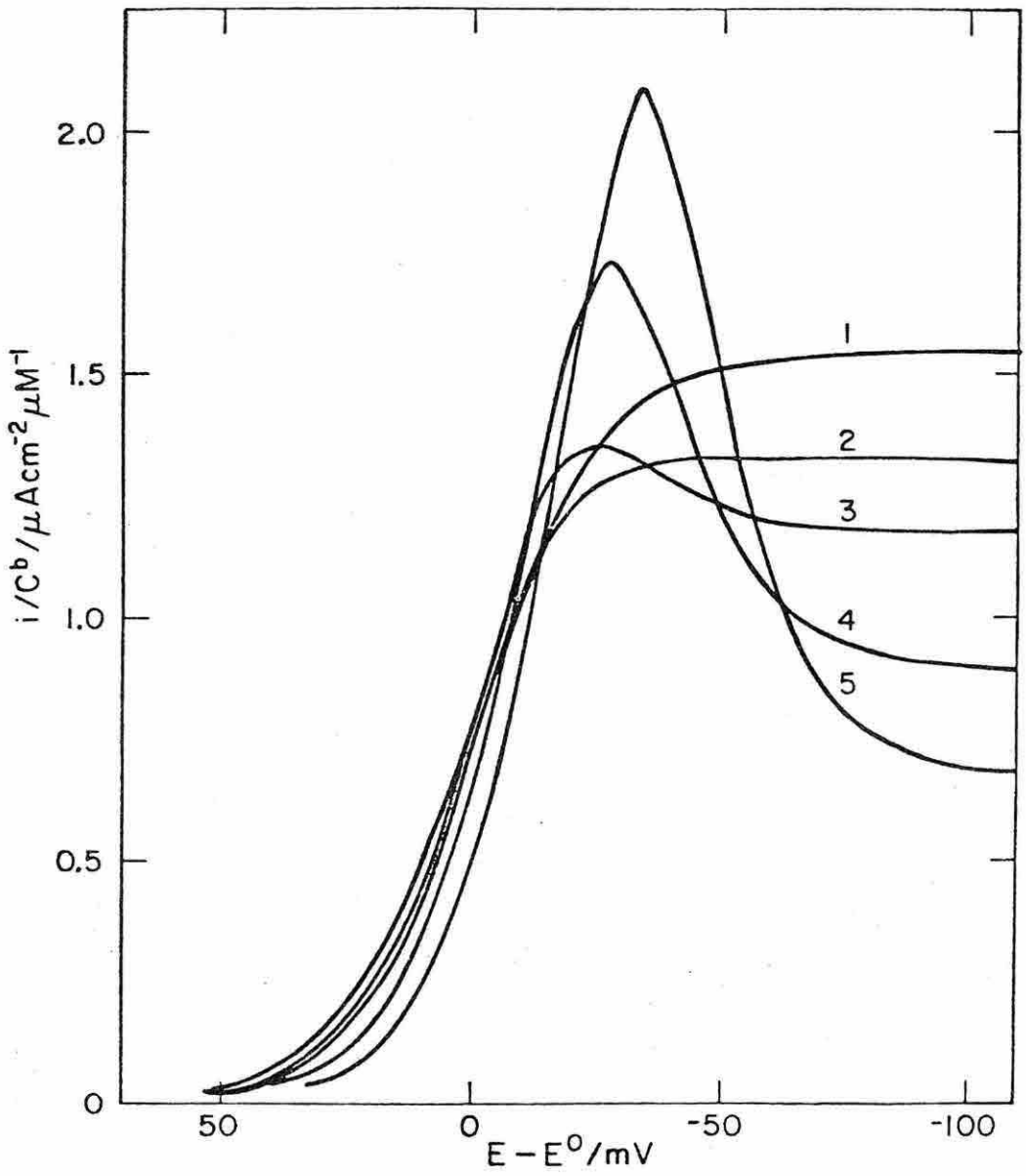

FIGURE 4.5

of the reactant was not included in their approximate calculations. It is evident from the curves in Fig. 4.5 that the current maximum is absent when the adsorption coefficient is 10^{-3} cm or less although significant depression of the limiting current persists. With non-linear isotherms similar behavior results at bulk reactant concentrations where the adsorption approaches the saturation value. In both cases the behavior can be dangerous analytically if reactant concentrations are being determined from limiting current magnitudes.

It should be noted that in the simulation employed here the adsorption coefficient was assumed to be independent of potential (Barker and Bolzan[1] used the same approximation). However, it is not difficult to estimate the qualitative effects that would be introduced by a potential dependence of the adsorption coefficient. If a reactant is adsorbed at the initial potential but not at potentials on the plateau of the wave depression of the limiting current arising from the depletion of reactant from solution will be the same whether or not the adsorption coefficient is potential dependent. The initially adsorbed reactant will react essentially instantaneously when the electrode potential is stepped to the diffusion limiting region whether or not it remains adsorbed.

In cases where the reaction product is not adsorbed the effect of desorption of the reactant at potentials on the rising portion of the wave because of a decrease in its adsorption coefficient will generally be to produce a maximum in the current-potential curve resulting from the enhancement of the reactant concentrations at the electrode surface. The converse case in which there is no adsorption of the reactant at the initial potential but increasing adsorption at potentials where the wave appears would be expected to exhibit shifted waves with altered shapes but the limiting current would not be affected since it remains a function only of the adsorption coefficient of the reactant at the initial potential.

Simulated Polarograms with Non-linear Adsorption Isotherms. When the reactant adsorption is governed by a linear isotherm the current maxima, limiting currents and half-wave potentials are not influenced by changes in the bulk concentrations of reactant. However, non-linear adsorption isotherms cause all three of these polarographic features to exhibit concentration dependences.

With non-linear isotherms and sufficiently large adsorption coefficients pre- and post-waves may appear in normal pulse polarograms. These waves originate for the same reasons that have been discussed in the cases of

differential pulse polarography, d.c. polarography,[3] linear potential scan voltammetry,[4] and chronocoulometry.[5] Figures 4.6 and 4.7 show a set of simulated polarograms for adsorbing reactants and products, respectively, which obey Langmuir adsorption isotherms. With reactant adsorption (Fig. 4.6) the post-wave appears in the form of a current maximum (curves 1, 2, 3). At low concentrations this post-wave so dominates the response that no vestige remains of the unperturbed main wave (curve 4). At higher concentrations where the electrode surface is saturated the post-wave becomes insignificant with respect to the main wave. Only over a rather narrow range of concentrations does a clear double wave appear (curve 3).

On the other hand, with product adsorption (Fig. 4.7) flat-topped pre-waves are obtained with shapes reminiscent of their counterparts in d.c. polarography. However, the concentration range within which the double waves develop is also quite restricted, spanning little more than one order of magnitude. The prominence of the waves is also a sensitive function of the adsorption coefficients of the product. As the coefficient is decreased the pre-waves eventually become imperceptible because their separation from the main wave decreases correspondingly.

The pre- and post-waves are most clearly separated from the main wave when the adsorption isotherms rise to

FIGURE 4.6

Simulated polarograms for an adsorbed reactant obeying a Langmuir isotherm. Bulk reactant concentrations, μM: (1) 1; (2) 50; (3) 200; (4) 1000. Adsorption coefficient: 0.5 cm; adsorption at saturation of the surface: 3×10^{-10} moles cm^{-2}. Other simulation parameters as in Fig. 4.3.

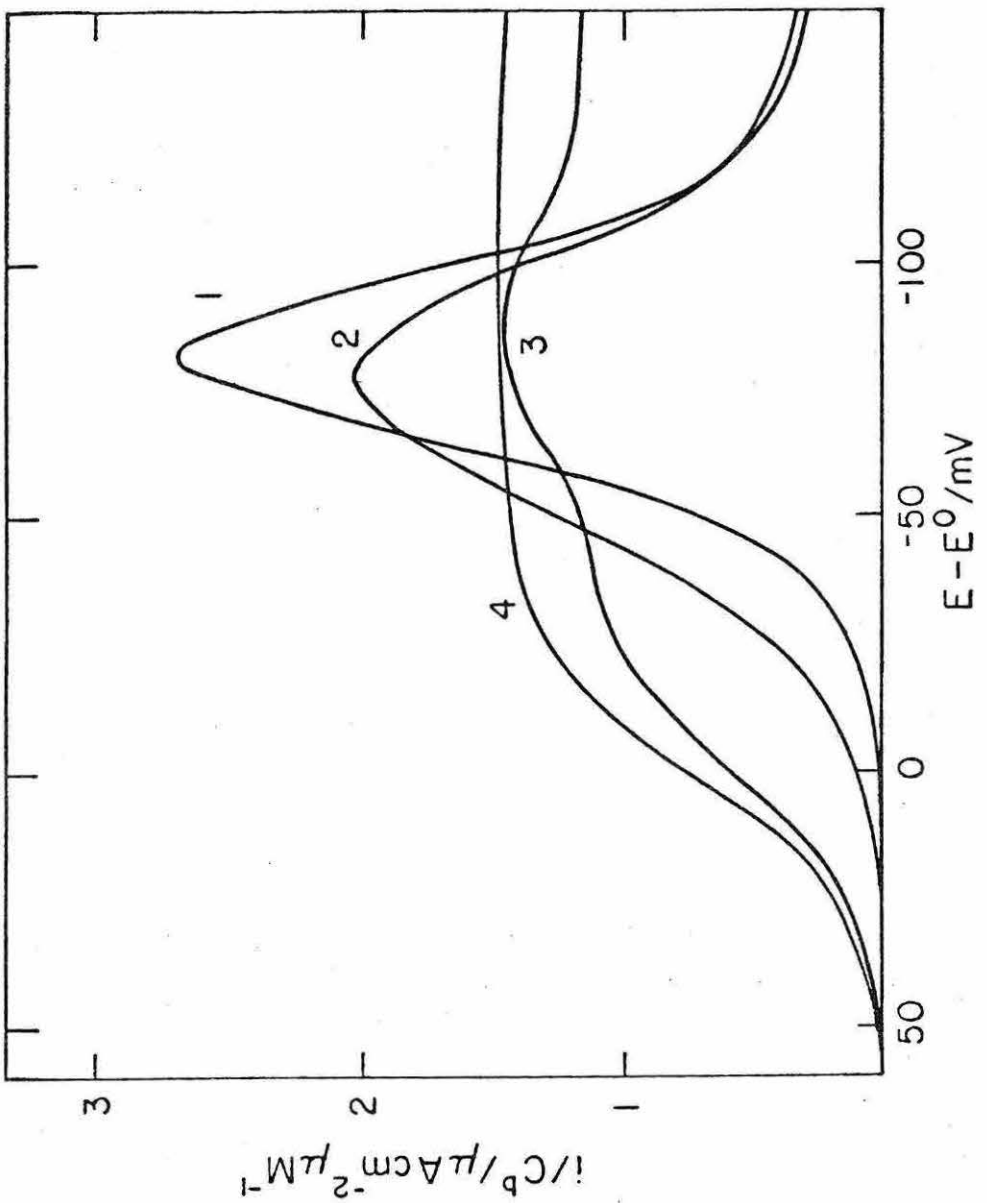

FIGURE 4.6

FIGURE 4.7

Simulated polarograms for an adsorbed product obeying a Langmuir isotherm. Bulk reactant concentrations, μM: (1) 1; (2) 50; (3) 300; (4) 400; (5) 500; (6) 1000. Other simulation parameters as in Fig. 4.6.

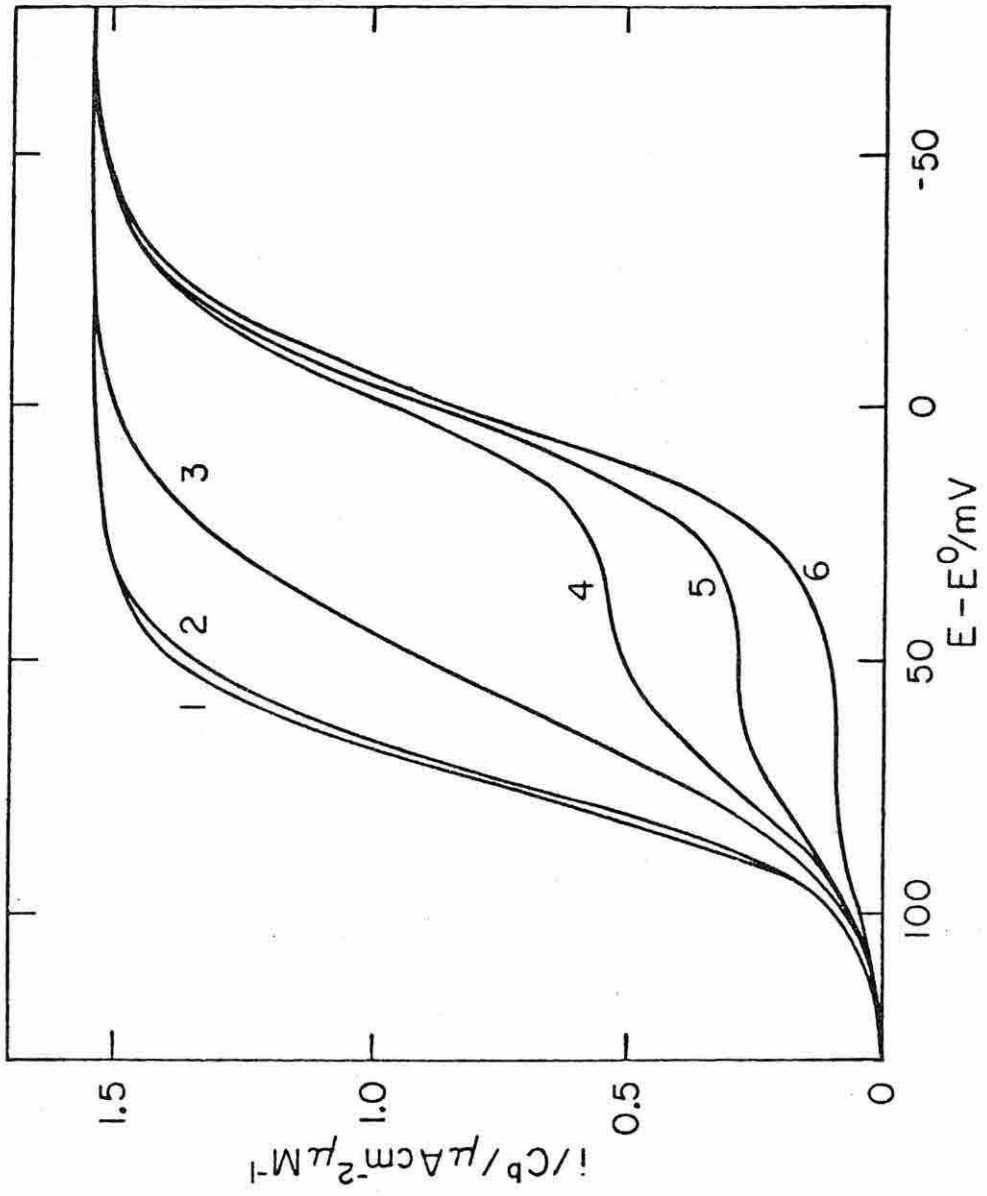

FIGURE 4.7

saturation coverage over a relatively narrow range of bulk concentrations as with the Langmuir isotherm or, especially, the Frumkin isotherm with an attractive interaction parameter.[6] Cd(II) in iodide electrolytes obeys a Frumkin isotherm with a repulsive interaction parameter and a smaller adsorption coefficient than was used in the simulations in Fig. 4.6. The net result is that a clear current maximum is observed in normal pulse polarograms for Cd(II) in iodide (Fig. 4.1), but no clearly separated post-wave (such as curve 3 in Fig. 4.6) is obtained at any concentration of Cd(II).

Figure 4.8 compares the concentration dependences of the experimentally measured values of the (normalized) maximum and limiting currents for Cd(II) in iodide electrolytes with those obtained from a digital simulation based on the Frumkin adsorption isotherm parameters that were determined previously by an independent technique. The good agreement between the experimental results, plotted as points, and the simulation which involved no adjustable parameters (the continuous lines) justifies the conclusion that the factors responsible for the current perturbations have been properly identified and satisfactorily accounted for in the simulation. For example, note that with the shorter drop time in Fig. 4.8 the current maximum is essentially absent at a concentration of 200 μM but

FIGURE 4.8

Concentration dependences of the peak currents and limiting currents for Cd(II) in 0.9 M KNO_3 - 0.1 M KI. The ordinate is the current density divided by bulk concentration of Cd(II). Experimental points are plotted, the numbered solid lines are simulated. 1, (○) maximum current, drop time = 5.2; 2, (●) Maximum current, drop time = 1 s; 3, (△) limiting current, drop time = 5 s; 4, (▲) limiting current, drop time = 1 s. Mercury flow rate: 1.06 mg s^{-1}; current sampling time: 48.5 ms; diffusion coefficients: Cd(Hg) = 1.5×10^{-5} cm^2 s^{-1}; Cd(II) = 10^{-5} cm^2 s^{-1}; Frumkin adsorption isotherm parameters [2] used in the simulation: adsorption coefficient = 0.04 cm; maximum adsorption 2.2×10^{-10} moles cm^{-2}; repulsive interaction parameter: 3.6.

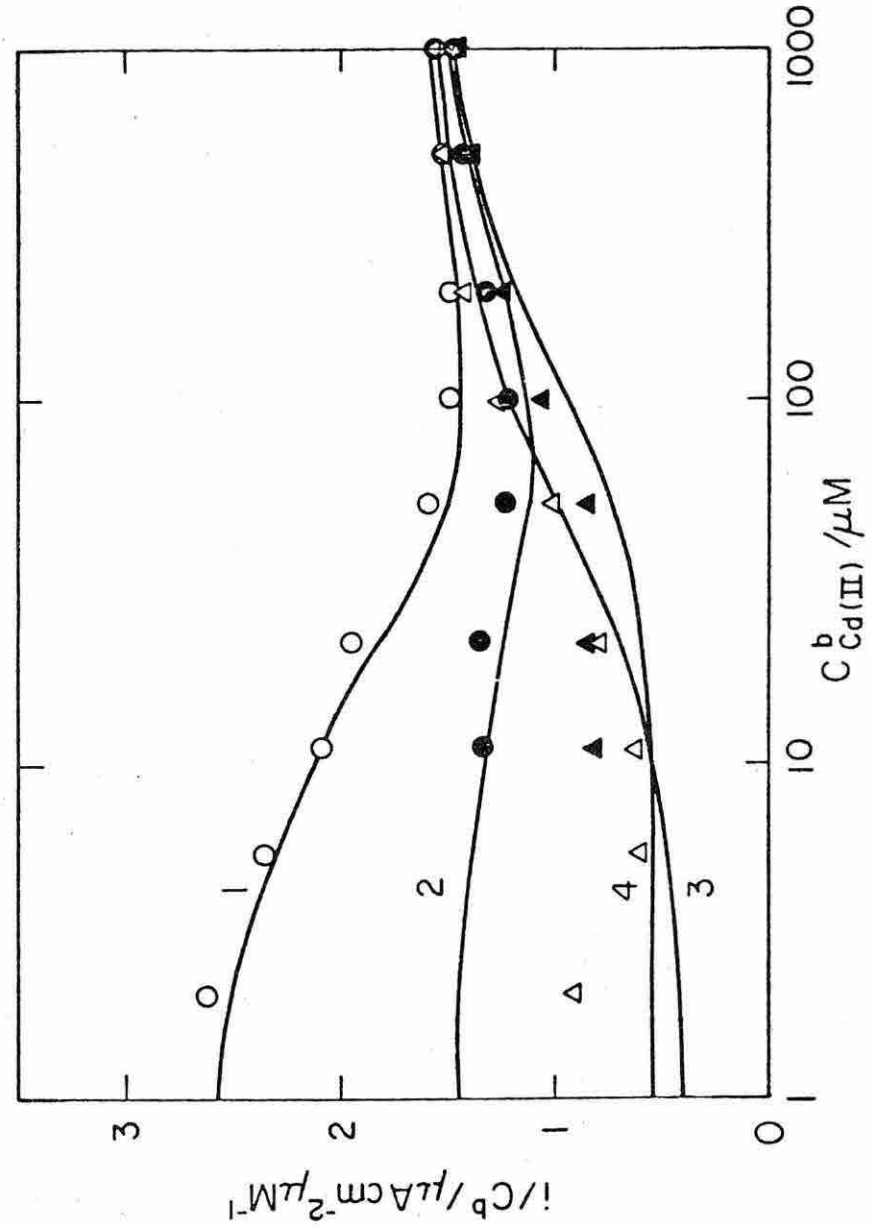

FIGURE 4.8

the normalized limiting current is still ca. 15% below the high concentration (no-adsorption) limit. Just such behavior was shown in Fig. 4.5 (curve 2) in the case of a linear isotherm.

CONCLUSIONS

Both the simulated and experimental results presented above make it clear that reactant adsorption can lead to normal pulse polarographic waves with anomalous features such as current maxima, double waves and depressed limiting currents. Although the shapes of the current maxima can resemble those of ordinary polarographic maxima[1] their origin is clearly different depending, as it does, on the coupling of adsorption, mass transfer and nernstian electrode kinetics rather than changes in interfacial tension and streaming at the surface of liquid mercury electrodes. Adsorption-induced current maxima may also appear in pulse polarograms obtained at solid electrodes with reversibly adsorbing, nernstian reactants.

The depression in normal pulse polarographic limiting currents which reactant adsorption induces can have serious analytical consequences because the linear relationship between the limiting current and bulk reactant concentration is lost. When both the reactant and the product of an electrode reaction are adsorbed the situation

becomes particularly troublesome if the normal pulse polarograms are being used for analytical purposes because severe depression of the limiting currents may result while the wave shapes give no hint that the adsorption is occurring (e.g., curves 4 in Figs. 4.3 and 4.4).

Whenever a current maximum is detected in a normal pulse polarogram obtained with a dropping mercury electrode the ensuing limiting current will be depressed but the electroanalyst has received a clear warning sign. When no maximum is observed other tests which may reveal the presence of adsorption include limiting currents which are very different on forward and reverse scans or anomalous dependences of the limiting currents on drop time or current sampling time.

REFERENCES

(1) G. C. Barker and J. A. Bolzan, Z. Analyt. Chem., 216, 215 (1966).

(2) K. B. Oldham and E. P. Parry, Anal. Chem., 42, 229 (1970).

(3) R. Bridicka, Z. Elektrochem., 48, 278, 686 (1942).

(4) R. H. Wopschall and J. Shain, Anal. Chem., 39, 1514 (1967).

(5) W. H. Reinmuth and K. Balasubramian, J. Electroanal. Chem., 38, 79 (1972).

(6) A. N. Frumkin and B. B. Damaskin in Modern Aspects of Electrochemistry, Vol. 3, J. O'M Bockris and B. E. Conway (Eds.), Butterworth, London, 1964, Ch. 3.

CHAPTER V[1]

Electron Transfer to and From Molecules Containing Multiple, Non-interacting Redox Centers. The Electrochemical Oxidation of Poly(vinylferrocene)

INTRODUCTION

The electrochemical behavior of molecules which contain several electroactive sites has been the subject of a number of studies.[2,3] The differences in potential between the half-reactions of the successive electron transfers to such molecules can depend upon the extent of interaction between the sites, solvation changes, ion pairing and structural changes of the molecule, but for molecules containing identical, non-interacting centers, the successive electron transfers will follow simple statistics. In the absence of significant molecular reorganization or solvation changes, the separations between successive formal potentials (as defined below) will depend only on the number of centers present. For example, with two centers present the separation is equal to (RT/F)ln4.[4] This situation is analogous to that of the separation in pK's of a molecule with non-interacting acidic groups.[5] As Ammar and Savéant have pointed out,[4] the nernstian voltammetric wave which results from such a situation has the shape of a one-electron transfer reaction, although more than one electron is transferred in the

overall reaction. In a recent paper[6] on the electroreduction of the polymers poly-2-vinylnaphthalene and poly-9-vinyl-anthracene evidence was presented for multi-electron transfer (up to 1200 electrons per molecule!) producing voltammetric waves with the overall shape of one-electron transfer reactions. Similarly in a recent study of the electrochemical oxidation of poly(vinylferrocene) (PVF) multi-electron transfers were observed.[7]

We report here a theoretical analysis of the expected current-potential characteristics for multiple electron transfers to a molecule containing any number of non-interacting redox centers and demonstrate that the statistical factors which govern the behavior produce a current-potential response with nernstian systems which, except for the larger limiting currents, has all the characteristics of a one-electron transfer reaction. Such behavior is demonstrated by the electrochemical oxidation of PVF for which coulometric measurements are employed to show that the total number of electrons transferred is equal to the number of ferrocene residues present in the molecule.

EXPERIMENTAL

Reagents. N,N-dimethylformamide (DMF) was stirred over anhydrous copper sulfate for 24 hours, distilled under reduced pressure, and stored under argon. Tetrahydrofuran (THF) was refluxed over sodium for 24 hours, distilled under

reduced pressure and stored under argon. Polarographic grade tetra-n-butylammonium perchlorate (TBAP) (Southwestern Analytical Chemicals, Austin, Texas), used as supporting electrolyte, was used as received after drying under vacuum. The samples of poly(vinylferrocene) were generously donated by Dr. Thomas W. Smith (Xerox Corp.); the synthesis purification, and measurement of molecular weights of these samples has been described.[7]

Apparatus. Cyclic voltammetry and coulometry experiments were carried out with a PAR Model 173 Potentiostat (Princeton Applied Research Corp., Princeton, NJ) driven by a PAR Model 175 Programmer. Current-voltage curves were recorded on a Tektronix Model 564 Oscilloscope or an X-Y Recorder. Pulse Polarography studies were performed with a PAR Model 174 instrument.

A conventional three-electrode cell was used in all experiments. The working electrode for voltammetric experiments was a platinum sphere with an area of 3.0 $mm.^3$ For coulometry a large platinum gauze electrode was employed. The reference electrode was a silver wire immersed in the test solution but isolated from the main chamber by a sintered-glass disk. The potential of this reference electrode was not particularly stable. Its potential was measured with respect to an aqueous saturated

calomel electrode (s.c.e.) to obtain the values of potential on this scale. The counter electrode was platinum and was isolated in a separate chamber of the cell. Positive feedback techniques were employed to minimize the effects of uncompensated resistance in the cyclic voltammetric measurements.

THEORY OF ELECTRON TRANSFER WITH REACTANTS HAVING MULTIPLE ELECTROACTIVE CENTERS

Consider a polymeric molecule containing n independent centers capable of accepting or donating one electron. Suppose that each center has the same standard potential, E_m^o, and adheres to the Nernst equation independently of the oxidation state of any of the other centers in the molecule; i.e., for each center there is a corresponding half-reaction with standard potential, E_m^o

$$\cdots XXOXX\cdots + e^- \underset{}{\overset{E_m^o}{\rightleftharpoons}} \cdots XXRXX\cdots$$

$$\cdots XXXXO\cdots + e^- \underset{}{\overset{E_m^o}{\rightleftharpoons}} \cdots XXXXR\cdots$$

$$\vdots$$

etc

where O and R represent the electroactive center in its oxidized and reduced states, respectively, and X represents

a center in either oxidation state. The probability that, at equilibrium, any site, i, is reduced is given by:

$$P(i=R) = \frac{1}{1+\theta} \tag{5.1}$$

where

$$\theta \equiv \exp\left[\frac{F}{RT}(E-E_m^{o})\right] \tag{5.2}$$

and E is the potential of an electrode with which the multiple-centered molecule is in equilibrium.

The "oxidation state" of such a polymeric molecule amounts to the sum of the monomeric components of the molecule that are in their oxidized states, namely (n-j), where j is the number of reduced sites. Application of standard probability theory[8] leads straightforwardly to a binomial distribution of the various forms of partially reduced polymer:

$$f_j = \binom{n}{j}\left(\frac{\theta}{1+\theta}\right)^{(n-j)}\left(\frac{1}{1+\theta}\right)^{j} \tag{5.3}$$

where f_j is the fraction of the polymer molecules present containing exactly j reduced centers (and (n-j) oxidized centers) at each value of θ.* $\frac{\theta}{1+\theta}$ and $\frac{1}{1+\theta}$ are the

---

*$\binom{n}{j} \equiv \frac{n!}{j!(n-j)!}$

probabilities that any particular monomeric center is oxidized or reduced, respectively.

If C_p is the bulk concentration of polymer, the equilibrium concentration, C_j, of molecules containing exactly j reduced sites (produced, for example, by controlled potential electrolysis of the solution at potential E) is given by:

$$C_j = C_p f_j \tag{5.4}$$

where f_j has the value corresponding to potential E. In many cases (discussed below) the same expression may be used to calculate concentrations at the electrode surface in voltammetric experiments.

Figure 5.1A shows calculated fractional concentration-potential curves for the reduction of a two-center molecule. The three curves represent the fractions, f_0, f_1 and f_2, of unreduced, half-reduced, and fully-reduced molecules, respectively. The curves intersect at the potentials for the two redox couples present. These are identified in Fig. 5.1 as E_1^F and E_2^F. The difference between these two intersection potentials is 35.6 mV (at T = 297° K), a result which has been discussed previously for molecules with two non-interacting centers by Ammar and Savéant.[4a] For the general case of molecules containing n non-interacting

FIGURE 5.1

Calculated fractional concentration-potential and current-potential curves for a reactant with two reducible centers. A - Fractional concentrations of unreduced (1), half-reduced (2) and fully-reduced (3) reactant. E_1^F and E_2^F are the formal potentials corresponding to the transfer of the first and second electrons to the molecule, respectively B - Current-potential curves for equal concentrations of (1) one-center and (2) two-center reactants. The currents have been corrected for differences in the diffusion coefficients of the one-center and two-center reactants. $i_{d,m}$ is the diffusion limited current for the one-center molecule. Curve 3 is the plot of $-\log(\frac{i}{i_d - i})$ for both current-potential curves. A temperature of 25° C is assumed

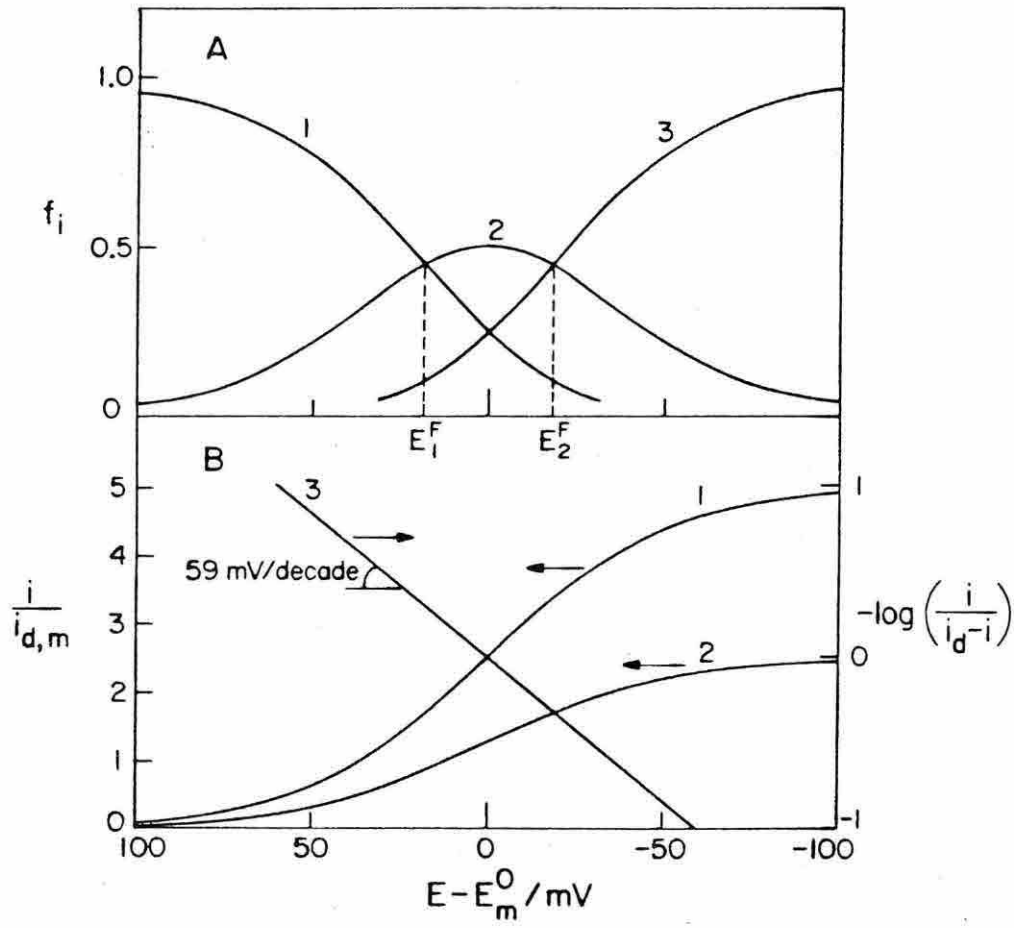
A
1.0
0.5
0
f_i
1
2
3
E_1^F
E_2^F
B
5
4
3
2
1
0
$\frac{i}{i_{d,m}}$
59 mV/decade
1
2
3
1
0
-1
$-\log\left(\frac{i}{i_d - i}\right)$
100
50
0
-50
-100
$E - E_m^0$ / mV

FIGURE 5.1

reducible centers it is possible to calculate the formal potentials, corresponding to each pair of successive oxidation states of the polymer.

At the formal potential E_j^F, the concentration fractions $f_{(j-i)}$ and f_j are equal:

$$f_{(j-i)} = f_j \tag{5.5}$$

substituting eqn (5.3) into both sides,

$$\binom{n}{j-1}\left(\frac{1}{1+\theta}\right)^{(n-j+1)}\left(\frac{\theta}{1+\theta}\right)^{j-1} = \binom{n}{j}\left(\frac{1}{1+\theta}\right)^{(n-j)}\left(\frac{\theta}{1+\theta}\right)^{j} \tag{5.6}$$

$$\binom{n}{j-1}\left(\frac{1}{1+\theta}\right) = \binom{n}{j}\left(\frac{\theta}{1+\theta}\right) \tag{5.7}$$

$$\theta = \frac{\binom{n}{j-1}}{\binom{n}{j}} = \frac{\frac{n!}{(n-j+1)!(j-1)!}}{\frac{n!}{(n-j)!j!}} \tag{5.8}$$

$$\theta = \frac{j}{n-j+1} \tag{5.9}$$

Substituting eqn (5.2):

$$E_j^F = E_m^o - \frac{RT}{F}\ln\left(\frac{j}{n-j+1}\right) \tag{5.10}$$

As an example, Fig. 5.2 illustrates fraction-potential and current-potential curves calculated for n = 5.[4b]

FIGURE 5.2

Calculated fractional concentration-potential and current-potential curves for a reactant with five reducible centers. The numbered curves have the corresponding significance to those identified in Fig. 5.1.

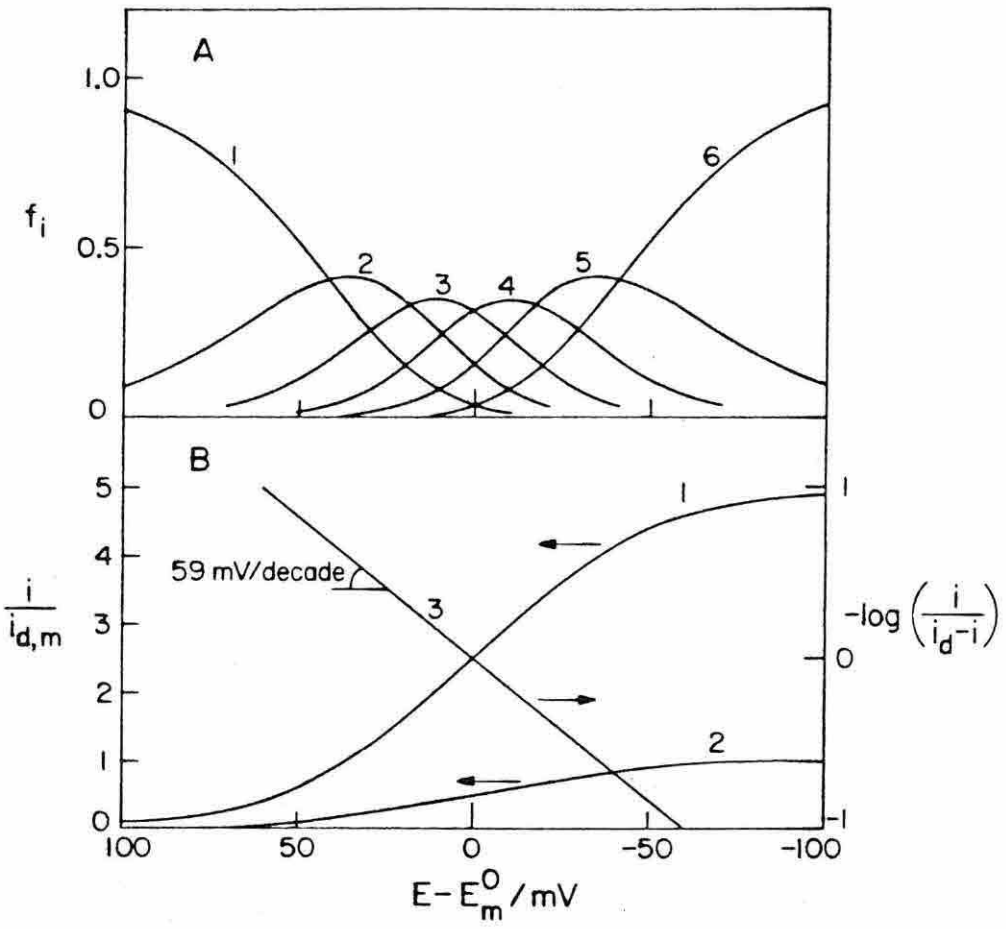
A
B
1.0
0.5
0
f_i
1
2
3
4
5
6
5
4
3
2
1
0
$\frac{i}{i_{d,m}}$
59 mV/decade
1
2
3
1
0
-1
$-\log\left(\frac{i}{i_d - i}\right)$
100
50
0
-50
-100
$E - E_m^0$ / mV

FIGURE 5.2

The difference between the formal potentials for the first and last pair of oxidation states in a molecule with n reducible centers is logarithmically related to n:

$$E_1^F - E_n^F = (2RT/F)\ln n \qquad (5.11)$$

For large n, this means that there will be large overlap of the concentrations of the various partially reduced species at potentials in the rising portion of a polarization curve, i.e., that the successive formal potential will fall increasingly close to each other as n increases. Note that the spacing between successive formal potentials becomes non-uniform for $n \geqslant 4$.

Comparison of the A and B portions of Figs. 5.1 and 5.2 reveals that the half-wave potential obtained with polymeric molecules matches the half-wave potential obtained with the corresponding molecule with one center and falls at the formal potential $E^F_{\frac{n+1}{2}}$ when n is odd. For even values of n, the half-wave potential falls between $E^F_{\frac{n}{2}}$ and $E^F_{\frac{n+2}{2}}$.

To calculate $Q_n(\theta)$ the total number of electrons consumed by a polymeric reactant of n centers during electrolysis from the completely oxidized state at a potential corresponding to θ, we multiply the amount of each reduced species formed by the number of electrons it

has accepted and sum for all j:

$$Q_n(\theta) = FN_T \sum_{j=o}^{n} j f_j \qquad (5.12)$$

where N_T is the total number of moles of polymer taken and F is the Faraday.

Under conditions where eqn (5.4) applies to concentrations at the electrode surface during voltammetric experiments, the shapes of the current-potential curves obtained may be calculated with the aid of eqn (5.12). (The magnitudes of currents will, of course, be scaled by diffusion coefficients and the experimental parameters applicable to each technique.) Voltammetric techniques in which the surface concentrations of reactant and product are directly reflected in the current-potential curves include d.c. polarography, normal pulse polarography, and voltammetry at rotating disk electrodes.

It can be shown that the shape of the current-potential curves obtained with these techniques will have the same shape as the corresponding curve for the species containing only a single reducible center but the limiting currents will be larger by a factor of n, the degree of polymerization. In terms of eqn (5.12) this correspondence can be expressed as

$$Q_n(\theta) = nQ_1(\theta) \qquad (5.13)$$

Equation (5.13) can be shown to be an identity by substituting eqn (5.12) into both sides and performing a few manipulations:

$$F\ N_T \sum_{j=o}^{n} j\ f_j \stackrel{?}{=} nF\ N_T \sum_{j=o}^{1} j\ f_j \tag{5.14}$$

Substituting eqn (5.3) into both sides:

$$F\ N_T \sum_{j=o}^{n} j \binom{n}{j} \left(\frac{\theta}{1+\theta}\right)^{n-j} \left(\frac{1}{1+\theta}\right)^{j} \stackrel{?}{=} n\ F\ N_T \left(\frac{1}{1+\theta}\right) \tag{5.15}$$

Noting that the 1.h.s. j = o term is zero, factoring out a term in $\frac{1}{1+\theta}$, and expanding the binomial coefficient $\binom{n}{j}$ yields:

$$F\ N_T \left(\frac{1}{1+\theta}\right) \sum_{j=1}^{n} \frac{jn!}{j!(n-j)!} \left(\frac{\theta}{1+\theta}\right)^{n-j} \left(\frac{1}{1+\theta}\right)^{j-1} \stackrel{?}{=} " \tag{5.16}$$

$$nF\ N_T \left(\frac{1}{1+\theta}\right) \sum_{j=1}^{n} \frac{(n-1)!}{(j-1)!(n-j)!} \left(\frac{\theta}{1+\theta}\right)^{n-j} \left(\frac{1}{1+\theta}\right)^{j-1} \stackrel{?}{=} " \tag{5.17}$$

Making the substitutions, k = j-1 and m = n-1,

$$nF\ N_T \left(\frac{1}{1+\theta}\right) \sum_{k=o}^{m} \frac{m!}{k!(m-k)!} \left(\frac{\theta}{1+\theta}\right)^{m-k} \left(\frac{1}{1+\theta}\right)^{k} \stackrel{?}{=} " \tag{5.18}$$

The sum is simply the binomial expansion of $\left(\frac{1+\theta}{1+\theta}\right)^{m}$ which is unity.

$$nF\ N_T \left(\frac{1}{1+\theta}\right) \cdot 1 = nF\ N_T \left(\frac{1}{1+\theta}\right) \tag{5.19}$$

Which was to be proved.

The current-potential identity corresponding to (5.13) is:

$$i_n(\theta) = ni_1(\theta)\left(\frac{D_p}{D_m}\right)^p \qquad (5.20)$$

where i_n is the current obtained at each value of θ with a polymer and i_1 the corresponding current for a monomeric sample when the concentrations of both polymer and monomer are equal. D_p and D_m are diffusion coefficients for polymer and monomer, respectively, and the exponent p depends on the voltammetric technique employed.

Figures 5.1B and 5.2B show the current-potential curves calculated for the reduction of two-center and five-center molecules, respectively, along with the corresponding plots of $\log\frac{i}{i_d-i}$ vs potential. The latter pair of plots, whose slopes reflect the steepness of the rising portions of the current-potential curves, are indistinguishable from each other and are identical to the plot that would result for the reduction of a monomeric one-electron reactant. Thus, the magnitudes but not the shapes of the current-potential curves are affected by the number of non-interacting reducible centers the reactant contains.

The current-potential responses obtained with techniques such as cyclic voltammetry, differential pulse polarography and a.c. polarography bear a more complex relation to the

concentrations of reactant and product at electrode surfaces so that simple equations analogous to (5.13) and (5.20) are not available. However, the shapes of cyclic voltammograms are discernable from those of corresponding polarographic or steady-state current-potential curves by means of semi-differentiation.[9] In this way it can be shown that cyclic voltammograms (as well as differential pulse and alternating current polarograms) for molecules with multiple, non-interacting redox centers will also exhibit shapes that match those of the corresponding species with a single center. Thus, the anodic and cathodic peak potentials and the peak and half-peak potentials should both be separated by 58 mV (25° C).[10]

The peak currents of cyclic voltammograms for polymeric reactants will obey eqn (5.20) with p = ½. This is true despite the fact that in the equation for the voltammetric peak current with nernstian reactants n, the number of electrons transferred, appears with the exponent 3/2 not 1.[10] The reason is that the equation for the peak current is derived for an electrode reaction in which n electrons are assumed to be transferred essentially simultaneously while the type of multi-centered reactant we have been discussing undergoes n successive, one-electron transfers per molecule.

Departures from Simple Theory. A variety of factors could cause departures from the behavior calculated on the

basis of the simple model employed thus far: Interactions between adjacent reducible centers; slow electron transfer at the electrode, i.e., non-nernstian behavior; structural changes in the polymer which accompany its reduction; adsorption or precipitation of reactants or products at the electrode surface; or changes in diffusion coefficients of reactants and products as charge is added or removed from the polymer.

The variety of experimental examples[11] in which molecules bearing several identical reducible (or oxidizable) centers exhibit multiple waves at separate potentials rather than a single, larger wave is presumably a result of one or more of these factors but electronic interaction between two centers seems most likely to be the major source of wave-splitting.

There are also cases in which the current-potential curves for a multi-centered reactant have slopes even greater than that for a one-electron reactant.[3] This can occur when the addition of the first electron produces a species which accepts additional electrons more readily than the original reactant. Simulated voltammograms corresponding to a variety of conditions have been discussed by Polcyn and Shain.[12]

EXPERIMENTAL RESULTS AND DISCUSSION

Voltammetric Studies. As discussed by Smith et al.,[7] finding a solvent in which PVG and its oxidation products are adequately soluble and in which adsorption or

precipitation of reactants or products does not distort cyclic voltammograms is difficult. We had the best success with DMF and THF. With DMF it was necessary to heat the DMF-polymer mixture to 150° C and then cool slowly to room temperature to dissolve mg amounts of PVG. Typical cyclic voltammograms of the monomer, vinylferrocene (VF), and PVF are shown in Fig. 5.3 and 5.4. The wave for VF shows characteristics of a reversible one-electron transfer with production of a soluble, stable product, i.e., $i_{pa}(\nu)^{-\frac{1}{2}}$ and E_{pa} independent of scan rate, $E_{pa} - E_{pc} \sim 60$ mV, and $i_{pc}/i_{pa} \sim 1$ (where i_{pa} and i_{pc} are the peak anodic and cathodic currents, respectively, E_{pa} and E_{pc} are the anodic and cathodic peak potentials, and ν is the scan rate). In DMF the 5 K polymer exhibits generally similar characteristics, but the 16 k PVF shows evidence of adsorption of the reactant in the form of overly sharp anodic peak currents (Fig. 5.3). For THF solutions adsorption of the reactant was not observed (i.e., $i_{pa}(\nu)^{-\frac{1}{2}}$ was independent of ν) but the cathodic wave on scan reversal showed that the oxidized product had accumulated at the electrode surface (Fig. 5.4). Smith *et al.*,[7] noticed similar behavior with methylene chloride as a solvent.

While the cyclic voltammetric behavior of the 5 K polymer in DMF shows the shape and peak separation expected of a reversible one-electron transfer, the adsorption and

FIGURE 5.3

Cyclic voltammograms for vinylferrocene (VF) and poly(vinyl-ferrocene) (PVF) in 10 m of DMF as solvent. A - 1.0 mg VF (Mol. Wt. = 212); B - 1.2 mg PVF of Mol. Wt. 4930; C - 1.0 mg PVF of Mol. Wt. 15750. The initial potential for all voltammograms was +250 mV vs. the silver wire reference electrode. More oxidizing potentials are to the right; oxidation currents are plotted upward. Supporting electrolyte: 0.1 M TBAP. Scan rate: 100 mV sec^{-1}.

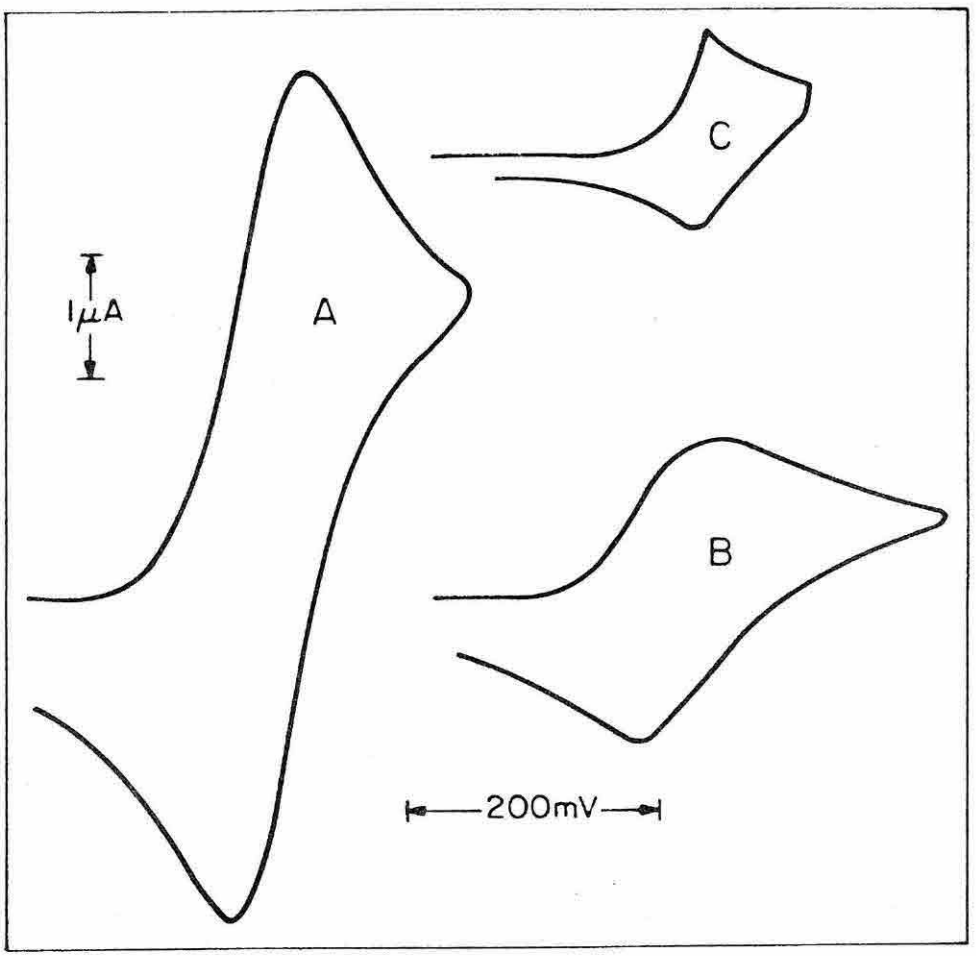

FIGURE 5.3

FIGURE 5.4

Cyclic voltammograms for poly(vinylferrocene) in 10 ml of THF as solvent. (——) - 0.94 mg PVF of Mol. Wt. 4930; (----) - 0.9 mg PVF of Mol. Wt. 15750. The initial potential was +100 mV vs. the silver wire reference electrode. More oxidizing potentials are to the right. Oxidation currents are plotted upward. Supporting electrolyte: 0.2 M TBAP. Scan rate: 100 mV sec^{-1}.

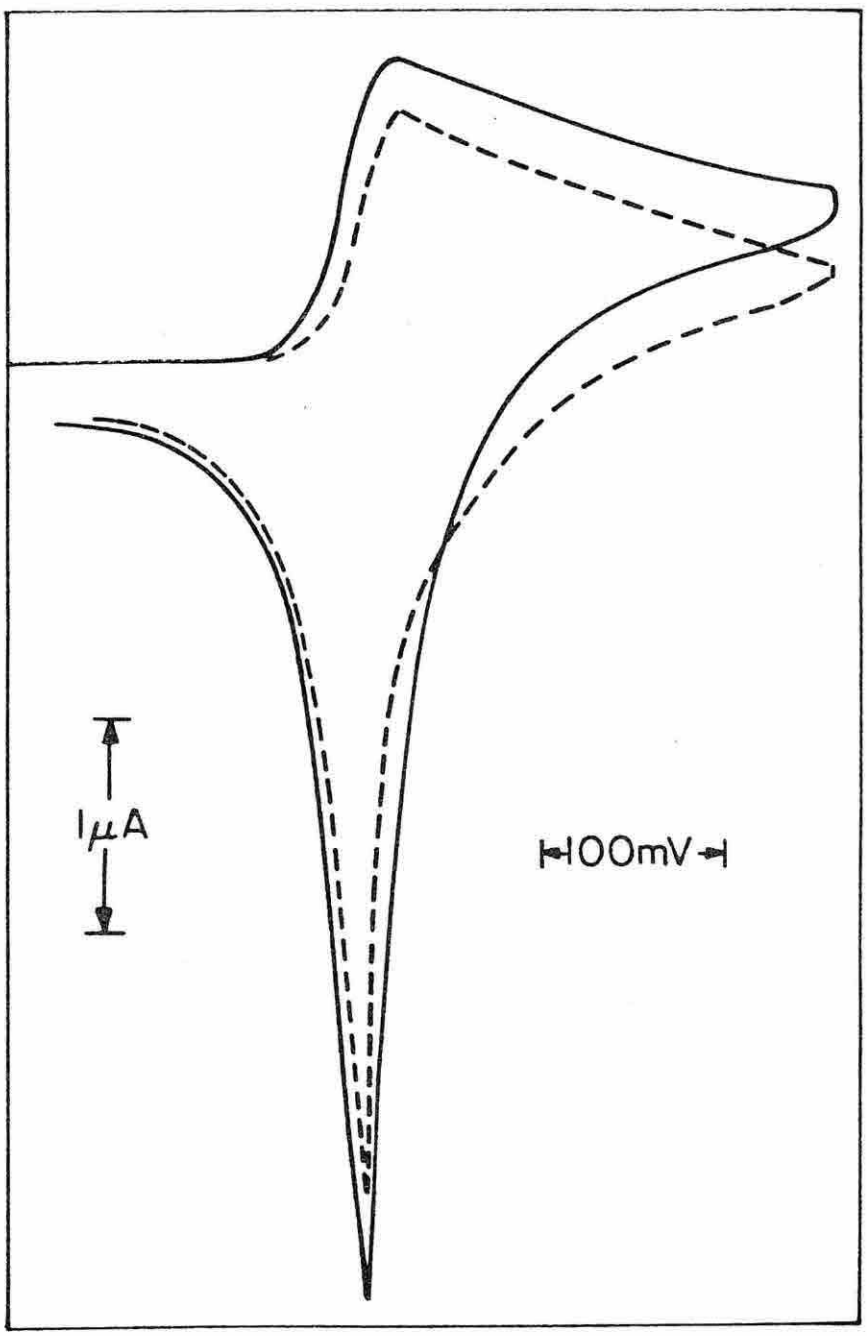

FIGURE 5.4

precipitation problems led us to use normal pulse voltammetry[13] as a means of determining the wave shape parameters and estimating the total number of electrons transferred per polymer molecule. In this technique adsorption or precipitation of the oxidized product should be of less importance, since a smaller amount will accumulate on the electrode surface during the brief pulse duration (~50 msec) and the oxidized product is reduced back to starting material during the time between pulses when the electrode is held at a potential at the foot of the anodic wave.[14] Typical normal pulse voltammograms are shown in Fig. 5.5 for both VF and PVF in THF. The limiting diffusion currents (i_d), slopes of E vs $\log(\frac{i_d - i}{i})$ plots, and half-wave potentials ($E_{\frac{1}{2}}$) obtained from the normal pulse polarograms are given in Table 5.1.

The total number of electrons transferred in the oxidation wave for the polymer (n_p) can be estimated from the limiting currents and approximate relative values of the diffusion coefficients of the monomer (D_m) and polymer (D_p).[6] From previous work on the relation between diffusion coefficient and molecular weight (M_m or M_p for monomer and polymer, respectively) the following relation seems most appropriate.[14]

$$D_p/D_m = (M_m/M_p)^{0.55} \qquad (5.21)$$

FIGURE 5.5

Normal pulse voltammograms for the oxidation of vinyl-ferrocene (VF) and poly(vinylferrocene) (PVF) in 10 ml of THF as solvent. A - 0.57 mg VF (Mol. Wt. - 212); B - 2.0 mg PVF of Mol. Wt. 15750. The initial potential was 0 mV vs. the silver wire reference electrode for both polarograms. Supporting electrolyte: 0.2 M TBAP. Scan rate: 2 mV sec^{-1}; Drop time: 5 sec.

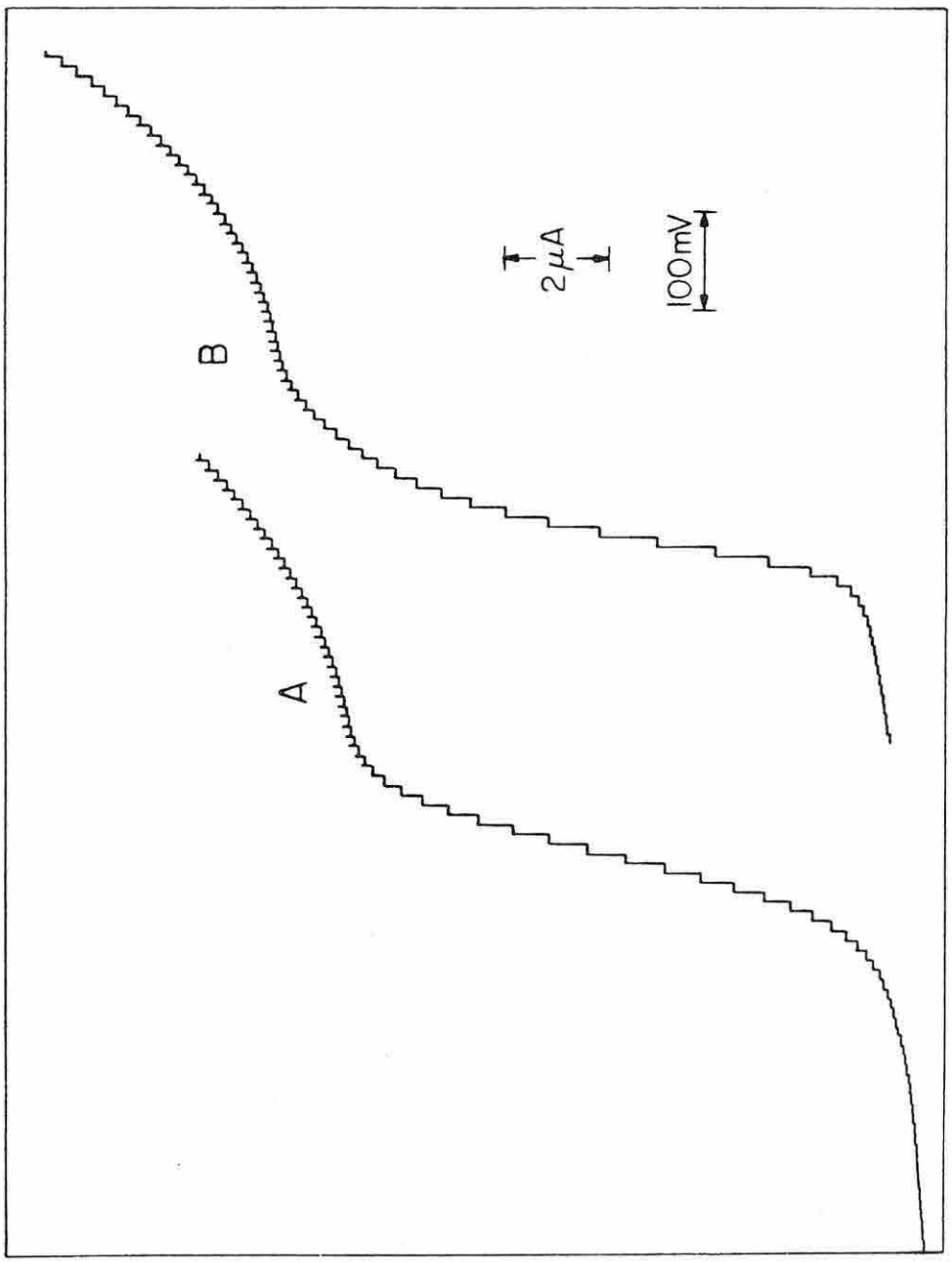

FIGURE 5.5

TABLE 5.1 Results of Normal Pulse Voltammetric Oxidation of Vinylferrocene and Poly(vinylferrocene)[a]

Compound	Amount taken, mg	Molec. wt.	Degree of Polymeriz.	i_d, μA	C μM	n_p[b]	log plot slope,[c] mV	$E_{1/2}$[d] (V vs. sce)
VF	0.57	212	1	9.6	260		61	0.56
PVF	0.55	4930	23.2	3.1	11	18	58	0.46
PVF	0.96	4930	23.2	6.1	19	21	60	0.45
PVF	0.54	15750	74.3	2.3	4	51	70	0.44
PVF	2.0	15750	74.3	10.6	12	75	66	0.48

[a] Experimental conditions are given in the caption to Figure 5.5

[b] Calculated using eqn. 5,22

[c] Slope of plot of E vs. $\log(\frac{i_d - i}{i})$

[d] The potential of the silver wire reference electrode employed was reproducible to only ca. ±50 mV but these potentials were subsequently confirmed (±15 mV) in experiments where an s.c.e. reference electrode was employed.

Assuming that the oxidation of VF is a one-electron reaction the value of M_p can be estimated by employing an equation derived previously for conventional d.c. polarography[6]

$$n_p = \frac{(i_{dp}/C_p)}{(i_{dm}/C_m)}\left(\frac{M_p}{M_m}\right)^{0.275} \qquad (5.22)$$

Values of n_p obtained in this way (Table 5.1) come close to matching the degree of polymerization of the polymer (DP), as was previously found for the reduction of poly-2-vinyl-naphthalene and poly-9-vinylanthracene.[6] Thus, the overall reaction results in the oxidation of essentially every ferrocene center in the PVF molecules. Smith and co-workers[7] made a similar estimation of n_p from anodic limiting currents in voltammetry at a rotating disk electrode with PVF in hexamethylphosphoramide. They assumed the Stokes-Einstein equation applied (i.e., $D \sim (M)^{-1/3}$) and reported values of DP/n_p which varied between 1.4 and 4.1 for PVF of different molecular weights. If their data are reanalyzed on the basis of eqn (5.21), we calculate values of DP/n_p which are more nearly constant but still vary from 1.3 to 2.6.

Note that the slopes of the log plots in Table 5.1 are quite close to the values corresponding to nernstian, multi-electron transfers to non-interacting groups in accord with the theoretical treatment presented above. Similar slopes were also observed in the rotating disk voltammetric studies at low concentrations of PVF.[7]

The difference in the values of $E_{1/2}$ for VF and PVF in Table 5.2 are not unexpected because the equivalence of $E_{1/2}$ values for polymeric and single-centered molecules predicted in the Theoretical Section assumed a comparison between polymer and "the corresponding molecule with a single center". A better comparison of $E_{1/2}$ values would be of PVF with monoethylferrocene. Monoethylferrocene has an $E_{1/2}$ value of 80 mV more positive than VF in acetonitrile as solvent.[10a] Subtracting 80 vF from the $E_{1/2}$ value for VF in Table 5.1 brings it quite close to the observed values for PVF in good accord with the theoretical prediction.

Coulometric Studies. To confirm the magnitude of the multi-electron transfers which occur in the oxidation of PVF without the need to estimate diffusion coefficients, coulometric oxidations of PVF at a large area platinum gauze electrode were carried out. The results are summarized in Table 5.2. Note the n_p calculated from the total coulombs consumed in the oxidation (Q_a) is very close to DP in agreement with the voltammetric results. The higher values of DP/n_p found in hexamethylphosphoramide as solvent by Smith, et al.,[7] (even when the diffusion coefficient is given the smaller value resulting from eqn (5.21) may be due to differences in the nature of the solvents employed which could lead to considerable differences in the extent of ion pair formation.

TABLE 5.2 Results of Controlled Potential Coulometric Oxidation of Poly(vinylferrocene)[a]

Compound	Amount taken, mg	Mol. Wt.	Degree Polymeriz.	Q_a,[b] C	n_p[c]	Q_c,[d] C
PVF	5.10	4930	23.2	2.3_5	23.6	1.9
PVF	4.92	15750	74.3	2.2	73.1	1.3_5
PVF	0.94	15750	74.3	0.43_5	75.1	0.21

[a] The electrolysis solution was ca. 15 ml. of THF containing 0.2 M TBAP.

[b] Charge consumed in the oxidation at +0.35 V vs. Ag reference electrode ($E_{1/2}$ was ca. 0.2 V vs. this reference electrode)

[c] $n_p = Q_a$/moles PVF

[d] Charge consumed in reduction of the oxidized solution at +0.1 V.

If a controlled potential reduction of the oxidized polymer is performed immediately following its oxidation the amount of charge required is less than was consumed during the oxidation. This is probably caused by precipitation of the oxidation product not all of which redissolves during the reduction step in THF. During the oxidation of the bright orange PVF a small amount of green, solid oxidation product is formed which persists following the reduction step.

Comparison with Results of Other Studies. It is of interest to contrast the results presented here for PVF with those that have been reported for several biferrocenes by Morrison, et al.,[11b] and for 1,1'-polyferrocenes by Brown, et.al.[11d] In the former study single polarographic waves were obtained with diffusion currents corresponding to a two-electron process when certain bridging groups connected the two ferrocene centers (Hg, C_2H_4, $(CH_3)_2CC(CH_3)_2$, and $-CH=CHC_6H_4CH=CH-$) but separated waves with one-electron diffusion currents resulted with other bridging groups. The slopes of plots of $\log(\frac{i}{i_d-i})$ vs potential for the biferrocenes which exhibited a single wave were 80 to 90 millivolts which matched the slope obtained with ferrocene itself. The authors, expecting the slope to be half as large for the biferrocenes as for ferrocene, explained the larger values in terms of electrochemical irreversibility. The present

treatment shows that their data are entirely compatible with comparable reversibility for both ferrocene and the biferrocenes: polarographic waves with one-electron slopes and two-electron diffusion currents are to be expected if the two ferrocene centers do not interact strongly. That diferrocenylethane exhibits such behavior is consistent with the results reported here for PVF since the ferrocene centers are separated by the same C_2H_4 bridging group in both cases.

In the previous electrochemical study of the oxidation of 1,1'-polyferrocenes[11d,h] the successive ferrocene groups are oxidized in a series of resolvable waves with values of $E_{1/2}$ separated by hundreds of millivolts. In these molecules the polymer chain is formed by direct linkage of the cyclopentadiene rings so that it is not surprising that strong interaction between the ferrocene residues apparently occurs. This is also suggested by the finding that the ease of oxidation of polyferrocene increases with chain length, i.e., the $E_{1/2}$ values for the first electron transfer increase in the order 1,1-quaterferrocene < 1,1'-terferrocene < biferrocene < ferrocene. For the PVF molecules the $E_{1/2}$ values are quite close to that for monoethylferrocene, as is expected (vida supra) as the ferrocene centers do not interact significantly.

CONCLUSION

Electron transfer to or from polymeric molecules containing identical, non-interacting electroactive centers will involve as many electrons as there are centers and will yield a voltammetric wave with the shape matching that of the corresponding molecule with a single electron active center but with a magnitude determined by the total number of centers present. This conclusion assumes the absence of complications arising from adsorption, precipitation or slow electron transfer kinetics.

ACKNOWLEDGEMENT

All experiments contained in this chapter were performed by Shlomo Margel.

REFERENCES AND NOTES

(1) James B. Flanagan, Shlomo Margel, Allen J. Bard and Fred C. Anson, J. Am. Chem. Soc., submitted for publication.

(2) A. J. Bard, Pure Appl. Chem., 25, 379 (1971) and references therein.

(3) F. Ammar and J. M. Savéant, J. Electroanal. Chem., 47, 115 (1973) and references therein.

(4) a. F. Ammar and J. M. Savéant, J. Electroanal. Chem., 47, 215 (1973);

b. It is important to note the difference between E_m^o and E_j^f. The latter is the potential at which the sum of all microscopic forms of a molecule having oxidation state j is equal to the sum of all forms having oxidation state j-1. The former is the common standard potential relating each microscopic center that is in its oxidized state to its reduced counterpart no matter what the overall oxidation state of the polymeric molecule happens to be.

(5) S. W. Benson, J. Am. Chem. Soc., 80, 5151 (1958).

(6) T. Saji, N. F. Pasch, S. E. Webber and A. J. Bard, J. Phys. Chem., submitted for publication.

(7) T. W. Smith, J. E. Kuder and D. Wychick, J. Polym. Sci., 14, 2433 (1976).

(8) M. R. Spiegel in "Statistics", McGraw-Hill Book Co., New York, N.Y., 1961, p. 122.

(9) a. J. C. Imbeaux and J. M. Savéant, J. Electroanal. Chem., 44, 169 (1973); M. Goto and K. B. Oldham, Anal. Chem., 45, 2043 (1973);

b. T. Kuwana, D. E. Bublitz and G. Hoh, J. Am. Chem. Soc., 82, 5211 (1960).

(10) R. S. Nicholson and I Shain, Anal. Chem., 36, 706 (1964).

(11) e.g., a. S. A. Adeyemi, J. N. Braddock, G. M. Brown, J. A. Ferguson, F. J. Miller and T. J. Meyer, J. Am. Chem. Soc., 94, 300 (1972);

b. W. H. Morrison, Jr., S. Krogsrud and D. N. Hendrickson, Inorg. Chem., 12, 1998 (1973);

c. C. Levanda, D. O. Cowan, C. Leitch and K. Beckgaard, J. Am. Chem. Soc., 96, 6788 (1973);

d. G. M. Brown, T. J. Meyer, D. O. Cowan, C. Levanda, F. Kaufman, P. V. Roling and M. D. Rausch, Inorg. Chem., 14, 506 (1975);

e. G. M. Tom and H. Taube, J. Am. Chem. Soc., 97, 5310, (1975);

f. M. J. Powers, R. W. Callahan, D. J. Salmon and T. J. Meyer, Inorg. Chem., 15, 894 (1976);

g. R. W. Callahan, F. R. Keene, T. J. Meyer and D. J. Salmon, J. Am. Chem. Soc., 99, 1064 (1977);

h. C. Levanda, K. Beckgaard, D. O. Cowan and M. D. Rausch, J. Am. Chem. Soc., 99, 2964 (1977).

(12) D. S. Polcyn and I. Shain, Anal. Chem., 38, 370 (1966).

(13) E. P. Parry and R. A. Osteryoung, Anal. Chem., 37, 1634 (1965).

(14) J. A. Turner, R. H. Abel and R. A. Osteryoung, Anal. Chem., 47, 1343 (1975).

(15) C. Tanford in "The Physical Chemistry of Macro-Molecules", John Wiley and Sons, Inc., New York, NY, 1961, p. 362.

CHAPTER VI

Molecules Containing Two Electron Transfer Centers: (1) Symmetric Centers with Interaction; (2) Asymmetric Centers

INTRODUCTION

The material presented here is a direct extension of the treatment of Chapter V[1] of multiple electron transfer centers. Example calculations are made for molecules containing two electron transfer centers. The results for symmetric dimeric molecules with interaction between centers and two-center asymmetric molecules can be generalized by the techniques described here and in the previous chapter to any particular molecule of interest. The dimer cases have been illustrated in some detail because of some interesting results relating to the magnitude of the "statistical factors" for the two cases. It is shown in the discussion section that these dimer results may in some cases be generalized to other molecules.

THEORETICAL

Current-potential Behavior of Interacting Electron Transfer Sites in Dimeric Molecules. Altered voltammetric response resulting from interactions between sites is frequently observed for compounds with dimeric or polymeric electron transfer sites. For simplicity we will discuss

only the case of an interacting dimer obeying nernstian electron transfer at both sites. In such a molecule the standard potential of an electron transfer at each site is dependent on the oxidation state of the other site. For the stepwise reduction of a completely oxidized dimer, the standard potential (E_1^o) of the first reduction may be shifted from the standard potential of the corresponding monomer by interaction with the other site or with the bridging portions of the molecule. The potential for reduction of a site when the neighboring site is reduced (denoted E_2^o) may be shifted in either the positive or negative direction from the first potential. If this shift is toward negative potentials, as in most of the cases reported by Ammar and Savéant,[2] the resulting reduction wave will be broadened or split into two waves. The usual cause for this effect is couloumbic repulsion of the second electron by the greater negative charge on the molecule. Occasionally a shift of the second reduction potential positive of the first is observed. This results in a wave more acutely sloped than the corresponding monomer wave.

It will be shown that statistical factors derived in Chapter V for non-interacting centers are still applicable when there is interaction. The total potential shifts are due to energetic component and a statistical component,

which are completely independent and add to determine the "formal potentials" of the complex formed by the sequential oxidation states of the total molecule. This result is as expected from simple thermodynamic considerations.[3]

The standard potential for either site to undergo electron transfer when the other site is oxidized is given by E_1^o, the resulting nernst equation expression is thus:

$$\theta_1 = \exp\left[\frac{F}{RT}(E-E_1^o)\right] = \frac{f_{o,o}}{f_{o,R}} = \frac{f_{o,o}}{f_{R,o}} \qquad (6.1)$$

where $f_{x,y}$ denotes the concentration fraction in which the first site is in state x and the second is in state y. The fractions $f_{o,R}$ and $f_{R,o}$ will be combined below, so that distinguishability of sites is not necessary.

With the other site reduced, the standard potential of a site is E_2^o,

$$\theta_2 = \exp\left[\frac{F}{RT}(E-E_2^o)\right] = \frac{f_{R,o}}{f_{R,R}} = \frac{f_{o,R}}{f_{R,R}} \qquad (6.2)$$

The difference $E_2^o - E_1^o$ is directly related to the energy of interaction $\Delta U = nF(E_2^o-E_1^o)$.

The fraction present with net molecular oxidation state one (one site oxidized, one reduced) is defined as f_1:

$$f_1 = 2f_{o,R} = 2f_{R,o} = f_{o,R} + f_{R,o} \qquad (6.3)$$

The fractions add up to unity:

$$f_{o,o} + f_1 + f_{R,R} = 1 \qquad (6.4)$$

Deriving from these equations the concentration fractions:

$$f_{R,R} = 1/(1 + 2\theta_2 + \theta_1\theta_2) \qquad (6.5)$$

$$f_1 = 2\theta_2/(1 + 2\theta_2 + \theta_1\theta_2) \qquad (6.6)$$

$$f_{o,o} = \theta_1\theta_2/(1 + 2\theta_2 + \theta_1\theta_2) \qquad (6.7)$$

Let the $Q_2(\theta)$ function be defined as in the previous section:

$$\frac{Q_2(n)}{FN_T} = f_1 + 2f_{R,R} = 2(1 + \theta_2)/(1 + 2\theta_2 + \theta_1\theta_2) \qquad (6.8)$$

The formal potentials are given by:

$$f_{oo} = f_1 \Longrightarrow E_1{}^F = E_1{}^o + \frac{RT}{F}\ln 2 \qquad (6.9)$$

$$f_1 = f_{RR} \Longrightarrow E_2{}^F = E_2{}^o - \frac{RT}{F}\ln 2 \qquad (6.10)$$

Thus the differences in these formal potentials as tabulated by Ammar and Savéant for some (interacting) organic dimers

includes an invariant statistical contribution of $\frac{RT}{F}\ln 4$.

Figure 6.1 shows concentration-potential and current-potential curves calculated assuming unfavorable energetics (first reduction makes second more difficult by 100 mV). Figure 6.2 was calculated assuming the first electron transfer more favorable energetically. Note that the results of the equations above are duplicated in the graphical determination of E^F's.

Transposition from the notation used here to the notation of Polcyn and Shain[4] is quite simple. They considered the reaction sequence:

$$A \overset{E_1^o}{\rightleftharpoons} A^- \overset{E_2^o}{\rightleftharpoons} A^{-2} \qquad (6.11)$$

These E_1^o and E_2^o are identical to the E_1^F and E_2^F of the treatment given here. Thus, for interacting dimeric centers, it is always necessary to include the factor of $\frac{RT}{F}\ln 4$ when converting from the formalism of eqn (6.11) to that employed here. Extension of this simple calculational method to polymers obeying linear free energy relationships with respect to number of sites oxidized or reduced should be trivial.

An example in which the statistical factor was properly taken into account was the study[7] of the electron

FIGURE 6.1

A. Calculated fractional concentration-potential curves for dimeric molecule with interaction. $E_1^o - E_2^o = 100$ mV. Curve (1): $f_{o,o}$; Curve (2): f_1; Curve (3): $f_{R,R}$.

B. Current-potential curves for same molecule. Current referred to hypothetical monomer limiting current of same diffusion coefficient. Note that the potentials corresponding to $\frac{i}{i_d} = 0.5$ and 1.5 are almost exactly equal to E_1^F and E_2^F respectively.

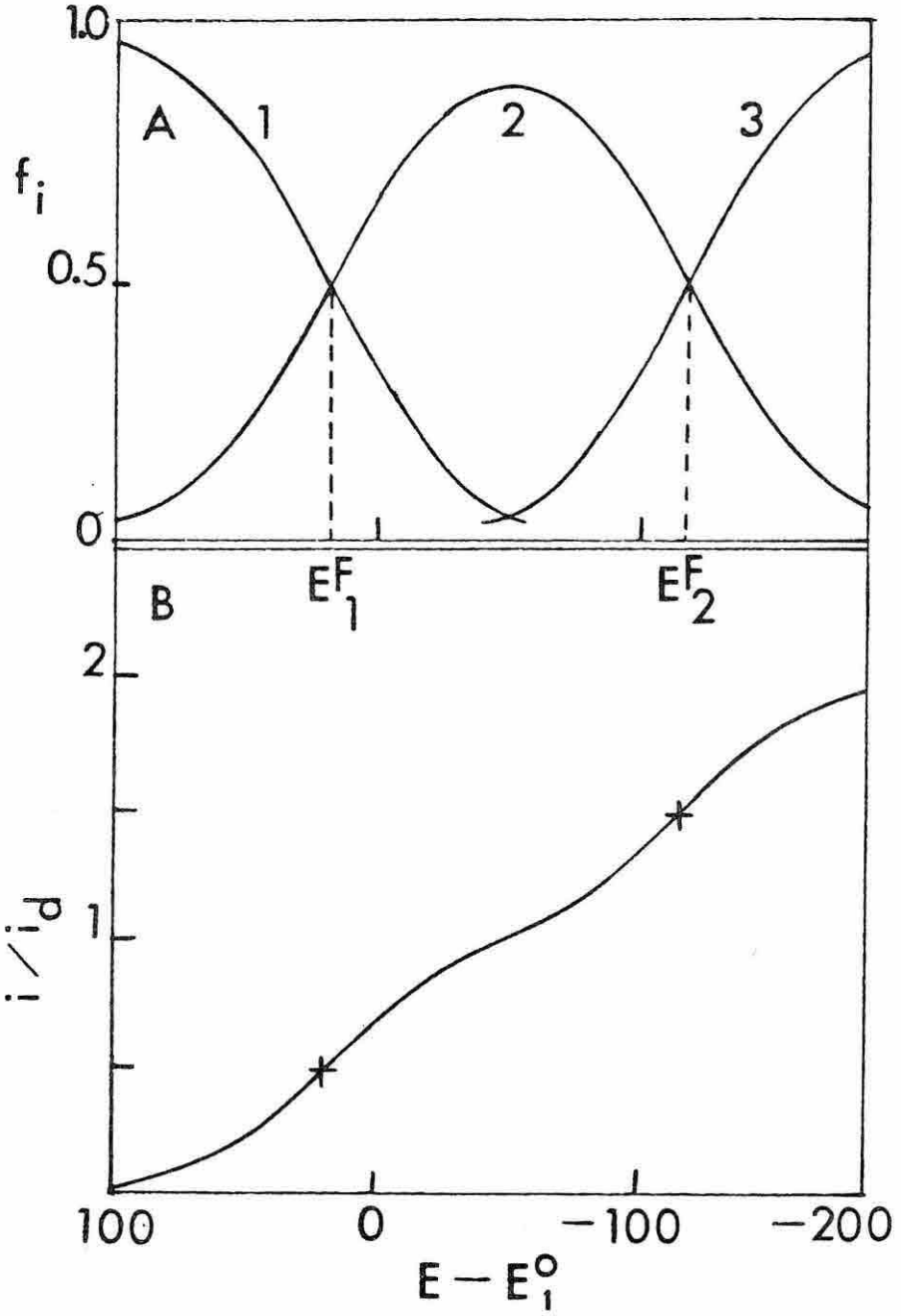

FIGURE 6.1

FIGURE 6.2

A. Calculated fractional concentration-potential curves for dimeric molecule with interaction. $E_1^o - E_2^o = -100$ mV. Curves have corresponding significance to Fig. 6.1.

B. Current-potential curves for same molecule. Current normalized as in Fig. 6.1. Potentials corresponding to $\frac{i}{i_d} = 0.5$ and 1.5 no longer equal E^F's.

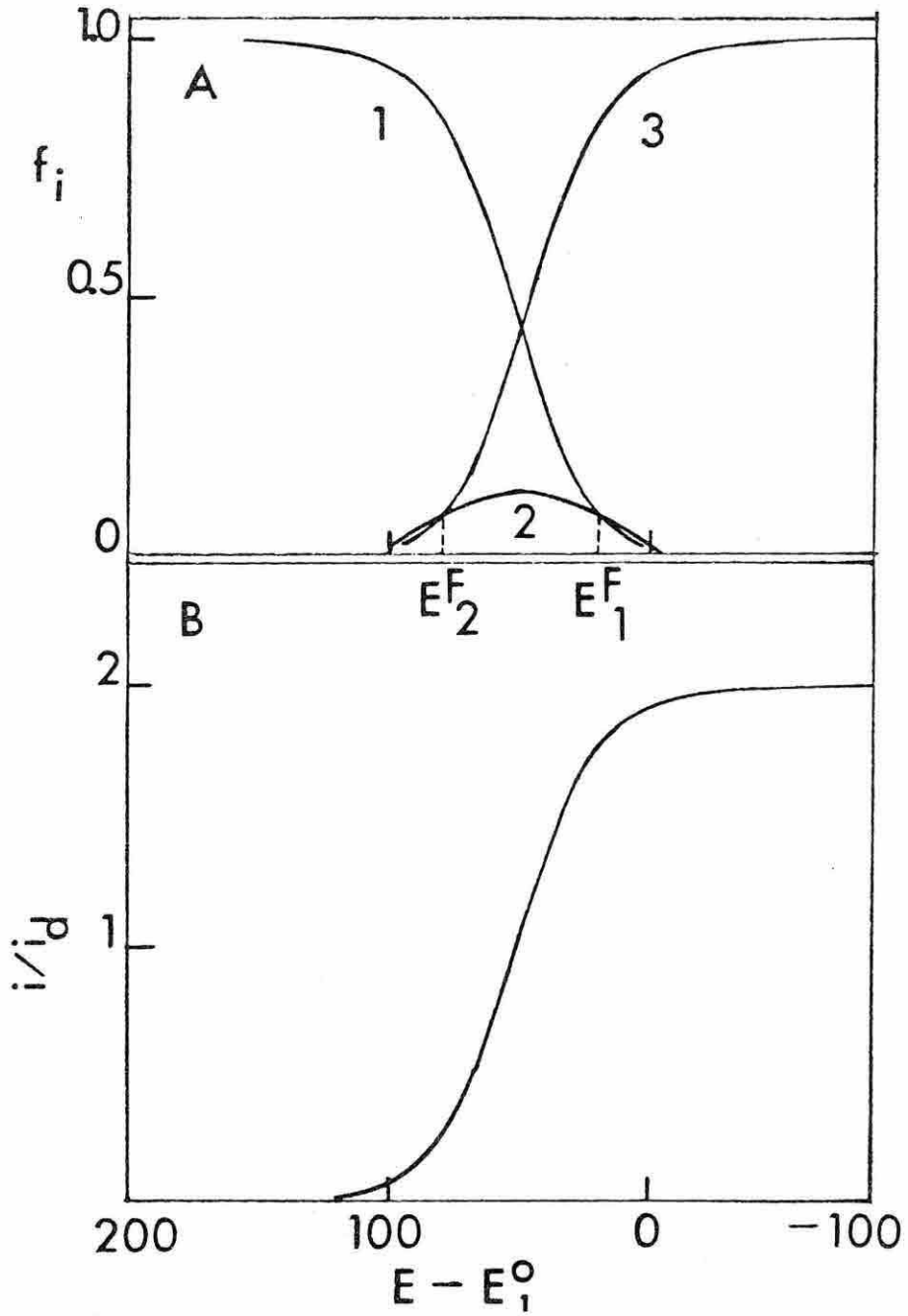

FIGURE 6.2

transfer and intervalence transitions of the compound $[(bpy)_2ClRu(pyz)RuCl(bpy)_2]^{+2,+3,+4}$. The authors found two waves for the couples denoted [3,3]/[2,3] and [2,3]/[2,2] where the abbreviations stand for the oxidation states of Ru in the compound. The waves appeared to be separated by ca. 120 mV, from which they calculated that the conproportionation constant, $K = [2,3]^2/[2,2][2,2]$, equal to about 100. Examination of Fig. 6.1 shows that even with closely spaced waves (ΔE^F = 136 mV), the "half wave potentials" of each of the poorly resolved waves (i.e., potentials corresponding to 0.25 and 0.75 of the eventual limiting current) correspond almost exactly to the E^F's from the concentration-potential curves.

Binuclear Noninteracting Electron Transfer Sites. For a molecule A-B composed of two nonidentical electron transfer sites, it is desired to calculate current-potential behavior. Since the centers are noninteracting, the standard potential E_A^o of center A is constant independent of the state of site B, and likewise for the standard potential E_B^o of site B. The fractions of the A or B sites oxidized or reduced are given by the nernst equation:

$$\theta_A = \frac{f_{oR}}{f_{RR}} = \frac{f_{oo}}{f_{Ro}} = \exp\left[\frac{nF}{RT}(E - E_A^o)\right] \qquad (6.12)$$

$$\theta_B = \frac{f_{Ro}}{f_{RR}} = \frac{f_{oo}}{f_{oR}} = \exp\left[\frac{nF}{RT}(E - E_A^o)\right] \qquad (6.13)$$

Where the f_{oR} etc denote concentration fractions: the first subscript is the state of center A; the second, center B. The compounds A_{ox}-B_R and A_R-B_{ox}, corresponding to the fractions f_{oR} and f_{Ro} respectively, are of course chemically different. It is useful, however, when spectroscopic or other methods for distinguishing these two species are for some reason not available and since electrons from either center are indistinguishable, to add their concentrations together and refer to them collectively as that fraction with one center oxidized and one center reduced, denoted f_1:

$$f_1 = f_{oR} + f_{Ro} \qquad (6.14)$$

The conservation of mass condition is:

$$f_{oo} + f_1 + f_{RR} = 1 \qquad (6.15)$$

From the above equations it is possible to derive expressions for the fractions of each species:

$$f_{oo} = \theta_A\theta_B/(\theta_A\theta_B + 1 + \theta_A + \theta_B) \qquad (6.16)$$

$$f_1 = (\theta_A + \theta_B)/(\theta_A\theta_B + 1 + \theta_A + \theta_B) \qquad (6.17)$$

$$f_{RR} = 1/(\theta_A\theta_B + 1 + \theta_A\theta_B) \qquad (6.18)$$

The Q function denoting the charge passed to bring N_T moles of completely oxidized compound to equilibrium with an electrode at potential E is:

$$\frac{Q(\theta_A,\theta_B)}{N_T F} = 2f_{RR} + f_1 = (2 + \theta_A + \theta_B)/(\theta_{A\ B} + 1 + \theta_A + \theta_B) \qquad (6.19)$$

It is convenient to extend the analogy with Polcyn and Shain,[4] and derive "formal potentials" for the couples f_{oo}/f_1 and f_1/f_{RR}. This choice of reference potential allows transposition to the following formalism:

$$(A\text{-}B) \overset{E_1{}^F}{\rightleftharpoons} (A\text{-}B)^- \overset{E_2{}^F}{\rightleftharpoons} (A\text{-}B)^{-2} \qquad (6.20)$$

Thus the E^F's can be extracted by mathematical analysis already developed for this simple mechanism.

The "formal potential" $E_1{}^F$ is defined as that potential at which $f_{oo} = f_1$ and $E_2{}^F$ such that $f_1 = f_{RR}$:

$$E_1{}^F = \frac{RT}{F}\ln\left(e^{-\frac{F}{RT}E_A{}^o} + e^{-\frac{F}{RT}E_B{}^o}\right) + E_A{}^o + E_B{}^o \qquad (6.21)$$

$$E_2{}^F = \frac{-RT}{F}\ln\left(e^{-\frac{F}{RT}E_A{}^o} + e^{-\frac{F}{RT}E_B{}^o}\right) \qquad (6.22)$$

Results calculated from these equations reveal that the statistical factor of $\frac{RT}{F}\ln 4$ between formal potentials

similarly defined for the symmetrical dimer case, both with and without interaction, is no longer constant and decreases rapidly as E_A^o and E_B^o diverge. Table 6.1 illustrates this behavior.

From the table it will be seen that for ΔE^o up to about 10 mV, the resulting wave is indistinguishable from an ordinary one-electron wave. For larger splittings observed in the wave it is necessary to apply results of the equations to calculate that portion due to the statistical factor. For very large splittings it is incorrect to use a statistical correction at all.

When a binuclear molecule of this type exhibits interaction between centers, it is necessary to determine if the a priori probability (i.e., the E_A^o and E_B^o) of reduction of one center is significantly different than the other, when both sites are oxidized. If so, it will be necessary to decrease the statistical correction below that applicable to the case of identical interacting centers.

The approach above using the nernst equation to derive equilibrium conditions as a function of potential and combining these with simple statistical theory has the advantage of being intuitively simple and providing concentration fractions and currents directly. Identical results could be obtained by a route couched in the

TABLE 6.1

Statistical Factors for Binuclear, Noninteracting Centers

(T = 298° k)

$\lvert E_A^o - E_B^o \rvert$	ΔE^F	$\Delta E^F_{STATISTICAL}$
0 mV	35.62 mV	35.62 mV
1	35.63	34.63
5	35.86	30.86
10	36.59	26.59
20	39.42	19.42
50	56.86	6.86
100	101.04	1.04
200	200.02	0.02

traditional thermodynamic formulation.[3] Some of the simple equations of thermodynamics may be invoked to enhance understanding. For example, the well known expressions, $\Delta G = -nF\Delta E$ and $\Delta G = \Delta U - T\Delta S$, where ΔG is free energy; ΔE is equilibrium potential; ΔU is enthalpy of reaction; ΔS is entropy and n, F and T have their usual significance. One observation which can be made from these simple equations is that energetic and entropic terms can affect the equilibrium potentials completely independently. Thus, in the section on dimeric interacting centers earlier in this chapter, it was shown that the entropic part of the wave separation was constant independent of the energetic part.

A case in which energetics does directly affect the entropic term is illustrated in this section on asymmetric noninteracting centers. In this case, the difference in standard potential of the two centers causes a change in the statistical contribution to the "formal potential" difference. It is possible to solve for the statistical contribution by considerations similar to those of Benson.[3]

For the molecule A-B where center A is more easily reduced than B, $E_A^o > E_B^o$. The probability p_A that A is reduced is:

$$p_A = \frac{1}{1 + \theta_A} \qquad (6.23)$$

and for site B reduced:

$$p_B = \frac{1}{1 + \theta_B} \tag{6.24}$$

from (6.12) and (6.13), we have

$$p_B = p_A \exp\left(\frac{nF}{RT}(E_2^o - E_1^o)\right) \tag{6.25}$$

If $p_A = p_B$, then we would have an (entropic) formal potential difference of $2\frac{RT}{F}\ln 2$ for a two center symmetric molecule. Since $p_B < p_A$, it is convenient to say that the molecule contains one-and-a-fraction A type centers. That is, the molecule contains the equivalent of $(1 + \frac{p_B}{p_A})$ centers of type A. From this point it is easy to invoke the arguments of Benson[3] with the result that,

$$\Delta E^F_{\text{STATISTICAL}} = 2\frac{RT}{F}\ln\left(1 + \exp\left(\frac{nF}{RT}(E_2^o - E_1^o)\right)\right) \tag{6.26}$$

which gives results identical with the last column of Table 6.1.

The study of bi-, ter- and quaterferrocenes of Brown et. al.[6] offers an opportunity to speculate on the operation of the factors reported here and in the previous chapter. These compounds, in which the ferrocene residues are directly linked without intervening atoms by single bonds between rings, exhibit cyclic voltammograms which have as many reversible waves as there are ferrocene residues in the compound. All such waves appear to be approximately reversible by the criteria of the authors.[6] This appears to be clear evidence for interactions of the type discussed in the first part of this chapter. Table 6.2 reproduces some of the observations for halfwave potentials for these compounds, ferrocene to quaterferrocene. The roughly equal separation of waves in quaterferrocene and the roughly equal average of the $E_{1/2}$ values from one compound to the next, suggests that a sort of linear free energy relationship exists between net charge and redox potentials. These compounds further illustrate the point of the second part of this chapter, that although two different sites exist in ter- and quaterferrocene (i.e., -fc- and fc-), the waves still appear to be reversible. Any small difference in intrinsic standard potential between the two types of sites was probably compensated for by the ΔE_{STAT}.

Table 6.2

Electrochemical Data for 1,1'-polyferrocene Compounds. Data from Brown et al.[6]

Compound	$E_{1/2}(1)$	$E_{1/2}(2)$	$E_{1/2}(3)$	$E_{1/2}(4)$	Average $E_{1/2}$
Ferrocene (fc)	0.40				0.40
Biferrocene (fc-fc)	0.31	0.65			0.48
1-1'-Terferrocene (fc-fc-fc)	0.22	0.44	0.82		0.49
1-1'-Quaterferrocene (fc-fc-fc-fc)	0.16	0.36	0.61	0.89	0.51

REFERENCES

(1) J. B. Flanagan, S. Margel, A. J. Bard and F. C. Anson, J. Am. Chem. Soc., Submitted for publication.

(2) F. Ammar and J. M. Savéant, J. Electroanal. Chem., 47, 115, 215 (1973).

(3) S. W. Benson, J. Amer. Chem. Soc., 80, 5151 (1958).

(4) D. S. P. Polcyn and I. Shain, Anal. Chem., 38, 370 (1966).

(5) R. W. Callahan, F. R. Kecne, T. J. Meyer and D. J. Salmon, J. Am. Chem. Soc., 99, 1064 (1977).

(6) G. M. Brown, T. J. Meyer, D. O. Cowan, C. LeVanda, F. Kaufman, P. V. Roling and M. D. Ransch, Inorg. Chem., 14, 506 (1975).

CHAPTER VII

Large Step Coulostatics

INTRODUCTION

A relatively new electrochemical technique called coulostatics has been proposed by Reinmuth[1] and Delahay[2] which has certain advantages over existing techniques. The experiment consists of injecting a charge onto an electrode and observing the open-circuit potential decay with time because of an electrochemical process of interest. Experimental application of large step coulostatics as reported here has been very limited, primarily because of the mathematical difficulties of predicting the response curves for the general case. Various approximations[3,4] have been proposed, but the limitations on experimental conditions have proved so severe that other "large step" methods such as chronocoulometry and chronopotentiometry have been preferred. The approach used here is similar to that proposed by Reinmuth[3] - the numerical solution of integro-differential equations. This numerical technique has been applied to a variety of electrochemical situations by Nicholson.[5] This numerical technique is to be differentiated from "digital simulation"[6] in that no concentration profile is generated. For this reason it is somewhat less flexible in the handling of second or higher

order solution reactions. The integro-differential equation method is, however, very amenable to certain numerical "tricks" to accelerate convergence. This numerical solution can be combined with nonlinear regression analysis to provide quantitative evaluations for experimental unknowns, in this case k^s and α for a simple electrode reaction.

Coulostatics was first proposed and is of interest now because of several significant advantages over other techniques for observing electron transfer kinetics: 1) Because no current is passed during the experiment, IR drops in dilute solutions are avoided. 2) The instrumentation is, at least in principle, rather simple since it is not necessary to use extremely fast and accurate potentiostats in order to look at processes in the microsecond region. 3) Since a potential range is spanned by the decay transient, it is possible to see potential dependent behavior in a single experiment. There are, of course, some disadvantages: 1) Certain parameters must be known <u>a priori</u> to high accuracy, especially double layer capacity and concentrations and in certain cases, the standard potential. Diffusion coefficients are less important, but must be known to within about 10% for both species. 2) Double layer reorganization and RC time delay reduce the ability to work at very short times in dilute supporting electrolytes. 3) Reliable switches and data

acquisiton hardware must work in the time range of one microsecond.

The form of the coulostatic response curve is shown in Fig. (7.1). In this figure, E_{pre} is the pre-potential imposed on the electrode by a potentiostat before charge injection. This potential should be well below the standard potential so that no current flows. The purpose of pre-potentiostating the electrode is to insure that the double layer is charged and the electrode potential stable before charge injection. E_{init} is the maximum value of the voltage achieved the instant after injection. The dotted line represents ideal response, while the solid line indicates the nature of nonidealities in actual response due to the RC time constant of the injection capacitor discharging through the solution resistance. Another method of injecting charge is by current pulse methods. The curve in Fig. (7.1) can be divided into two regions. Region I is a section of the curve in which the potential is decaying rapidly and is controlled only by the hetergeneous electron transfer rate. If it were possible to extrapolate to t = 0 the initial slope would be dependent only upon the initial bulk concentrations and the effective rate constant at E_{init}. In region II, the slope is much smaller because of concentration polarization and back reaction if any. Although mass transfer seems

FIGURE 7.1

General representation of a coulostatic transient. E_{pre} - potential imposed by potentiostat before injection; t=0 - instant of injection; E_{init} - instantaneous potential achieved after "ideal" charge injection; Region I - region of greatest charge transfer information; Region II - region in which diffusion control becomes important.

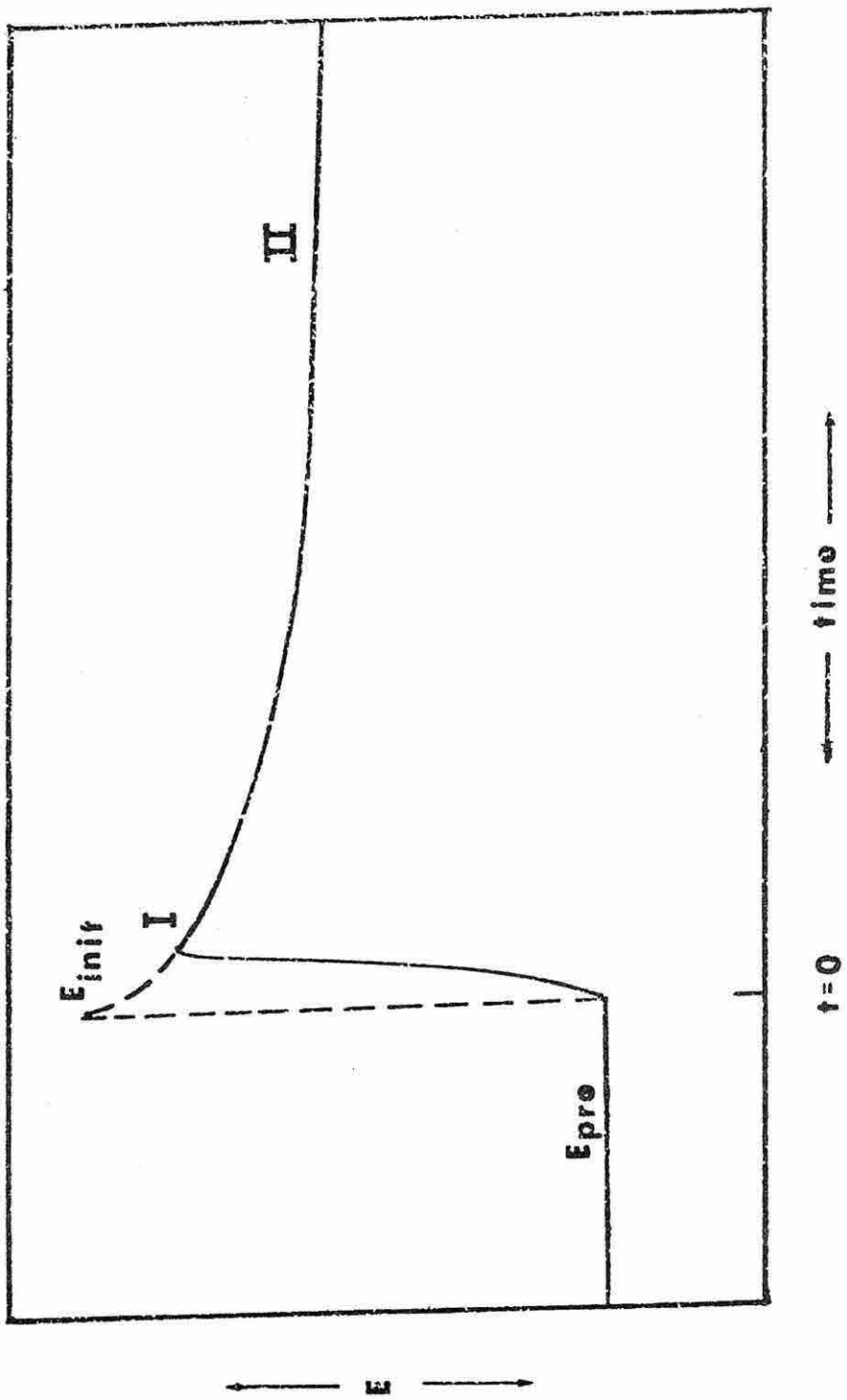

FIGURE 7.1

to be the limiting process in the potential decay, it will be shown that this region contains much useful information.

Instrumentation. A schematic diagram of the experimental setup used in the bulk of the experimental work is shown in Fig. (7.2). The working electrode may be solid, hanging mercury drop or dropping mercury. Because of the high precision required in drop area and surface reproducibility, a mercury electrode is preferred in the present study. Referring to the figure, C_{inj} is the injection capacitor, charged by V_{inj} which is on the order of 10 to 40 volts. A few microseconds before the charge is to be injected, the potentiostat is disconnected from the cell by opening S1. The follower is also disconnected at this time by S2 in order to protect it from the potential surge to be expected the reference electrode. Note that diode clamping of the follower will not work, since the current will flow through the reference electrode, causing its potential to shift from its equilibrium values. At t = 0, S3 is closed, injecting the charge that was on C_{inj} onto the working electrode. A few microseconds later S2 is closed again, reconnecting the follower which follows the potential decay and relays it to the data acquisition device, a fast A/D converter. The switches are driven and the data stored by the PDP 11/40 digital computer. The ability to switch and acquire data digitally on the

FIGURE 7.2

Block diagram of experimental setup.

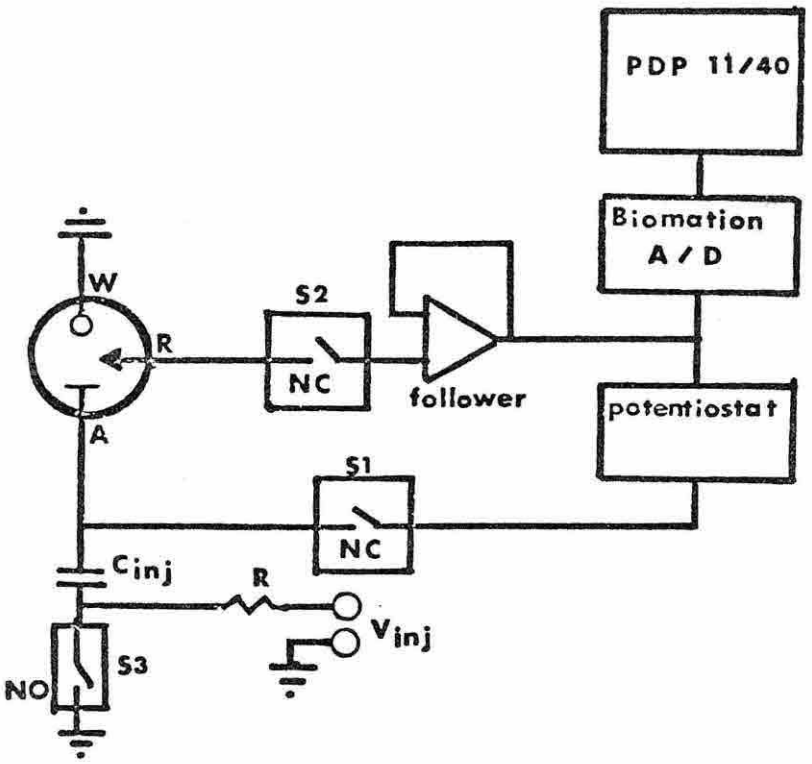
PDP 11/40
Biomation
A/D
potentiostat
follower
S2
NC
S1
NC
S3
NO
W
R
A
Cinj
R
Vinj

FIGURE 7.2

microsecond time scale has not been possible until recently with the advent of the laboratory computer. The switches are nonmechanical solid state devices made by Teledyne Co. The A/D conversion and rapid storage are done by a Biomation 802 transient recorder, which is capable of converting and storing 1000 8-bit data points in 500 microseconds. The follower which relays the analogue signal is a Burr Brown 3400B op-amp with extremely high slewing rate and frequency response. The potentiostat circuitry is not at all critical since the prepotential is applied for several seconds at low current.

The circuit described above is extremely simple but has the drawback that if solution resistance is high the RC injection time constant may become very long. An alternative approach is to apply a current pulse for a known time interval.

THEORETICAL

Electrode Kinetics. Let us now investigate the coulostatic experiment in more detail. The process of interest in the present work is the heterogeneous electron transfer process

$$A + ne^- \underset{k_r}{\overset{k_f}{\rightleftharpoons}} B \qquad (7.1)$$

The only restrictions on A and B are that they are soluble

in a liquid phase, either the solvent or the mercury electrode. Adsorption, homogeneous kinetics, double layer effects and similar complications will not be discussed in detail below, but are simple extensions of the approach.

The forward and reverse rate constants are given by the standard expressions (notation in Table 7.1):

$$k_f = k^s \left\{ \exp\left(\frac{-\alpha n F}{RT}(E-E^o)\right) \right\} \tag{7.2}$$

$$k_r = k^s \left\{ \exp\left((1-\alpha)\frac{nF}{RT}(E-E^o)\right) \right\} \tag{7.3}$$

Coulostatics takes advantage of the fact that the electrode immersed in the solution acts as a capacitor. A typical graph of differential double layer capacity as a function of potential in a simple electrolyte (0.01 m NaF) is shown in Fig. (7.3).[7] The differential capacitance is the quantity

$$C(E) = \frac{dq}{dE} \tag{7.4}$$

where q is double layer charge as a function of potential. Net capacity for a finite potential step is given by

$$C_{dl} = \frac{\int_{E}^{E+\Delta E} C(E)\,dE}{\Delta E} \tag{7.5}$$

Table 7.1

Summary of Notation

Symbol	Explanation	Units
E_{pre}	Potential just before charge injection	V
E_{init}	Potential just after charge injection	V
q	Injected charge	coul
V_{inj}	Voltage to which V_{inj} is charged	V
C_{inj}	Injection capacitance	fd
E(t)	Potential as a function of time	V
t	Time after injection	sec
R	Gas constant	1-atm/deg-mole
T	Temperature	°K
n	Number of electrons	--
F	Faraday constant	coul/mole
k_s	Apparent standard rate constant	cm/sec
C_A^o	Surface concentration of oxidant	moles/cm^3
C_B^o	Surface concentration of reductant	moles/cm^3
α	Transfer coefficient	--
D_A	Diffusion coefficient of oxidant	cm^2/sec
D_B	Diffusion coefficient of reductant	cm^2/sec
C^b	Initial bulk concentration of A	moles/cm^3

FIGURE 7.3

Typical double layer capacity-potential curve.[7]
Mercury electrode in aqueous 0.01 M NaF, 25° C.
Potentials referred to potential of zero charge.

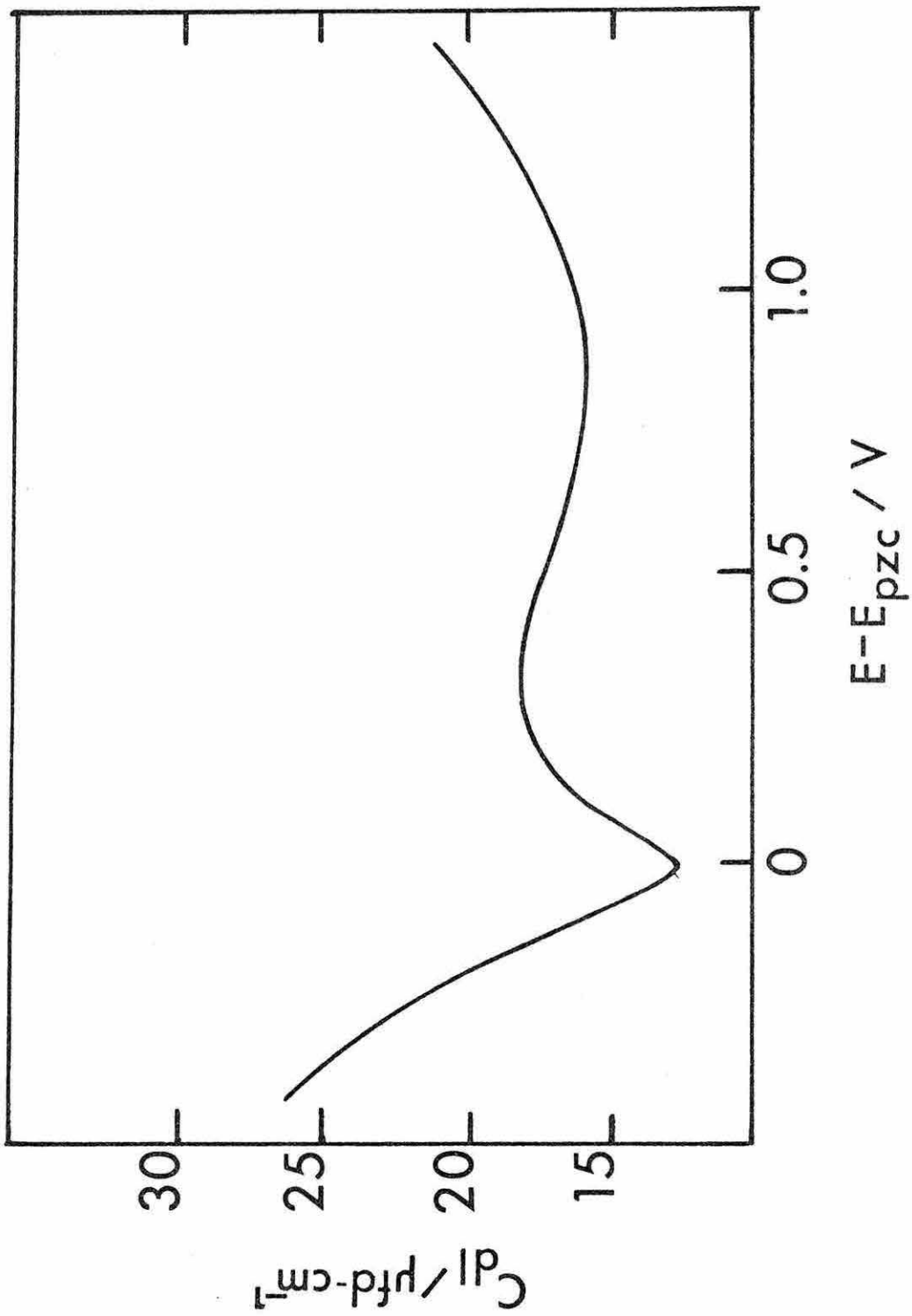

FIGURE 7.3

When C(E) is relatively constant as at potentials well anodic of the zero charge potential, the effective capacitance is very close to the differential capacitance. Capacitance of the electrode will be considered constant in the analysis below although it is simple extension to use an empirical fit of C vs. E in the simulation. Using this approximation, the initial charge injected on an electrode of double layer capacitance C_{dl} and area A is given by

$$\Delta E = \frac{C_{inj} \cdot V_{inj}}{C_{dl} \cdot A + C_{inj}} \tag{7.6}$$

If C_{inj} is small in comparison with $C_{dl} \cdot A$, this becomes

$$\Delta E \approx \frac{C_{inj} \cdot V_{inj}}{C_{dl} \cdot A} \tag{7.7}$$

If C_{inj} is not small its effect must also be considered in the more complex relations to follow. In order to avoid this, C_{inj} is kept at about 0.1% of the total electrode capacitance or about 500 - 2000 pfd. The current pulse technique, of course, has very low load capacitance.

Let us now consider the events taking place during the course of a single experiment in more detail. The DME is knocked from the capillary when a pulse is sent to the drop knocker from the computer. The computer times the

life of the drop from this point. While the drop is growing the prepotential E_{pre} is imposed on the electrode. If no current is drawn at this potential, no potential relaxation will occur during the period between disconnectio of the potentiostat and the time at which charge is injected. The potential then takes an excursion from E_{pre} to E_{init} which is $E_{pre} + \Delta E$ (from eqn. (7.7). The potential will then relax toward the prepotential as electrons charging the double layer are consumed in a Faradaic process. The general equation governing the rate of this process is

$$\frac{dq}{dt} = nF\frac{dA}{dt} = k_r C_B^o - k_f C_A^o \qquad (7.8)$$

where $\frac{dA}{dt}$ is the conversion rate of species A, and the C^o are surface concentrations of the two species refered to in eqn. (7.1). The change in potential as a result of this process is

$$\frac{dE}{dt} = \frac{1}{C_{dl} \cdot A}\frac{dq}{dt} \qquad (7.9)$$

The problem which must be solved by simulation is the derivation of the C^o as a function of time, a problem involving diffusion to an electrode of varying potential.

Data acquisition on the Biomation transient recorder is initiated by the computer at the same instant that the

switch injecting the charge is closed. Total acquisition time can range from 500 microseconds to 500 milliseconds, the range being chosen as a function of the magnitude of the standard rate constant k^s and the potential. As will be shown below, the information content varies widely with the rate of the process. A few (less than 30) data points are selected from the digitized data for least squares nonlinear regression analysis. Since the curve is rather uninteresting visually, the conventional approach of comparing the experimental transients with complete "working curves" generated by simulation is not the approach of choice. Only a few points from the curve need be selected since the curve is monotonic and if a smoothing procedure is used on the raw data, not much additional information is gained by using additional points. For the purposes of the information density study it was found that 5 generated data points including typical random errors contained enough information to very adequately fit k^s and α.

Nonlinear Regression. Nonlinear regression refers to methods of evaluating implicit parameters in equations of the form

$$Y_i = f(x_i^1, x_i^2, \ldots; a_1, a_2, \ldots; b_1, b_2 \ldots) \qquad (7.10)$$

where the x_i are independent variables such as time, injection charge, etc., which serve to distinguish data points. The a_1, a_2... are the parameters to be determined - in this case k^s and α. The b_1, b_2... are constants such as diffusion coefficients, concentration and temperature which are not varied independently and which are the same for all points in a single fit. The parameters to be determined are varied systematically in order to minimize the sum of squares of the deviations S^2:

$$S^2 = \sum(Y_i - y_i)^2 \qquad (7.11)$$

where the y_i are experimental data points and Y_i are the function evaluations using a trial set of unknowns. The procedure for locating the minimum is based on iterative numerical procedures for searching the S^2 hypersurface. The method used in this study is that due to Marquardt.[8] The fortran programs for this segment of the problem were adapted from Bevington.[9] The Marquardt procedure is a very fast efficient method which is an empirical combination of gradient search and parabolic expansion methods. Gradient search is simply following the path of steepest descent on the S^2 surface. This method is good for convergence far away from the true minimum, because it will avoid false minima as long as S^2 decreases along some path to the true minimum. Near the minimum, however, it

becomes quite slow and inaccurate. The parabolic expansion technique involves taking the derivatives of S^2 numerically with respect to the "a" parameters and expanding the surface in a Taylor series truncated after the quadratic term. This method is valid only very near the true minimum where the surface is approximately parabolic. In the Marquardt combination, these procedures complement each other to make a very fast and accurate routine. Another advantage of the Marquardt program is that the curvature of the S^2 surface is known at its minimum. This curvature may be used to estimate information density, since the steeper the curvature, the more precise the estimate of the true value of the unknown. This is analogous to a Gaussian distribution in which the standard deviation is related to the curvature and therefore the width of the curve.

Since the fitting routine is an empirical iterative process, the function Y in eqns (7.10) and (7.11) must be called many times, typically 10 - 50 times per data point. Since the numerical derivatives of S^2 are taken by finite difference of two function evaluations, the function must be highly accurate and consistent. In order to use a digital simulation for the generating function Y, it was necessary to satisfy both of these criteria simultaneously. This problem has now been partially solved using classical numerical techniques.

Numerical Methods. Digital simulation refers to numerical techniques used to model physical problems mathematically, using a digital computer to carry out the extensive iterative calculations usually required. In electrochemistry, simulation is used to solve diffusion-boundary value problems which frequently arise. A typical electrochemical simulation consists of some or all of the following: diffusion, heterogeneous kinetics, hydrodynamics, complex geometric complications, homogeneous kinetics, adsorption and double layer effects. The central problem is that of diffusion-boundary value problem, which is coupled to the other features in a complex way. A large amount of work has been done on simulating the diffusion problem alone because of its importance in heat conduction problems which arise in many engineering applications. When the other conditions of the experiment are suitably coupled to the diffusion problem, the computer can approximate the behavior of the experiment. In recent years, digital simulation has been used to model thin layer electrodes,[10] ESR cells,[11] homogeneous kinetics in solution preceeding or following the electrode reaction,[12,13] perturbations in response due to geometry,[14] and the geometric and hydrodynamically complicated problems of the rotating ring-disk[15,16] and tubular electrodes.[17] At least two major approaches have appeared in the electrochemical literature.

The first, due to Nicholson,[5] is based on calculation of the semi-integral of the current numerically. In the second method, popularized by Feldberg,[6] and discussed in many engineering texts (e.g., reference 18), a diffusion profile is calculated explicitly. The second method is considerably more general than the first in its ability to handle arbitrarily complicated problems, but it has the drawback of being somewhat slower due to the necessity of calculating a large number of concentrations in the diffusion layer. The latter approach was used in Chapters II, III and IV and will not be discussed here. The integral equation method of Nicholson has been modified for the coulostatic work.

In this method the problem is couched in integral equation form which still requires numerical techniques to evaluate. Because of the preliminary mathematical processing required in setting up the integral equations, this approach may under certain circumstances be more limited than the simulation based on explicit calculation of the diffusion profiles. Such cases include solution reactions and two dimensional diffusion.

For coulostatics the appropriate integral equation is given by Reinmuth:[3]

$$C_{dl}\frac{dE}{Dt} = nFk^{s}\left\{C_{A}^{b} - (nF(\pi D_{A})^{\frac{1}{2}})^{-1}\int_{0}^{t}\frac{C_{dl}(dE/d\tau)}{\sqrt{t-\tau}}\,d\tau\right\}$$

$$\cdot \exp((-\alpha nF/RT)(E-E^{o}))$$

$$-nFk^{s}\left\{C_{B}^{b} - (nF(\pi D_{B})^{\frac{1}{2}})^{-1}\int_{0}^{t}\frac{C_{dl}(dE/d\tau)}{\sqrt{t-\tau}}\,d\tau\right\}$$

$$\cdot \exp((1-\alpha)nF/RT)(E-E^{o})) \qquad (7.12)$$

Note that the integral expression in the above is identical to the semi-integral which has been used recently in other electrochemical studies.[19,20,21] The only other place in eqn (7.12) where finite differences are necessary is in calculation of the integral. Since the quantity dE/dt is already known as a function of time, the integral can be approximated as a sum:

$$\int_{0}^{t}\frac{dE/d\tau}{\sqrt{t-\tau}}\,d\tau \approx \sum_{j=1}^{n=t/\Delta t}\frac{\Delta E}{\sqrt{n-j+1}} \qquad (7.13)$$

For the first iteration from t = 0 to t = Δt, the integral is taken to be zero. Subsequent iterations calculate the surface concentration by means of the sum in eqn (7.13). Note the similarity between eqn (7.12) and eqn (7.8). The expressions in brackets are the instantaneous surface concentrations. For the coulostatic simulation, eqn (7.12)

was evaluated as in implicit difference equation in ΔE.

A Method of Accelerating Convergence. In this simulation approach an error in time of order Δt to the first power is the leading term of the truncated Taylor series. It is possible to use this fact in order to increase the speed and accuracy of the simulation, something which is very desirable when it is to be used as a fitting function. If $f(t)$ is the true value of a function and $f_j'(t)$ is an approximate numerical value achieved after j iterations, then since $\Delta t = t/j$, we have:

$$f(t) = f_j'(t) + \varepsilon_1(\Delta t) + \varepsilon_2(\Delta t) + \ldots \qquad (7.14)$$

by doubling the number of iterations, we have,

$$f(t) = f_{2j}' + \varepsilon_1(\tfrac{\Delta t}{2}) + \varepsilon_2(\tfrac{\Delta t}{2}) + \ldots \qquad (7.15)$$

Subtracting eqn (7.15) from twice eqn (7.14) yields:

$$f(t) = 2f_{2j}'(t) - f_j'(t) + \varepsilon_2'(\tfrac{\Delta t}{2})^2 + \ldots \qquad (7.16)$$

The quantity $f_{2j}'' = 2f_{2j}' - f_j'$ is clearly a better approximation to the true value than either of the others. This procedure of doubling the number of interactions and eleminating terms

in the error series is widely known as the Richardson extrapolation method and has been applied in many different sorts of numerical calculations. By repeating the process above, succeeding terms in the series can be eliminated. This method applied to the coulostatic simulation has resulted in accuracy of 0.001% in only a few total iterations. It is to be noted that this technique will work only if the original simulations are convergent. Nonconvergent simulations cannot be saved. Table 7.2 shows results using the technique on a typical coulostatic simulation. The generating parameters are chosen to be somewhat similar to those of zinc and are given in Appendix A. This simulation is of a long time, 10000 μsec., and the first few results are therefore nonconvergent. Note that the 4-iteration row is missing because of overflow errors caused by violent nonconvergence. Following rows with larger numbers of iterations and smaller Δt begin to converge. The last two columns converge in a total of 127 iterations. After 512 iterations the uncorrected column has not quite converged. The saving in computation time is the ratio of the number of iterations squared, so the net savings is a factor of 16. The time required for the first 127 iterations is approximately 1.5 seconds on the PDP 11/40 with floating point hardware.

Table 7.2

An Example of a Coulostatic Simulation with Accelerated Convergence. Total time 10000.μsec. Other Parameters Given in Fig. 7.4.

j	f_j'	f_j''	f_j'''
1	0.11816E 00		
2	-0.20403E 02		
8	-0.13398E 00		
16	-0.13419E 00	-0.13441E 00	
32	-0.13439E 00	-0.13458E 00	-0.13464E 00
64	-0.13449E 00	-0.13460E 00	-0.13460E 00
128	-0.13455E 00	-0.13460E 00	-0.13460E 00
256	-0.13457E 00	-0.13460E 00	-0.13460E 00
512	-0.13459E 00	-0.13460E 00	-0.13460E 00

RESULTS AND DISCUSSION

Information Density Study. Before doing an experiment, it is necessary to determine time scale of the experiment which will yield optimum accuracy in the results. Since the reciprocal square root of the curvature of the S^2 surface is proportional to the standard deviation of the quantity involved, it was possible to use generated data to investigate the information content of coulostatic transients. Results of such a study are shown in Fig. 7.4, 7.5 and 7.6. Five equally spaced data points were generated, and they were used as input to the fitting routine. After the program had converged to the correct k^s and α, the "standard deviations" were scaled and plotted as a function of the interval between points. Figure 7.4 shows the information densities of k^s and α when the potential was stepped from an overpotential of +200 mV to +20 mV by means of an injection voltage of -50 v. The parameters used to generate the data are given in the caption of Fig. 7.4, and are similar to those for zinc reduction in a typical experiment. In this region, the reaction is rather slow and back reaction is very important. Also plotted in all these figures is the potential spanned by the five points used. The minima are quite pronounced and coincide with the maximum in the potential spanned by the points. This is exactly as would be expected, especially for α, since

FIGURE 7.4

Information density study for k^s and α. Five points used in fit. Interval between points = (time span)/5.

Parameters used for data generation and fit:

k^s=0.001 cm/sec; α=0.4; C_{dl}=20 μfd/cm^2;

C^b=1.0 mM; $D_A=D_B=10^{-5}$cm^2/sec; n=2.

Curve 1 - Potential spanned by the 5 data points

Curve 2 - σ_α

Curve 3 - σ_{k^s}

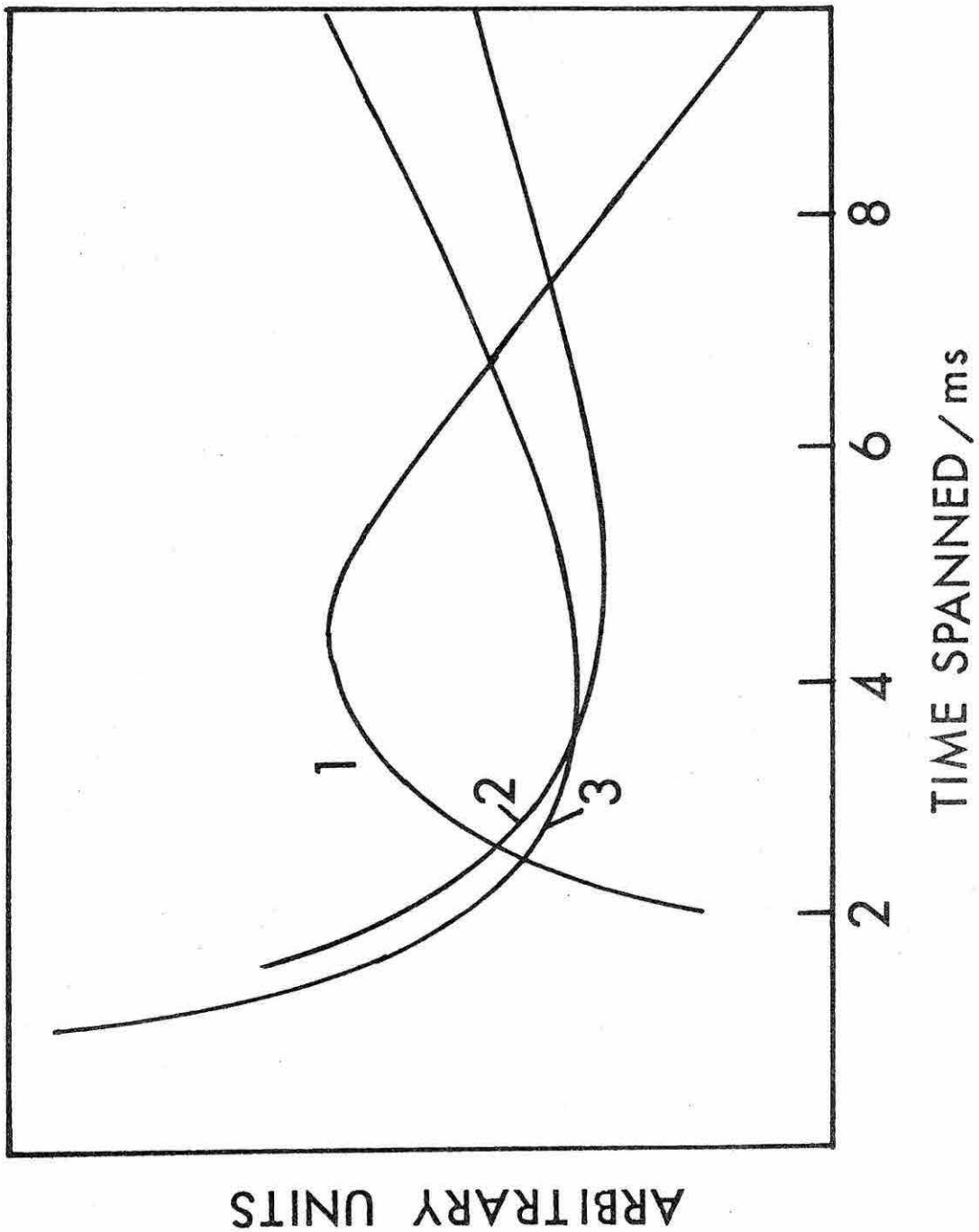

FIGURE 7.4

FIGURE 7.5

Information density study for k_s and α. Five data points used. Parameters and numbered curves as in Fig. 7.4. V_{inj}=-70 V.

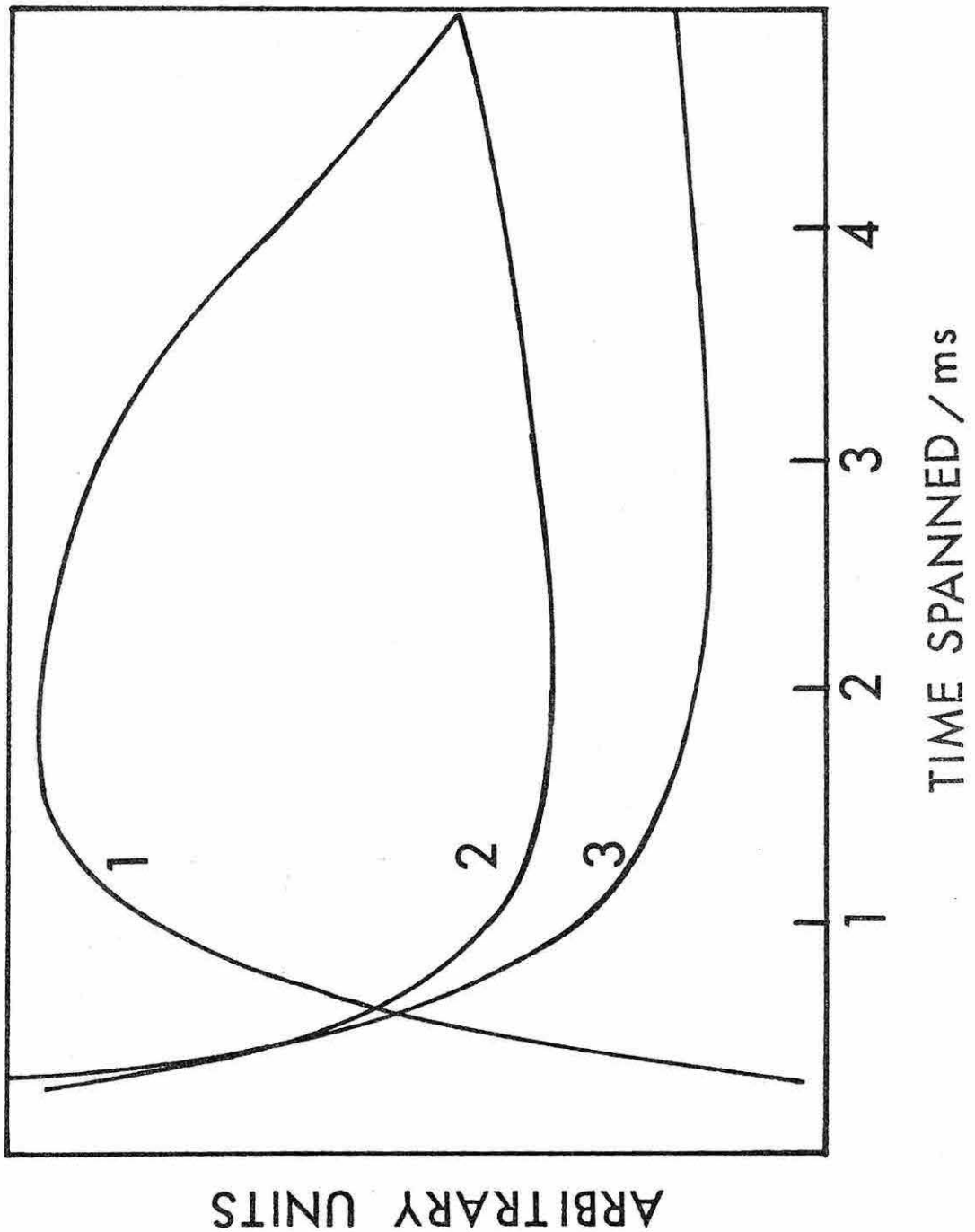

FIGURE 7.5

FIGURE 7.6

Information density study. V_{inj}=-80 V. Parameters and numbered curves as in Fig. 7.4.

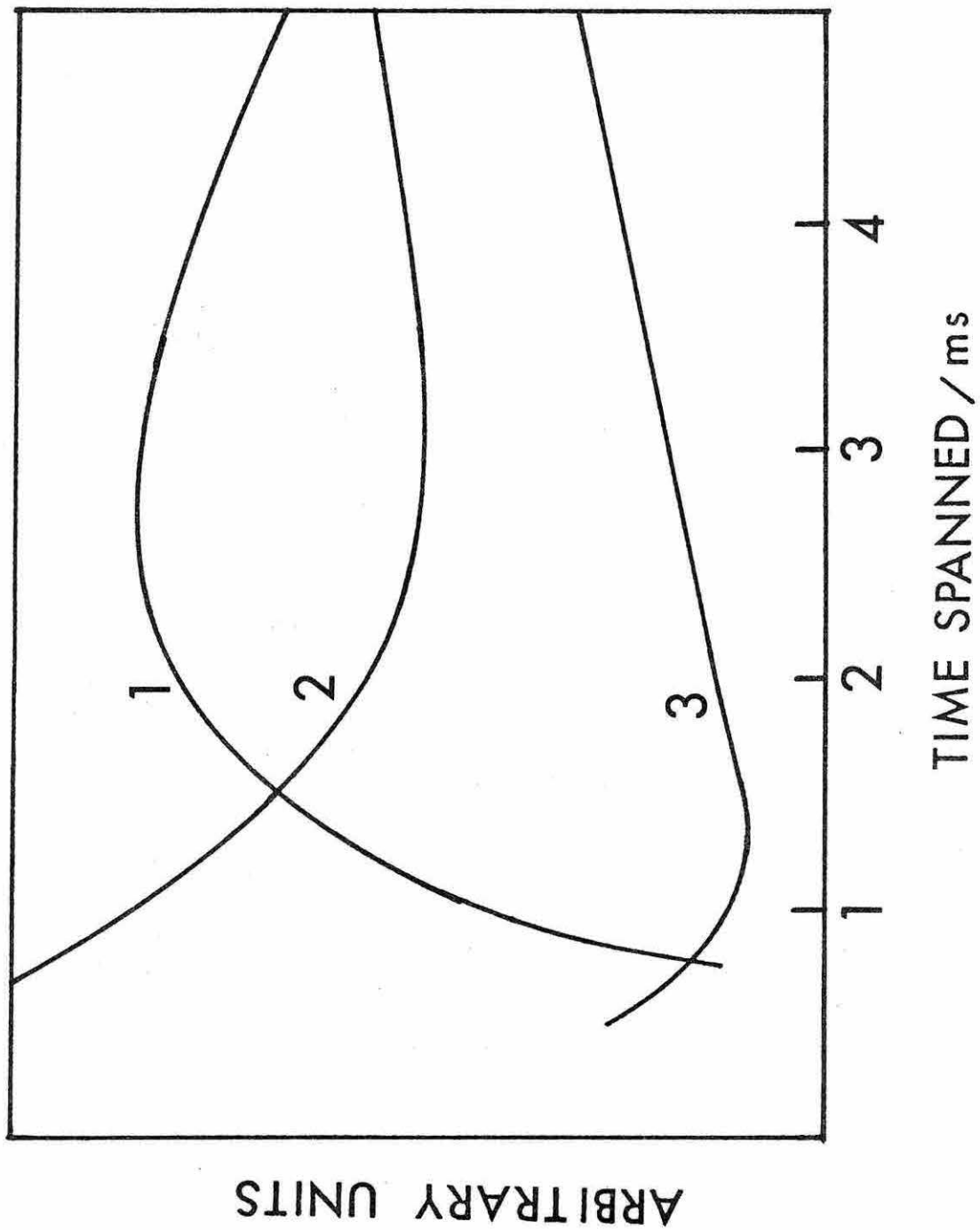

FIGURE 7.6

its influence on rate is especially pronounced as the potential changes. Figures 7.5 and 7.6 are the information studies for injection voltages of -70 and -80 volts respectively. The same general behavior is observed, but the minima occur at shorter times, as would be expected since the forward rate constants are faster at the higher overpotentials and concentration polarization would be expected to set in sooner. Figure 7.7 shows the raw transients generated by the simulation. The effect of concentration polarization can be seen at the trailing end of the transients.

Figure 7.4, 7.5 and 7.6 showed that near the beginning of the transient the information density is strongly dependent on potential span. In order to avoid this effect and to look directly at the information density in different parts of the curves, sections of one curve were sampled at constant potential span. Five equally spaced points were taken from different areas of the V_{inj} = -50 v transient. Since the slope of the curve was decreasing, it was necessary to take longer segments of the curve at longer times. The results are shown in Table 7.3. The effects of concentration polarization decreasing the available information is clearly evident here, although the potential span remains nearly constant.

Another effect which has been noted in these studies of generated data is that in some cases a sample of data

FIGURE 7.7

Simulated raw coulostatic transients. The potential axis is referenced to E_{pre}, which is 200 mV positive of E° for the A-B couple. Parameters as in Fig. 7.4.

V_{inj}: Curve 1, -80 V.

Curve 2, -70 V.

Curve 3, -60 V.

Curve 4, -50 V.

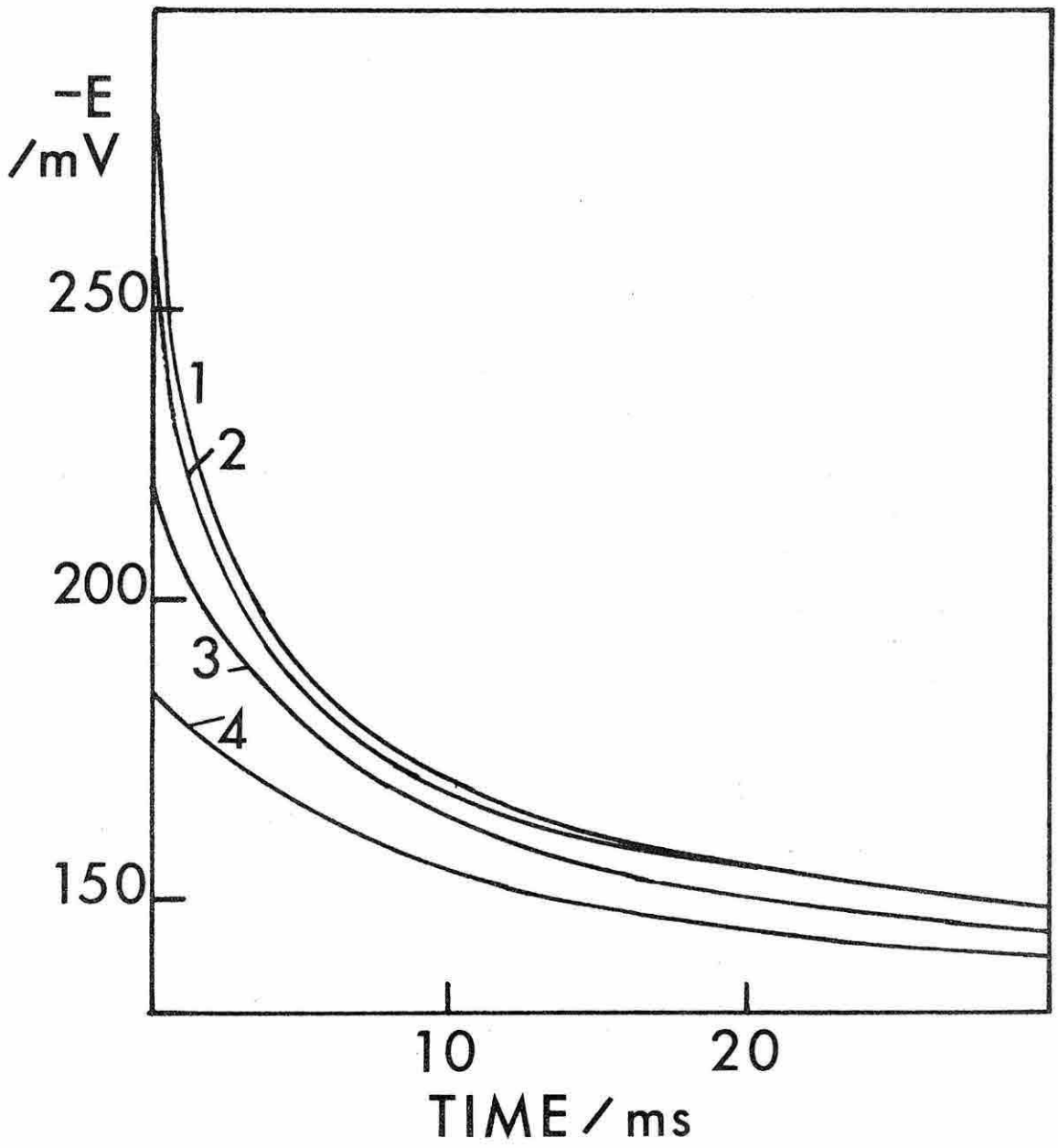

FIGURE 7.7

Table 7.2

Effect of Concentration Polarization Constant Potential Span of 10 mV. V_{inj} = -50 v.

Times sec	Pot1 mv	Pot1 Span mv	"σ_α"	"σ_{k^s}"
1000	-179.7			
1650	-176.6			
2300	-173.9	10.5	40.8	0.0721
2950	-171.5			
3600	-169.2			
10000	-154.5			
12500	-151.1			
15000	-148.3	10.2	156.6	0.454
17500	-146.1			
20000	-144.2			
30000	-139.4			
47500	-135.0			
65000	-132.6	9.8	487.8	1.84
82500	-130.9			
100000	0129.6			

taken in a narrow band of times may have higher information than samples taken over a much wider range. For example, Table 7.4 shows two simulation-fits of 5 data points each. The first fit is of points taken at 2000 μsec. intervals to 10000 μsec. The second is a fit to five points taken from the interval 6000 - 7000 μsec. Even though the potential span is much smaller in the second case, the information density is greater. This phenomenon has not been studied in detail, but it is possible that by taking closely spaced points, more information about the details of the curvature of the transient is available. A detailed study of other methods of sampling such as geometric spacing, random spacing or taking points from several transients could be done to optimize the experiment.

Error Propagation Study. A knowledge of the effects of inaccuracies in the parameters assumed as known for the fit is very important in assigning confidence limits in the results. This points out a problem with the coulostatic method, namely that preliminary experiments must be done to determine these constants to high accuracy. Probably the most important of these measurements is the very precise determination of the double layer capacitance which can be estimated with the coulostat using a blank solution, if it is assumed that the reactant does not change C_{dl}.

Table 7.4

Information Density of Closely vs. Widely Spaced Points.

V_{inj} = -80 v.

Time sec	Potl mv	Potl Span mv	"σ_α"	"σ_{k^s}"
2000	-215.6			
4000	-195.0			
6000	-180.5	52.0	3.69	0.0147
8000	-171.1			
10000	-163.6			
6000	-180.5			
6250	-179.2			
6500	-177.9	5.0	3.04	0.0078
6750	-176.7			
7000	-175.5			

The technique is similar to that of the previous section on information density - points are generated by simulation and then fit. Between generation of the raw data and the fit to that data, one of the assumed constants is changed slightly. It was found in general that even when such a change affected the fit values of k^s and α, the curvature of the S^2 surface as reflected in the information density coefficients remained rather constant. This can be expressed as the relative error derivative, RED, or the derivative of the relative change in k^s or α with respect to relative change in the parameter in question. For example,

$$RED_\alpha \equiv \{\text{rel. change in } \alpha\}/\{\text{rel. change in parameter}\} \quad (7.17)$$

Using the parameters in Appendix A and choosing 5 equally spaced points which yield maximum information density as determined in the previous section, the error propagation was studied for several different parameters. The results are shown in Table 7.5. The data were generated assuming $k^s = 0.001$ and $\alpha = 0.4$. The resulting values of k_s and α are shown as well as the RED for each case. Although these results are valid only for these numbers, they should be qualitatively similar for other electrode reactions following the simple mechanism of eqn (7.1). The results

Table 7.5

Error Propagation Study. Zinc Parameters (Fig. 7.4) Used. V_{inj} = -60 v., 5 points at 2500 μs. intervals.

Changed Parameter	α_{fit}	k^s_{fit}	RED_α	RED_{k^s}
$D_{ox}=D_r= 1.5 \times 10^{-5}$	.417	.00099	.085	-.02
$D_{oc}=1.1 \times 10^{-5}$	.400	.00100	small	small
$D_r = 1.1 \times 10^{-5}$	.404	.000999	.1	-.01
C_{ox} = .00101	.401	.000990	.25	-1.0
C_{dl} = 20.2	.382	.000971	-4.5	-2.9
C_{inj} = .00101	.415	.00104	3.95	4.0

show that diffusion coefficients are relatively unimportant but that parameters directly affecting the double layer capacitance or the initial potential have a large effect. For example, a 1% error in the double layer capacitance will induce a -4.5% error in α and a -2.9% error in k^s. This points out the high accuracy which must be maintained in calibrations and measurements before the experiment itself. Careful determination of the capacity-potential relationship is especially important and should be done with a blank solution on the same apparatus as the actual experiment. The effect of errors in the standard potential were not simulated since it could not be changed in the same way as the other parameters, but its effect is expected to be large. The accurate determination of this quantity must be done by a separate experiment such as D.C. polarography with correction for diffusion coefficients and for spherical diffusion. Large error propagation might be partially overcome by using other data sampling schemes or by changing the approach of the fit to include extrapolation to E_{init}. An analogous sort of extrapolation to zero time was done by Abel[22] to find the initial charge in a non-linear regression for chronocoulometry. There may be problems with this approach, however, since it introduces another adjustable parameter which might cause bias in the fit for k^s and α.

The $Zn^{+2}/Zn(Hg)$ Reaction and an Alternative Data Analysis Technique. An example of some experimental considerations in coulostatics is illustrated here by its application to the $Zn^{+2}/Zn(Hg)$ reduction, using a simplified data analysis scheme. The inherent experimental advantages of coulostatics - speed and usability with highly resistive solvents as well as the flexibility of the simulation method will be discussed in the context of this reaction.

Some question exists as to the mechanism of the Zn^{+2} reduction[23,24,25,26] because of a break in apparent transfer coefficient. The net reaction is:

$$Zn^{+2} + 2e^- \rightleftharpoons Zn(Hg) \qquad (7.18)$$

The break in apparent transfer coefficient can be explained quite easily in a qualitative way if the two step mechanism[26] is assumed:

$$Zn^{+2} + e^- \rightleftharpoons Zn^+ \qquad (7.19)$$

$$Zn^+ + e^- \rightleftharpoons Zn(Hg) \qquad (7.20)$$

Evaluation of eqn (7.12) at the instant of charge injection, yields:

$$\left(\frac{dE}{dt}\right)_{t=0} = \frac{nFC_A^b}{C_{dl}} k^s \exp\left(\frac{-\alpha nF}{RT}(E_{init} - E^o)\right) \qquad (7.21)$$

Taking the natural logarithm of both sides of eqn (7.21) yields,

$$\ln\left(\frac{dE}{dt}\right) = K + \frac{-\alpha n F}{RT}(E_{init} - E^o) \qquad (7.22)$$

where K is a collection of constants. If the quantity $\ln\left(\frac{dE}{dt}\right)$ at t = 0 is plotted against $E - E^o$, the slope will be $\frac{-\alpha n F}{RT}$. Such a diagram is similar to a Tafel plot with back reaction correction. Thus, if $\ln\left(\frac{dE}{dt}\right)_{t = 0}$ is plotted against $E_{init} - E^o$ the slope will be $\frac{-\alpha n F}{RT}$.

Figure 7.8 shows the results of a Tafel-like plot constructed from coulostatic data for 1.05 mM Zn^{+2} in 0.1 M $NaClO_4$ at a DME. Only oxidant was present in the bulk at the beginning of the experiment. The overpotentials available start at about +50 mV and extend cathodic to an overpotential of -300 mV. The transients all appeared similar to those in Figures 7.1 and 7.7. The t = 0 decay slope needed for the Tafel analysis was obtained by the crude but effective strategy of fitting the initial portions of the decay transient to a three-point parabola. The value of E_{init} was calculated from the known double layer capacity, drop area, and injection charge. The other two points needed for the parabola were obtained from the experimental transient. The slope of the parabola was then calculated at t = 0 and plotted as a function of

E_{init}. The error bars in the figure represent the scatter due to taking different points of the transient to define the parabola. Clearly, as the figure shows, the crude application of coulostatics qualitatively confirms the results. The simple parabolic fit method is rather useful in qualitative understanding of this electron transfer. This experiment shows clearly one advantage of coulostatics - its ability to deal with fast reactions at large overpotentials. Since there is no curvature or systematic deviation at these very high overpotentials, it is likely that the method might be used for even faster rates.

Attempted application of the nonlinear regression technique developed in the beginning of this chapter was not found to be very effective with an actual experimental system, $Zn^{+2}/Zn(Hg)$. Table 7.6 illustrates some of the results of the technique for the simultaneous fit of k^s, α and C_{dl} to raw data. Even when care was taken to include points in potential ranges in which one reaction step was rate limiting (i.e., on linear portions of the plot of Fig. 7.8), large uncertainties are found in the resulting parameters. This may be due to strong cross-correlations of parameters similar to effects to be discussed in Chapter VIII.

Table 7.6

Results of Large Step Nonlinear Regression Procedure on Raw Data for $Zn^{+2}/Zn(Hg)$ Systems.

$C^{b}_{Zn^{+2}}$ = 1.00 mM in 1M $NaClO_4$, pH 3

$D_{ox} = 8 \times 10^{-6}$, $D_R = 1.6 \times 10^{-5}$ cm^2/sec

$E^{o} = -1000$ mV vs. SCE

$V_{inj} = -8$ and -40 V, $E_{pre} = -800$ mV vs. SCE

$C_{inj} = .002 - .004$ µfd.

$A = 0.032$ cm^2

No. Points	V_{inj}	C_{inj}	Potl. Span	k^s	α	C_{dl}
--	V	µfd	V	cm/sec	-	µfd/cm^2
5	-40	.004	-1.227 - -1.099	.0025	.30	16.2
10	-40	.0025	-1.095 - -1.044	.0045	.20	16.8
	-40	.0020				
20	-40	.004	-1.227 - -1.044	.0048	.16	18.2
	-40	.003				
	-40	.0025				
	-40	.002				

FIGURE 7.8

Tafel-like plot generated by parabolic extrapolation of coulostatic transients. 1.05 mM Zn^{+2} in 0.1 M $NaClO_4$, pH 3. Values for αn were found to be 0.75 and 0.30 for the segments anodic and cathodic of the breakpoint potential.

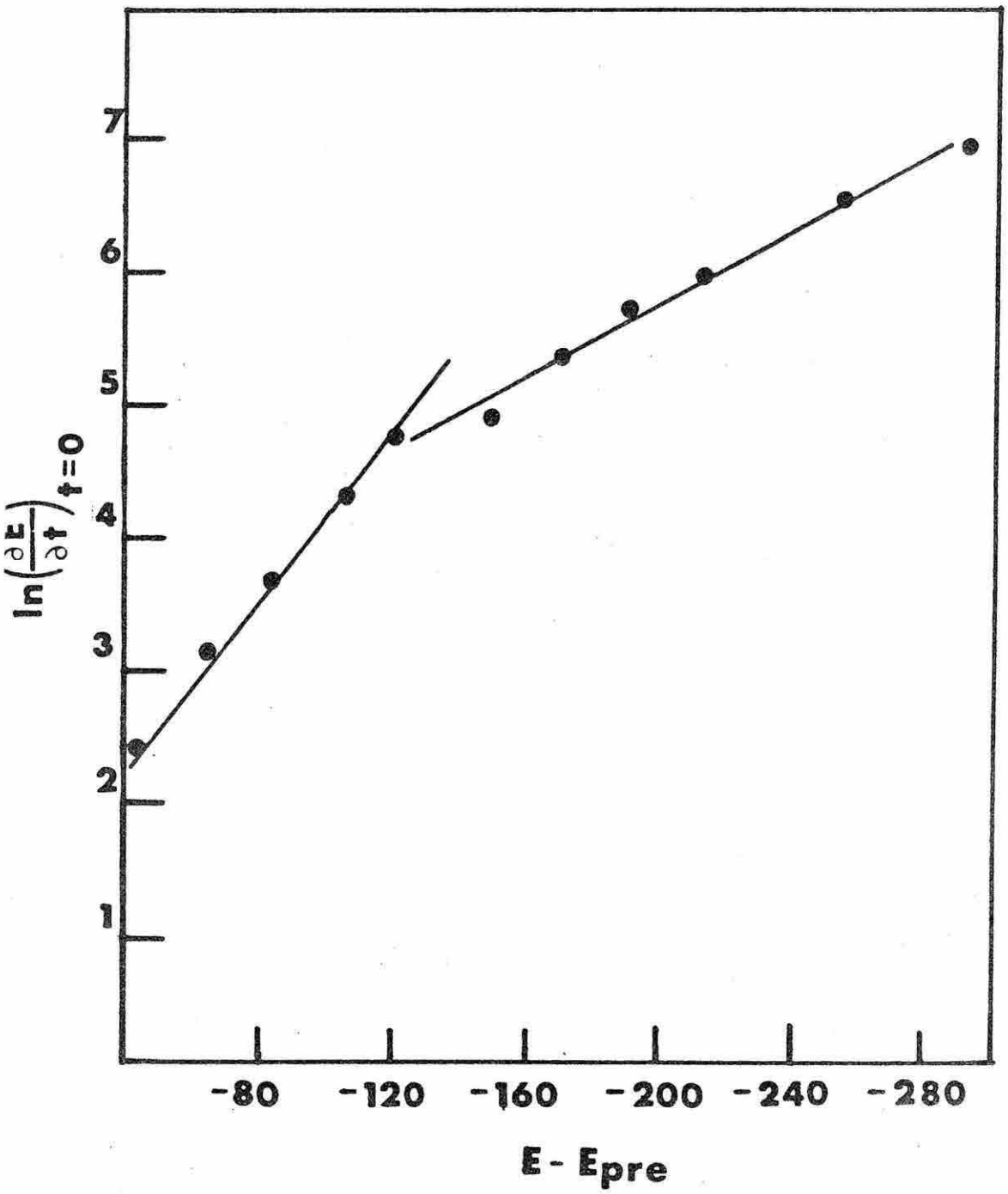
7
6
5
4
3
2
1
$\ln\left(\frac{\partial E}{\partial t}\right)_{t=0}$
-80
-120
-160
-200
-240
-280
E - Epre

FIGURE 7.8

REFERENCES

(1) W. H. Reinmuth and C. E. Wilson, Anal. Chem., 34, 1159 (1962).

(2) P. Delahay, Anal. Chem. 34, 1161 (1962).

(3) W. H. Reinmuth, Anal. Chem., 34, 1272 (1962).

(4) P. Delahay, Anal. Chem., 34, 1267 (1962),

(5) R. S. Nicholson, Anal. Chem., 37, 667 (1965).

(6) S. W. Feldberg, "Electroanalytical Chemistry, A Series of Advances," Vol. 3, A. J. Bard, Ed., Marcel Dekker, New York, N.Y., 1969, p. 199.

(7) D. C. Grahame, J. Am. Chem. Soc., 76, 4819 (1954).

(8) D. M. Marquardt, J. Soc. Ind. Appl. Math., 11, 431 (1963).

(9) P. R. Bevington, "Data Reduction and Analysis for the Physical Sciences," Mc Graw-Hill, New York, N.Y., 1969, Ch. 11.

(10) I. B. Goldberg and A. J. Bard, J. Electroanal. Chem., 38, 313 (1972).

(11) I. B. Goldberg and A. J. Bard, J. Phys. Chem., 45, 3281 (1971).

(12) M. D. Hawley and S. W. Feldberg, J. Phys. Chem., 70, 3459 (1966).

(13) L. Marcoux, J. Phys. Chem., 76, 3254 (1972).

(14) J. B. Flanagan and L. Marcoux, J. Phys. Chem., 77, 1051 (1973).

(15) A. J. Bard and K. B. Prater, J. Electrochem Soc., 117, 207 (1970).

(16) A. J. Bard and K. B. Prater, J. Electrochem. Soc., 117, 207 (1970).

(17) J. B. Flanagan and L. Marcoux, J. Phys. Chem., 78, 719 (1974).

(18) B. Carnahan, H. A. Luther and J. O. Wilkes, "Applied Numerical Methods," Wiley, New York, N.Y., 1969, Ch. 7.

(19) K. B. Oldham, Anal. Chem., 41, 1904 (1969).

(20) M. Grenness and K. B. Oldham, Anal. Chem., 44, 1121 (1972).

(21) J. C. Imbeaux and J. M. Savéant, Electroanal. Chem., 44, 169 (1973).

(22) R. H. Abel, Ph. D. Thesis. California Institute of Technology, 1971.

(23) J. Blackledge and N. S. Hush, J. Electroanal. Chem., 5, 435 (1963).

(24) P. Teppema, M. Sluyters-Rehbach and J. H. Sluyters, J. Electroanal. Chem., 16, 165 (1968).

(25) M. Sluyters-Rehback, J. S. M. C. Breukel and J. H. Sluyters, J. Electroanal. Chem., 19, 85 (1968).

(26) E. Eriksrud, J. Electroanal. Chem., 67, 69 (1976).

CHAPTER VIII

Alternative Data Analysis Schemes in the Use of Small Step Coulostatics with In Situ Generation of Reactants For the Measurement of Electrode Kinetics

INTRODUCTION

Small step coulostatics refers to the technique in which the charge injected onto an electrode perturbs the potential only a few millivolts from the equilibrium potential established before charge injection. This technique is valuable in the coulostatic evaluation of electron transfer rate constants because it allows closed-form equations describing the relaxation of potential toward the equilibrium potential to be used. The in situ generation of reactants at the surface of the electrode is important because it is an alternative to the troublesome procedure of mixing known quantities of oxidant and reductant before each experiment. This procedure which is analogous to the d.c. component of the potential applied in a.c. polarography or the initial potential applied in differential pulse polarography is the source of some difficulty in the analysis of the results of coulostatics, particularly at higher rates of electron transfer. Some alternative methods of data analysis will be presented in the following to illustrate some of these

difficulties and the importance of careful choice of unknowns in the nonlinear regression analysis.

When used to experimentally determine the rates of electron transfer processes, the small step technique has the advantages discussed in the previous chapter for coulostatics in general: Freedom from uncertainty in potential due to uncompensated resistance and very rapid application of the perturbation compared with potential step techniques. Only A.C. methods seem at present to offer competition with coulostatics in the ability to measure very rapid electron transfer rates in solutions of high resistivity. The ultimate limit on the ability of coulostatics to measure fast rates is finally determined by the electronics of charge injection and data acquisition and by the solubility of the reactant.

It is in the small step format that the coulostatic technique was first proposed by Reinmuth[1] and Delahay.[2] A thorough summary of the equations governing use of the small step technique for electrode kinetics was given by Reinmuth.[3] Kudirka and Enke[4] showed by numerical calculations that the potential change induced by the charge injection could be larger than was previously thought for the linearization condition used by Reinmuth to continue to hold.

Small step coulostatics shares with differential pulse polarography and A.C. polarography the feature that the

measurement is made as a perturbation of an electrode initially at equilibrium. As in the two techniques cited, the equilibrium may be virtual rather than real, the only requirement being that the D.C. component of the response be much smaller than, or at least separable from the response resulting from the perturbation. In A.C. techniques, the D.C component is removed by phase-selective detection or high pass filtering. In differential pulse, the correction is made by subtraction of the current flowing just before the potential perturbation from the sampled current. In coulostatics, the optimum technique is probably analogous to that used in alternate drop differential pulse polarography: The potential decay experienced by the electrode without charge injection is subtracted from the observed experimental transient. This component is usually very small on the time scales to be considered and could even be neglected in most of the work presented below.

THEORETICAL

The basis for the evaluation of small step data is the theory developed by Reinmuth.[3] The electrode is initially assumed to be in quasi equilibrium at potential E_{pre}, corresponding to overpotential $\eta = 0$. A small charge, q, is injected a few microseconds after potential control (if any) is released. The initial perturbation of

potential is:

$$\eta_o = q/C_{dl} = (V_{inj}+C_{inj})/(C_{dl}+C_{inj}) \qquad (8.1)$$

where notation is summarized in Table 8.1.

The relaxation of potential for purely diffusion-controlled electron transfer ($Ox + ne^- \rightleftharpoons R$):

$$\eta(t) = \eta_o \exp(t/\tau_D)\,\mathrm{erfc}(t/\tau_D)^{\frac{1}{2}} \qquad (8.2)$$

A rational function approximation developed by the author for $\exp(x^2)\mathrm{erfc}(x)$ is given in subroutine E2EC in Appendix A. Equation (8.2) is the limiting case for very rapid charge transfer, the Nernstian case. The time constants τ_C and τ_D are given by

$$\tau_C = RTC_{dl}/nFI^o \qquad (8.3)$$

where

$$I^o = nFk^s C^o_{ox} \exp((-\alpha nF/RT)(E-E^o)) \qquad (8.4)$$

and

$$\tau_D = \{(RTC_{dl}/n^2F^2)(\frac{1}{C^o_{ox}D^{\frac{1}{2}}_{ox}} + \frac{1}{C^o_R D^{\frac{1}{2}}_R})\}^2 \qquad (8.5)$$

Table 8.1

Summary of Notation

Symbol	Explanation	Units
$\eta=0$	Potential just before charge injection	V
η_o	Potential just after charge injection	V
V_{inj}	Voltage to which C_{inj} is charged	V
C_{inj}	Injection capacitance	fd
C_{dl}	Double layer capaciatance	fd
$\eta(t)$	Overpotential as a function of time	V
t	Time after injection	sec
τ_D	Diffusional time constant	sec
τ_C	Charge transfer time constant	sec
R	Gas constant	1-atm/deg-mole
T	Temperature	°K
n	number of electrons	--
F	Faraday constant	coul/mole
I^o	Exchange current density	A/cm^2
k_s	Apparent standard rate constant	cm/sec
C^o_{ox}	Surface concentration of oxidant	$moles/cm^3$
C^o_R	Surface concentration of reductant	$moles/cm^3$
α	Transfer coefficient	--
$D_{ox,R}$	Diffusion coefficient of oxidant, reductant	cm^2/sec
ξ	$(D_{ox}/D_R)^{1/2}$	--
θ	(C^o_{ox}/C^o_R) from Nernst equation	--
C^b	Initial bulk concentration of Ox	$moles/cm^3$

For relaxation of the perturbation with charge transfer limiting conditions:

$$\eta(t) = \eta_o \exp(-t/\tau_C) \tag{8.6}$$

Finally, for mixed control of the electrochemical discharge of the perturbing charge:

$$\eta = \eta_o \frac{1}{(\gamma-\beta)} \{\gamma \exp(\beta^2 t)\operatorname{erfc}(\beta t^{\frac{1}{2}}) - \beta \exp(\gamma^2 t)\operatorname{erfc}(\gamma t^{\frac{1}{2}})\} \tag{8.7}$$

where,

$$\beta = \tau_D^{\frac{1}{2}}/2\tau_C + (\tau_D/4\tau_C - 1)^{\frac{1}{2}}/\tau_C \tag{8.8}$$

and,

$$\gamma = \tau_D^{\frac{1}{2}}/2\tau_C - (\tau_D/4\tau_C - 1)^{\frac{1}{2}}/\tau_C \tag{8.9}$$

Curve Fitting. The Marquardt Algorithm[5] and the criteria for nonlinear least squares analysis of data are discussed in the previous chapter. Briefly, it was desired to solve for certain unknown parameters subject to the criterion of least squares:

$$S^2 = \sum^{\text{all data}} (f(t, C_{dl}, \tau_D, \tau_C, q) - E(t))^2 = \min \tag{8.10}$$

where $(f(t,C_{dl},\tau_C,\tau_D,q)$ refers to the potential calculated via eqns (8.1), (8.3) or (8.6). Unlike the situation in the previous chapter, all data used in the fit refer to a single initial potential and injection charge. No attempt is made at this stage to calculate directly k^s and α as before.

After eqn (8.10) is solved by the fitting routine for the parameters which minimize S^2, it is possible to use eqn (8.4) to solve for I^o and by (8.4), if C_{ox} is accurately known, it is possible to find k_f. If E^o is known, it is possible to make a plot of the forward rate constant, k_f which is given by:[6]

$$k_f = k^s \exp(1-\alpha nF/RT)(E-E^o)) \qquad (8.11)$$

or from eqn (8.4):

$$k_f = \frac{I_o}{nFC^o_{ox}} \qquad (8.12)$$

If C_{ox} and C_R could be known <u>a priori</u>, it would be possible to derive the k_f vs potential relations independent of knowledge of E^o for the reaction. If the reaction is assumed to be Nernstian on the time scale of the pre-electrolysis, the surface concentrations are calculated from simple Nernstian polarographic theory:[7]

$$C_{ox}^{o} = \frac{\xi\theta}{1+\xi\theta} \tag{8.13}$$

$$C_{R}^{o} = \frac{1}{1+\xi\theta} \tag{8.14}$$

Thus, if E^o and diffusion coefficients are known, it is possible to construct the graph of k_f vs $E - E^o$ from which k^s and α may be extracted. Correction for double layer effects via conventional Frumkin correction[14] may be applied after reduction of raw data to the k_f vs E format.

EXPERIMENTAL

Coulostatic injection, data acquisition and experimental control functions were performed on the computerized instrumentation described in the previous chapter. The only change in experimental procedure relative to that work was use of smaller injection capacitors and/or injection voltages. The electrode used was a conventional hanging mercury drop electrode of area 0.032 cm^2 or a PAR universal electrode model 802 which could be triggered by computer and which yielded a drop of area 0.0192 cm^2. Ordinary blunt capillaries were used.

Solutions of 2 mM Eu^{+3} in 9.5 mM ClO_4^- and 3.5 mM H^+ were prepared by Bruce Parkinson. Cr(III)(edta) was prepared and three times recrystallized by Akifumi Yamada. Analytical reagent grade sodium chloride, glacial acetic

acid and sodium hydroxide were used as received in preparation of the electrolyte for the Cr(edta) experiments. All measurements were made at room temperature 23 ±2° C.

RESULTS

One major problem with coulostatic analysis is the strong dependence of the transient shape on double layer capacitance. This dependence is not present in potentiostatic methods because the faradaic current is not at all dependent on C_{dl}. Equations (8.1), (8.2), (8.6) and (8.7) illustrate the direct interrelationship between observed potential and the double layer capacitance. In the analysis of real data, the random errors and the inability to record the potential at its instantaneous value just after charge injection, but before any decay occurs, combine to make data analysis quite difficult without a priori knowledge of the double layer capacitance. Consider the simulated potential decay transients in Fig. (8.2), where curves 1 and 2 correspond to curves 3 and 4, respectively, of Fig. (8.1), but on a shorter time scale. Curve 2 is the diffusion controlled limit, eqn (8.2), and curve 1 is for mixed diffusion-charge transfer. Clearly from the figure it can be seen that if the first $0.01 \cdot \tau_D$ sec. of the transient were unavailable it would be impossible to differentiate curve 1 from curve 2, apart from the uniform displacement in overpotential. This difference

FIGURE 8.1

Potential relaxation with mixed charge transfer and diffusion control.

Curve 1 - $\tau_C/\tau_D = 10$

Curve 2 - $\tau_C/\tau_D = 1$

Curve 3 - $\tau_C/\tau_D = 0.1$

Curve 4 - $\tau_C/\tau_D = 0.$ (diffusion control)

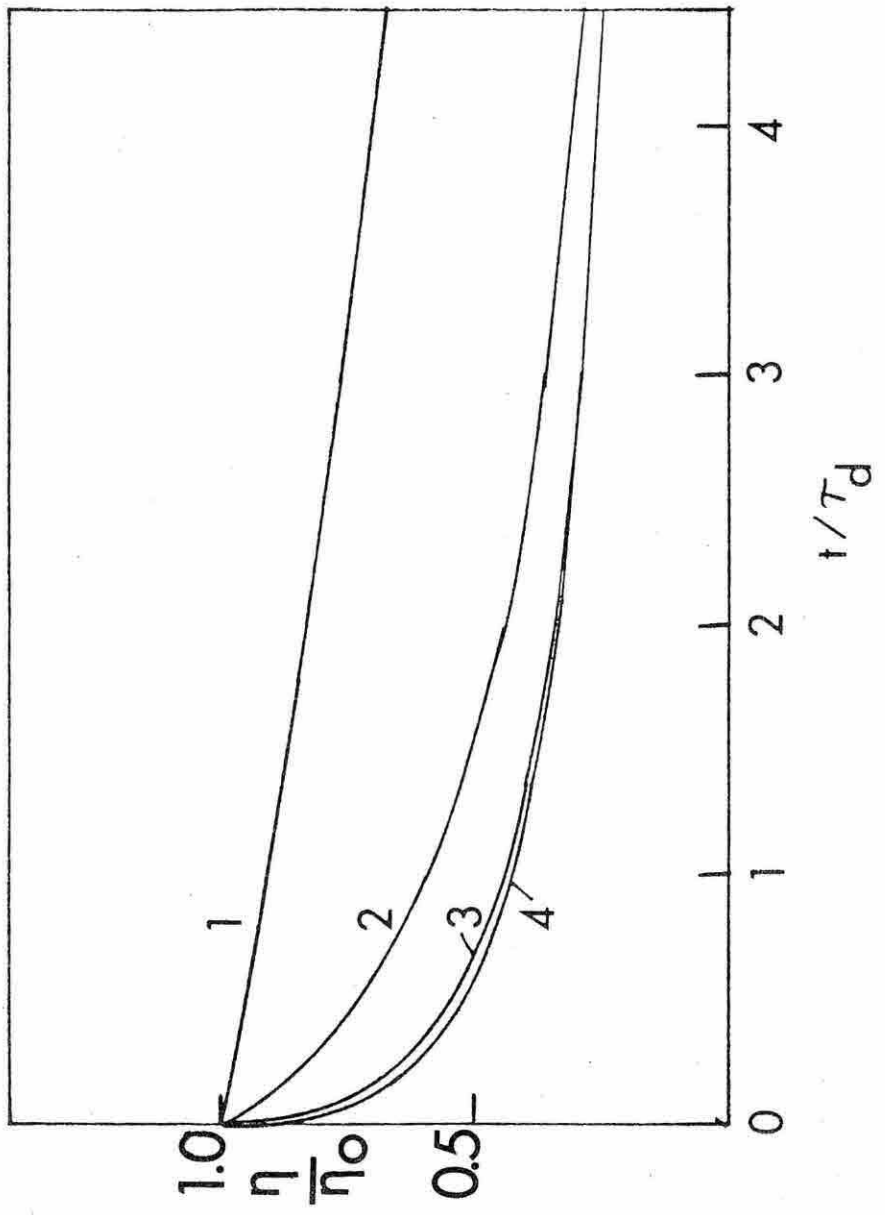

FIGURE 8.1

FIGURE 8.2

Potential relaxation, expanded time scale.

Curve 1 - $\tau_C/\tau_D = 0.1$

Curve 2 - $\tau_C/\tau_D = 0.$ (diffusion control)

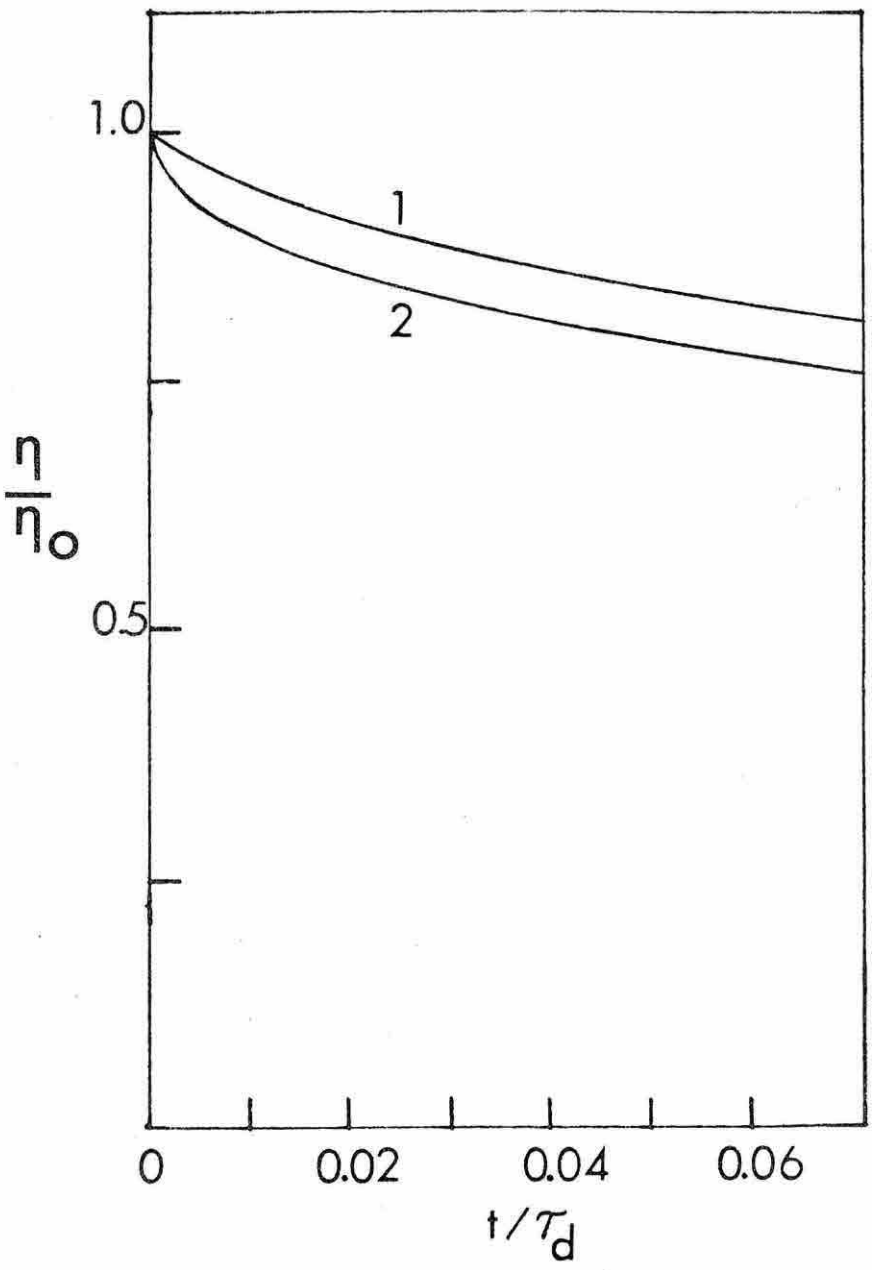

FIGURE 8.2

overpotential due to charge transfer kinetics could be confused with uncertainty in double layer capacitance. Thus it is necessary to have a priori knowledge of the double layer capacity in the presence of reactants in situations in which the mixed control equation (8.7) is to be applied. A nonlinear regression procedure which finds simultaneously C_{dl} and a parameter related to charge transfer (usually I_o or τ_C) is subject to this difficulty. Martin and Davis[8] probably encountered this phenomenon in their coulostatic study of the kinetics of cyanide hemichrome and ferri/ferro cyanide, using simultaneous nonlinear regression to determine I^o and C_{dl}. In varying the bulk concentration of reactants between 11.0 and 30.7 mM, the value of C_{dl} derived varied from 17.3 to 21.7 $\mu F/cm^2$, or about 22%. The values of k^s found varied by 100%, from 0.045 cm/sec to 0.088 cm/sec, very poor results for a rate of reaction 10^2 slower than the upper limit reached by A.C. techniques. For the cyanide hemichrome system it was necessary to manually vary C_{dl} and diffusion coefficients in order to estimate a range of possible rate constants of 2 to 7 cm/sec.

A further illustration of this interrelationship was observed in a simulation study to determine if the rate constant of the $Ru(NH_3)_6^{+2/+3}$ couple could be determined coulostatically. Table (8.2) shows the results of generating data via eqn (8.7), adding a known amount of

Table 8.2

Small Step Coulostatics. Curve Fit to Synthetic Data With Random Noise Added. For simulation of $Ru(NH_3)_6^{+2/+3}$ case, $D_{ox} = 4.75 \times 10^{-6}$. $D_R = 4.9 \times 10^{-6}$ cm^2/sec. n = 1. C^b_{Ru} = 1.67 mM. $E_{init} - E^o = 0$. q = 0.0625 μC/cm^2.

Times Used, μs			Input Parameters				Results of Fit			
t_{min} μs	t_{max} μs	Δt μs	C_{dl} $\frac{\mu fd}{cm^2}$	τ_C μs	τ_D μs	σ mV	C_{dl} $\frac{\mu fd}{cm^2}$	τ_C μs	τ_D μs	σ mV
100	500	10	35	112.5	104.9	0.05	31.8	80.8	86.7	0.055
50	250	5	35	112.5	104.9	0.05	33.7	75.4	97.5	0.052
5	50	5	35	112.5	104.9	0.05	32.4	88.3	89.6	0.048
5	50	5	35	112.5	104.9	0.25	24.9	51.7	52.9	0.251
100	500	20	35	11.3	104.9	0.025	32.4	0.4	90.0	0.030
5	50	5	35	11.3	104.9	0.025	11.3	96.6	33.6	0.026
5	50	5	35	11.3	104.9	0.05	11.5	89.3	32.3	0.052
5	50	5	35	11.3	104.9	0.1	12.7	77.8	30.0	0.103

random noise, then using a three term regression (τ_C, τ_D and C_{dl}) to try to recover the original information present. The added random noise is of a magnitude comparable to that found in experiment. The results illustrate the inaccuracies inherent in trying to determine several strongly cross-correlated parameters simultaneously as is the case here. Results of actual experiments on the $Ru(NH_3)^{+2/+3}$ couple were inconclusive and no reliable differentation from diffusion control could be made.

For reactants with rate constants yielding τ_C long with respect to τ_D, the (linear) logarithmic fit may be used. This procedure has the advantage that the double layer capacitance can be calculated directly from the t = 0 intercept of the ln(η) vs t plot. Figure (8.3) illustrates the results of eqns (8.6) and (8.7), plotted as forward rate constant vs potential. Thus it appears that for the slower electron transfer rates (relative to data acquisition rates and reactant concentrations,[3] the exact function (8.7) is nearly as well behaved as the logarithmic analysis. In situ generation of Eu^{+2} was used.

With the in situ generation of reduced product, the back-calculation of k_f from τ_C or I^o via eqns (8.11) - (8.14), contributes another source of uncertainty because of the necessity of knowing the standard potential very

FIGURE 8.3

Results of logarithmic fit (eqn (8.6)) vs. eqn (8.7) for $Eu^{+2/+3}$. (O) log approximation (yields τ_C and C_{dl}). (●) exact (simulation fit to τ_C and C_{dl}).

Assumed:

$D_{Eu^{+3}} = 9 \times 10^{-6}$. $D_{Eu^{+2}} = 7 \times 10^{-6}$ cm^2/sec.

$n = 1$. $E^O = -620$ vs SCE.

Solution contained: 2 mM Eu^{+3}, 9.5 mM ClO_4^- and 3.5 mM H^+.

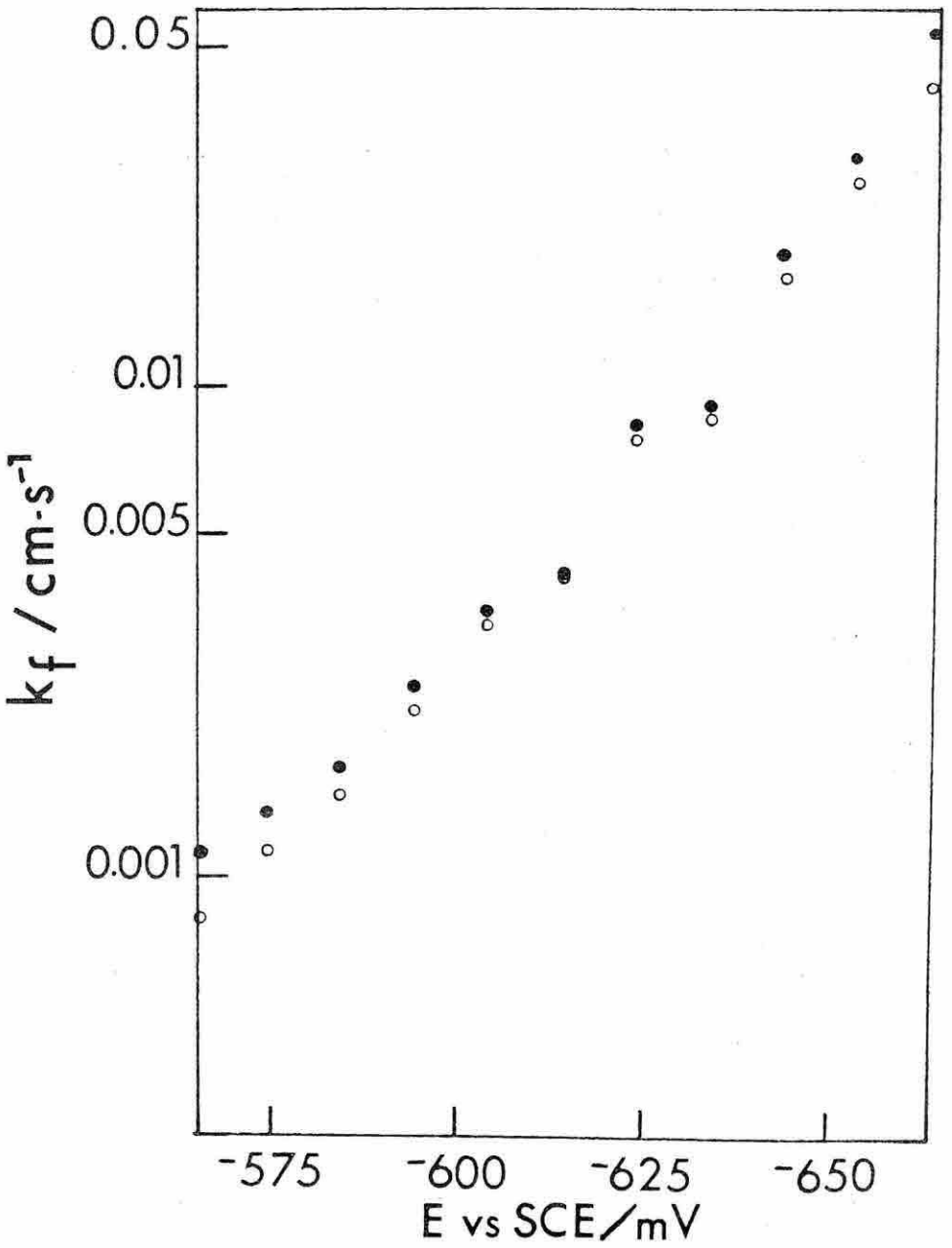

FIGURE 8.3

accurately. Consider the Cr(edta) couple which has a relatively large standard rate constant of electron transfer. Yamada and Tanaka[9] have determined by chronoamperometry in 0.4 M NaCl with 0.1 M pH 5 acetate buffer electron transfer parameters k^s = 0.2 cm/sec and α = 0.6. Figure (8.4) compares their results with the results of small step coulostatics. These results are for a two-term regression in τ_C and C_{dl}. Although the coulostatic results are of the same order of magnitude as theirs, there is a marked disagreement in slope, and hence in α. Much of the vertical scatter may be attributed to the simultaneous fit of C_{dl} and τ_C discussed above. The filled circles represent calculation of k_f and τ_C using our best estimate of E^o of -1220 mV vs. SCE. The open circles represent the results of similar data evaluated for E^0 = -1215 mV. That this difference is due to the difference of standard potentials assumed in translating τ_C to k_f can be seen by the comparison of the line in Fig. (8.4) with the open triangles. The line represents the findings of Yamada and Tanaka,[9] of k^s = 0.2, α = 0.6. The open trangles are the result when data generated artificially using these values and E^o = -1220 mV are fit by a program assuming E^o = -1215 mV. Thus it is seen that even a small error in assumed standard potential, such as could be caused by a liquid junction potential,

FIGURE 8.4

Formal rate constant vs potential for Cr(edta), 0.4 M NaCl and 0.1 M pH5 acetate buffer. Regression in τ_C and C_{dl}.

(●) E^o assumed -1220.

(O) E^o assumed -1215

(△) Regression on simulated data, $E^o_{FIT} = E^o_{GEN} + 5$ mV.

/ - Calculated for $k^s_a = 0.2$, $\alpha_a = 0.6$ (reference 9).

$D_{ox} = 6.33 \times 10^{-6}$ cm²/sec

$D_R = 5.63 \times 10^{-6}$ cm²/sec

$n = 1$

$A_{drop} = 0.032$ cm²

$C_{inj} = -10$ V

$V_{inj} = 100$ pfd

Data taken at various intervals and ranges between 10 and 500 μsec.

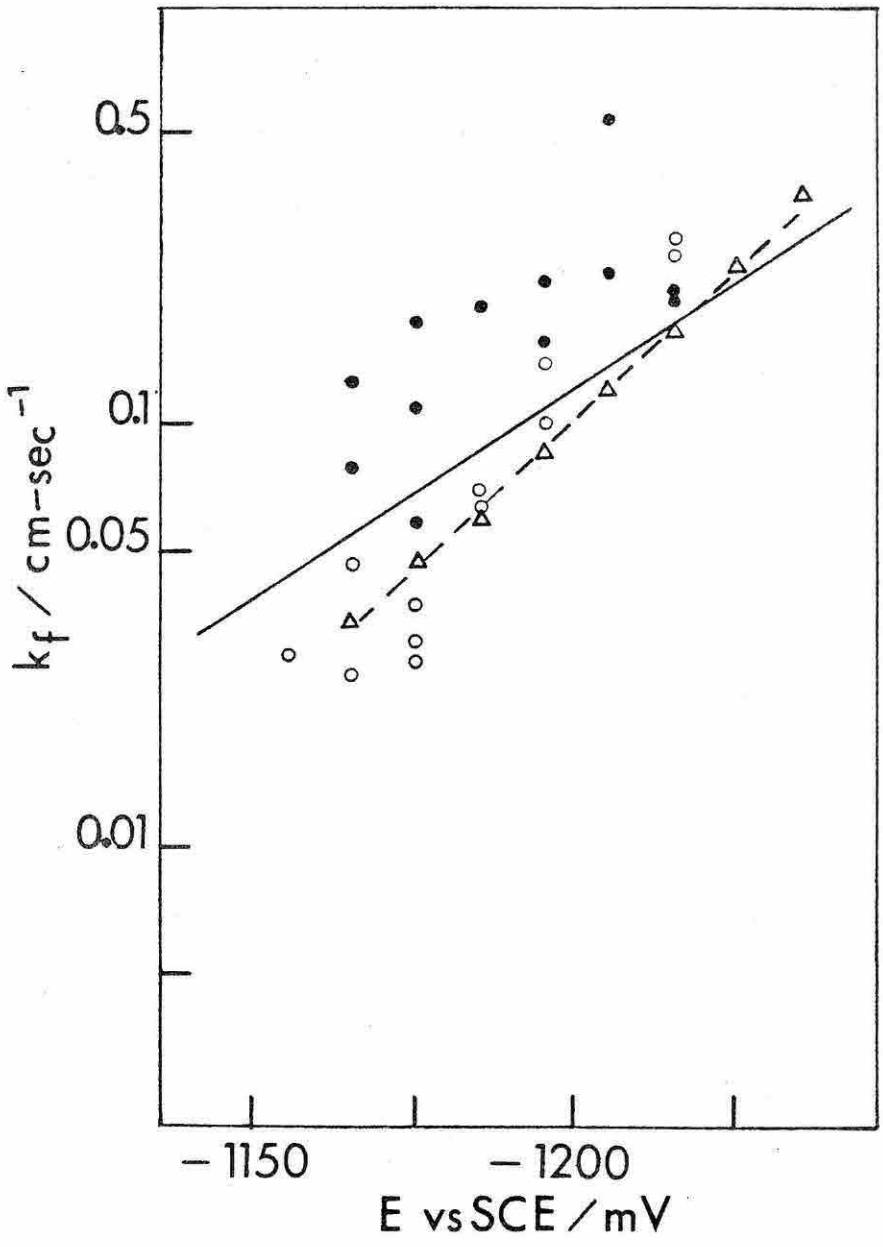

FIGURE 8,4

a defective reference electrode, or a change in electrolyte composition can cause severe problems, particularly in the interpretation of α.

Figure (8.5) shows the reduction in vertical scatter resulting from a single-term regression, τ_C only, with C_{dl} estimated from coulostatics of electrolyte solution without reactant present. The reduction in vertical scatter over Fig. (8.4) may be due to choosing a uniform sampling frequency and range. The potential of -1220 vs SCE for E^o assumed for the fit apparently causes the slope to match closely that obtained assuming the literature value of 0.6 (solid line).

Since the results shown in Fig. (8.4) imply that exact knowledge of the standard potential is necessary in order to obtain information about the transfer coefficient in the in situ generation experiment, it would be desirable to obtain this parameter directly, if possible, from the coulostatic results.

Information about the surface concentrations is present in τ_D through eqns (8.5), (8.13), (8.14), and $\xi = (\frac{D_o}{D_R})^{\frac{1}{2}}$. Let us define K such that:

$$K \equiv \left(\frac{1}{C_{ox}^{o} D_{ox}^{\frac{1}{2}}} + \frac{1}{C_{R}^{o} D_{R}^{\frac{1}{2}}}\right) \qquad (8.15)$$

FIGURE 8.5

Single term regression for Cr(edta) data. (●) - regression assumes C_{dl} = 15.0 μfd/cm². (O) - C_{dl} assumed 15.3 μfd/cm². Points taken 25 to 100 μsec in intervals of 5 μsec. Other parameters as in Fig. (8.4).

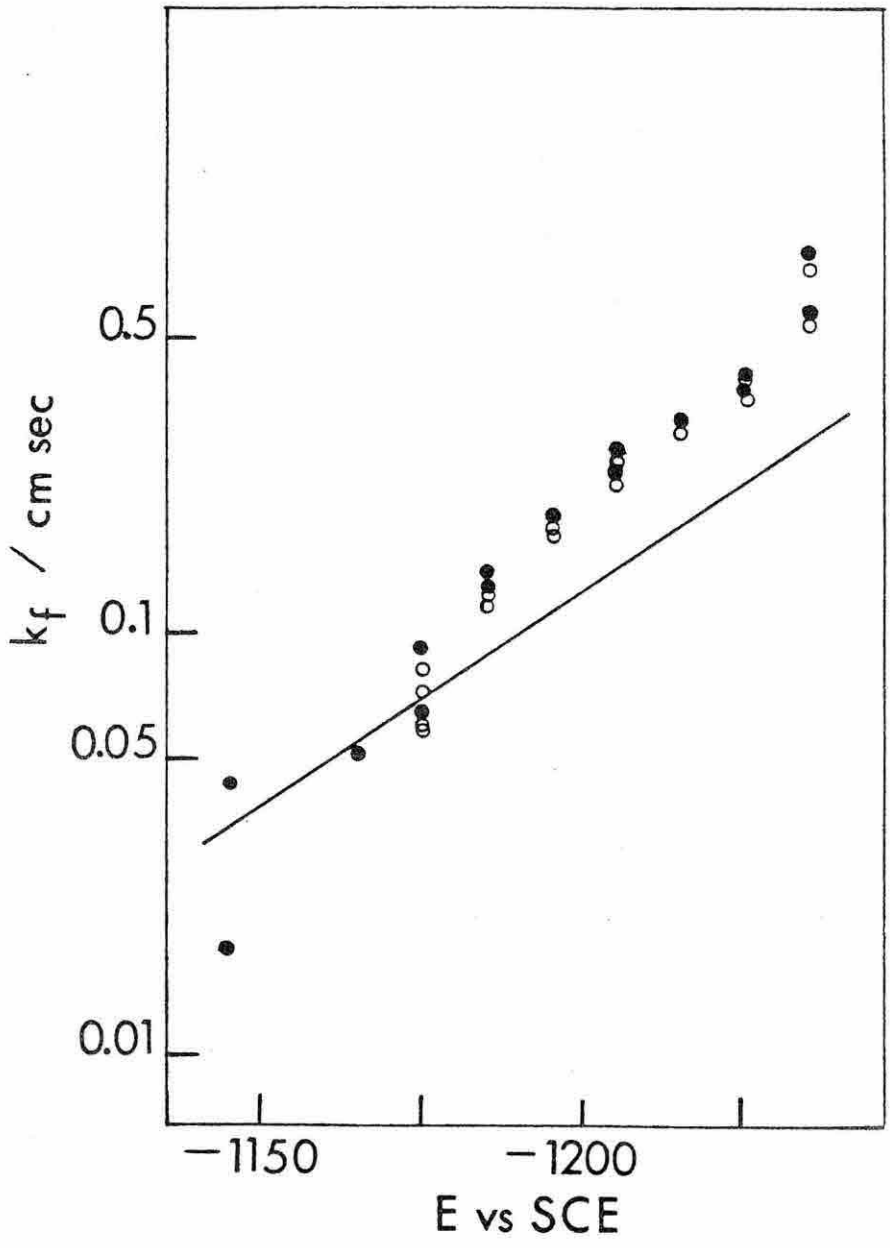

FIGURE 8.5

so that,

$$K = \frac{\tau_D^{\frac{1}{2}} n^2 F^2 C^b}{RTC_{d1}} = \frac{1+\xi\theta}{\xi\theta D_o^{\frac{1}{2}}} + \frac{1+\xi\theta}{\xi D_R^{\frac{1}{2}}} \tag{8.16}$$

rearranging,

$$K = \frac{1+2\xi\theta+\theta^2\xi^2}{\xi\theta D_o^{\frac{1}{2}}} \tag{8.17}$$

whence,

$$0 = \xi^2\theta^2+\theta(2\xi-K\xi D_o^{\frac{1}{2}})+1 \tag{8.18}$$

or finally,

$$0 = \xi^2\theta^2+\theta(2\xi-\frac{\tau_D^{\frac{1}{2}} n^2 F^2 D_o C^b}{RTC_{d1} D_R^{\frac{1}{2}}})+1 \tag{8.19}$$

which can be solved directly for θ:

$$\theta = \frac{-b\pm\sqrt{b^2-4ac}}{2a} \tag{8.20}$$

where

$$a = \xi^2\theta^2 \tag{8.21}$$

$$b = 2\xi - \frac{\tau_D^{\frac{1}{2}} n^2 F^2 D_o C^b}{RTC_{d1} D_R^{\frac{1}{2}}} \tag{8.22}$$

$$c = 1 \tag{8.23}$$

Assuming that all the parameters in (8.20) are known to high accuracy, one can now calculate directly the surface concentrations and hence the standard potential directly from coulostatic data. Of course, the cost of this advantage is the necessity of another unknown to be found by regression.

Figure (8.6) is the result when this theory is applied to experimental results on the Cr(edta) system. The undesirable result of an imaginary root near the standard potential is the result of eqn (8.20). The reason for this imaginary root is a slight error in the assumed parameters, particularly the diffusion coefficients, bulk concentration, double layer capacitance or temperature; or it could reflect a value of τ_D from the regression routine which was too small because of the difficulties alluded to above for strongly cross-correlated unknowns.

An attempt was made to avoid the problem of imaginary roots of eqn (8.19) by changing some of the assumed input parameters until the minimum value of $b^2 - 4ac$ in eqn (8.20) no longer became negative at any potential. The resulting "fudge factor" was incorporated in two different parameters, C^b and D_{ox}. The two methods give slightly different results in both the values of θ and k_f. The potential corresponding to $\theta=1$ which

FIGURE 8.6

Regression in τ_C and τ_D for Cr(edta) system illustrating use of eqns (8.19) - (8.22). (●) - C_{dl} = 16 μfd/cm². (O) - C_{dl} = 15 μfd/cm². / - drawn for k^s = 0.2, α = 0.6 (reference 9).

A. Computed standard rate constants vs. potential.

B. θ vs Potential via eqn (8.20).

Note imaginary roots at E = -1240 mV (corresponding k_f was calculated assuming θ = 1). Simulation parameters as in Fig. (8.4).

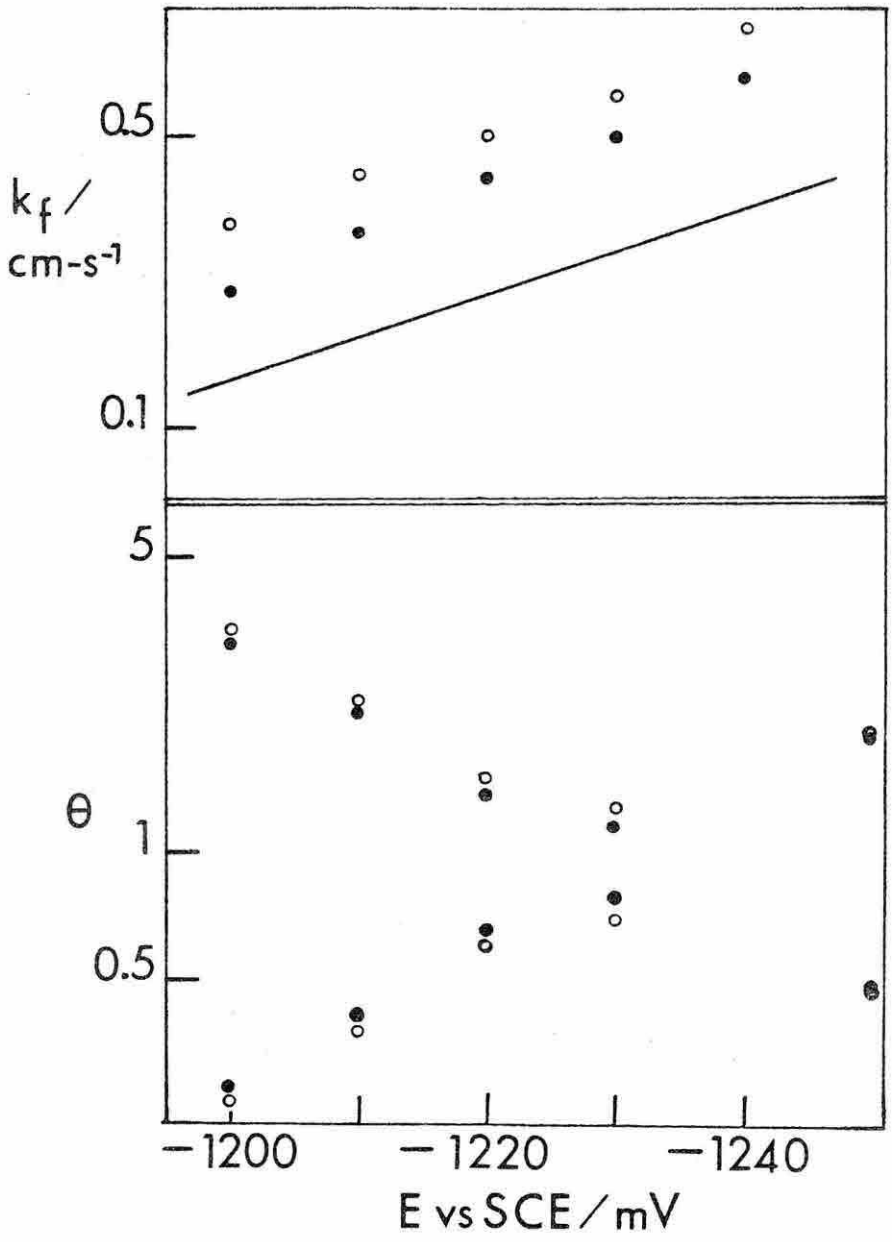

FIGURE 8.6

FIGURE 8.7

Reanalysis of data in Fig. (8.6) incorporating parameter adjustments which avoid imaginary roots in eqn (8.20). (●) - D_o = 6.33 x 10^{-6} cm^2/sec; C^b = 1.13 mM; C_{dl} = 16 $\mu fd/cm^2$. (O) D_o = 8.08 x 10^{-6} cm^2/sec; C^b = 1.00 mM; C_{dl} = 16 mM. All other regression parameters as in Fig. (8.4).

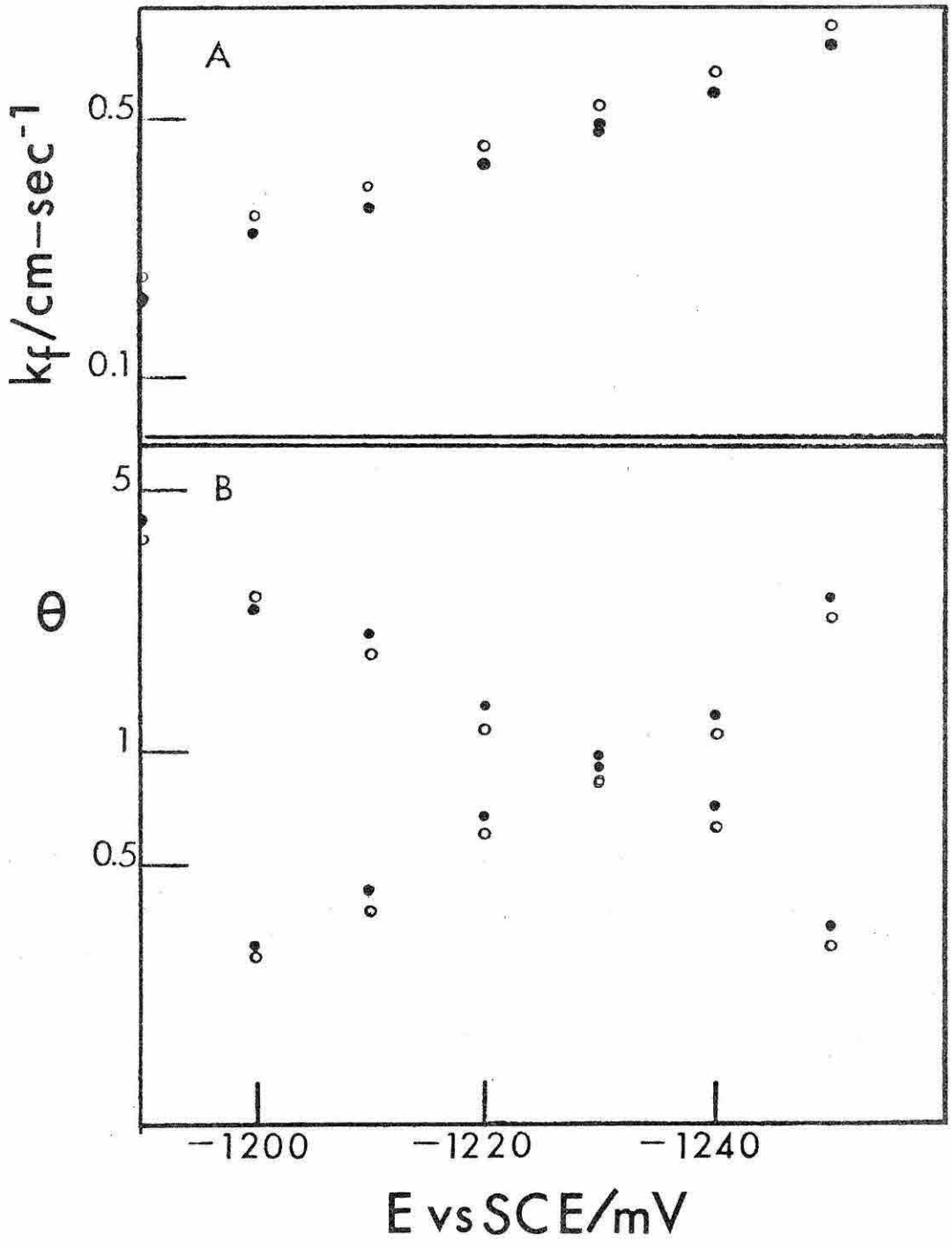

FIGURE 8.7

theoretically would be E^o for the reaction varies between -1225 and -1230 mV vs SCE, slightly higher than the literature values.

CONCLUSIONS

It was found that strong cross-correlations exist in the data analysis of coulostatic transients via eqn (8,7) between double layer capacitance, charge transfer parameters, and the diffusional relaxation parameters. In order to separate and quantize any one of these factors, it is necessary that the other two be well defined *a priori*. The logarithmic approximation eqn (8,6) is better suited to the analysis of data because it yields an independent estimate of C_{dl} and during the fit of the raw data is independent of the diffusional factors. Under those conditions in which this approximation can be made to hold by increasing the reactant concentration and decreasing sample time, this alternative should yield more consistent results.

REFERENCES

(1) W. H. Reinmuth and C. E. Wilson, Anal. Chem., 34, 1159(1962).

(2) P. Delahay, Anal. Chem., 34, 1161(1962).

(3) W. H. Reinmuth, Anal. Chem., 34, 1272(1962).

(4) J. M. Kudirka and C. G. Enke, Anal. Chem., 44, 614(1972).

(5) P. R. Bevington, "Data Reduction and Analysis for the Physical Sciences," McGraw-Hill, New York, N. Y., 1969, Ch. 11.

(6) P. Delahay, "Double Layer and Electrode Kinetics," Interscience, New York, N. Y., 1965, Ch. 7.

(7) P. Delahay, "New Instrumental Methods in Electrochemistry," Interscience, New York, N. Y., 1954, p. 54.

(8) R. F. Martin and D. G. Davis, Biochemistry, 7, 3906(1968).

(9) A. Yamada and N. Tanaka, Science Reports of the Tohoku University, Series I, Vol. LII, June 1969, p. 73.

APPENDIX A

Computer Program to Calculate Differential Pulse Current Function

INTRODUCTION

Equation 2.4, an approximate analytical expression for current-potential response of a nernstian system with adsorbed product and/or reactant, was evaluated by means of a computer program on the PDP-11/40. Because of the extreme complexity of this equation, use of the computer was a virtual necessity to generate simulated differential pulse polarograms.

Main program All.FTN was used for all input/output, scanning of potential, and calculation of eqn (2.4). Subroutine E2EC.FTN generator the function $\exp(x^2)\mathrm{erfc}(x)$ by means of rational function approximation developed by the author. Subroutine VARIN.FTN is a utility keyboard I/O program. Listings are shown on the following pages.

```
      BYTE PRINT
      CALL VARIN(FN,'N = ',4,0.,10.)
      CALL VARIN(DOX,'DOX= ',5,0.,.01)
      CALL VARIN(DRED,'DRED= ',6,0.,.01)
      CALL VARIN(CSTAR,'C*, MOLAR= ',11,0.,20.)
      CSTAR=CSTAR*1.E-3
      CALL VARIN(T,'SAMP. TIME, SEC= ',17,0.,100.)
      CALL VARIN(DE,'DELTA E, MV= ',13,-1000.,1000.)
      DE=ABS(DE)/1000.
      WRITE (6,3)
3     FORMAT ('$PRINTOUT? ')
      READ (6,4) PRINT
4     FORMAT (1A1)
1     CALL VARIN(FKO,'K OX, CM-1= ',12,0.,0.)
      CALL VARIN(FKR,'K RED, CM-1= ',13,0.,0.)
      CPND=0.
      CPADS=0.
      DO 5 I=1,100
      E=(50-I)/1000.
      EJ=E-DE
      THETA0=EXP(38.92*FN*E)
      THETA1=EXP(38.92*FN*EJ)
      XI=SQRT(DOX/DRED)
      SDO=SQRT(DOX)
      SDR=SQRT(DRED)
      SPT=SQRT(3.14159*T)
      BETA=(THETA1*SDO+SDR)/(FKO*THETA1+FKR)
      CO=CSTAR*THETA0*XI/(THETA0*XI+1.)
      CR=CSTAR*XI/(THETA0*XI+1.)
      G=CO/THETA1-CR
      COTRLL=FN*96400./SPT*SDO
      COTRLL=COTRLL*G*THETA1/(1.+THETA1*XI)
      CUR1=FN*96400.*G*THETA1/(FKO*THETA1+FKR)
      CUR2=(SDO*FKR+SDR*FKO-BETA*FKO*FKR)/SPT
      CUR3=(FKO*FKR*BETA*BETA-BETA*(SDO*FKR+SDR*FKO)+SDO*SDR)
      CURR=CUR1*(CUR2+CUR3*E2EC(BETA*SQRT(T)))
      RATIO=CURR/COTRLL
      CO=CSTAR
      CR=CSTAR/THETA0
      G=CO/THETA1-CR
      CUR1=FN*96400.*G*THETA1/(FKO*THETA1+FKR)
      CUR2=(SDO*FKR+SDR*FKO-BETA*FKO*FKR)/SPT
      CUR3=(FKO*FKR*BETA*BETA-BETA*(SDO*FKR+SDR*FKO)+SDO*SDR)
      CURRL=CUR1*(CUR2+CUR3*E2EC(BETA*SQRT(T)))
      IF (ABS(CURR).LT.ABS(CPADS)) GO TO 6
      CPADS=CURR
      EPADS=E
6     IF (ABS(COTRLL).GE.ABS(CPND)) CPND=COTRLL
      IF (PRINT.NE."131) GO TO 5
      WRITE (6,10) I,E,CURR,COTRLL,RATIO,CURRL
10    FORMAT (I5,5(1PE12.3))
5     CONTINUE
      RATCP=CPADS/CPND
      WRITE (6,21) FKO,FKR,EPADS,RATCP
21    FORMAT (4F10.4)
      GO TO 1
      END
```

```
      REAL*8 FUNCTION E2EC(XX)
      IMPLICIT REAL*8 (A-H),(O-Z)
      IF (XX.GT.2.) GO TO 20
      P=1.000000401D0+XX*(.54417793909D0+XX*(.14536558998
     1     -XX* 000653025051380D0))
      Q=1.D0+XX*(1.6725632231D0+XX*(1 0325517836D0
     1     +XX*.24473362473D0))
      GO TO 30
20    Y=1./XX/XX
      P=(.5641895D0+Y*(1.76366D0+Y* 479275D0))/XX
      Q=1.D0+Y*(3.625876+Y*1 918612)
30    E2EC=P/Q
      RETURN
      END
```

```
C       SUBROUTINE VARIN(X,ALPHA,IPRINT,XMIN,XMAX)
C
C       X=INPUT VARIABLE
C       ALPHA=A STRING OF ALPHA-NUMERIC CHARACTERS
C       IPRINT=# OF CHARACTERS IN ALPHA (<81)
C       XMIN=MIN BOUND ON X
C       XMAX=MAX BOUND ON X
C
C       IF XMIN=XMAX, NO BOUNDS TEST WILL BE MADE
C
        SUBROUTINE VARIN(X,ALPHA,IPRINT,XMIN,XMAX)
        BYTE ALPHA(80)
        CALL SETERR (6,-1)
10      IF (IPRINT GE.1) WRITE (6,20) (ALPHA(I), I=1,IPRINT)
20      FORMAT ('$',80A1,X)
        READ (6,30) X
30      FORMAT (F20.0)
        CALL TSTERR(6,IER)
        GO TO (50,40), IER
40      IF (XMIN EQ.XMAX) RETURN
        IF (X LT.XMIN.OR.X.GT XMAX) GO TO 70
        RETURN
50      WRITE (6,60)
60      FORMAT (' CONVERSION ERROR')
        GO TO 10
70      WRITE (6,80) XMIN,XMAX
80      FORMAT (' ERROR:',G10.4,' < X <',G10.4)
        GO TO 10
        END
```

APPENDIX B

Digital Simulation Program for Differential Pulse

INTRODUCTION

This digital simulation calculates differential pulse currents for the following Nernstian electron transfer reaction

$$O_x + ne \rightleftharpoons Red \qquad (B.1)$$

In which either or both reactants may be adsorbed according to (independent) Frumkin isotherms:

$$\frac{K_i C_i^0}{\Gamma_i^m} = \frac{\theta_i}{1 - \theta_i} e^{A_i \theta_i} \qquad (B.2)$$

where K_i is the Henry's law coefficient (units of cm), Γ_i^m is maximum coverage, θ_i is Γ_i/Γ_i^m, A_i is the Frumkin interaction parameter (positive = repulsive; negative = attractive). If A is zero this reduces to a Langmuir isotherm:

$$\frac{K_i C_i^0}{\Gamma_i^m} = \frac{\theta_i}{1 - \theta_i} \qquad (B.3)$$

If Γ^m is very large, this in turn reduces to a linear isotherm (Henry's law):

$$\Gamma_i = K_i C_i^0 \tag{B.4}$$

The subroutine FMKISO calculates Γ_i and $\left(\frac{d\Gamma_i}{dC_i}\right)$ given Γ_i^m, K_i, A_i, and C_i^0. If the isotherm reduces to (B.3) or (B.4), a direct calculation of Γ_i is possible. If not, an iterative Newton-Raphson procedure is used to calculate Γ_i.

The long pre-electrolysis drop-growth period $0 < t < t_d$ is divided into ITER discrete steps of duration $\Delta t_1 = \frac{t_d}{ITER}$. The much shorter stage after the potential step $t_d < t < t_d + t_s$ is likewise divided into ITER steps of duration $\Delta t_2 = \frac{t_s}{ITER}$.

During the drop-growth phase, concentrations are evaluated at large grid spacings, Δx_1:

$$\Delta x_1 = \sqrt{\max(D_{OX}, D_{RED}) \cdot \Delta t_1 / 0.45} \tag{B.5}$$

So that the stability criterion $\frac{D\Delta t}{(\Delta x)^2} < 0.5$ is satisfied. A similar formula is used to calculate Δx_1 given Δt_2. In

order to convert the old concentration profile to the new grid spacing, a linear interpolation scheme is used.

Boundary Conditions

The boundary conditions during the second phase, after the applied potential is stepped to E + ΔE, is perhaps the most unusual aspect of this simulation. Because of uncompensated resistance in the circuit, it was necessary to calculate the potential loss as a function of the cell current at each time step. Since the current drawn is a function of potential of the working electrode through the Nernst equation and through the equation for charging the double layer capacities, it was necessary to solve for i and E_w self-consistently. Another problem was the fact that it was necessary to solve for the amount of surface material in the adsorbed state and in solution at X = 0. If all that is known is conservation of mass in the zeroth volume element,

$$C_{tot}^{0} = C_{ox}^{0} + C_R^{0} + \Gamma_{ox}/\Delta x + \Gamma_R/\Delta x \qquad (B.6)$$

and

$$C_{ox}^{0} = f(\Gamma_{ox});\ C_R^{0} = g(\Gamma_R) \qquad (B.7)$$

and the Nernst equation, it is necessary to calculate simultaneously for C^0's and Γ's which satisfy the isotherm. For a general nonlinear isotherm, it takes a few iterations of a Newton-Raphson calculation to solve for the C^0's and Γ's. Since this calculation is nested within the calculation for E_w and i ($C_{ox}^{\ 0}$ and $C_R^{\ 0}$ being a function of E_w *via* the Nernst equation) the boundary value calculation requires as much or more computer time as diffusion and drop growth. The complete flow chart is in Fig. B.1. A flow chart of the boundary condition calculation is given in Fig. B.2.

FIGURE B.1

Flowchart of differential pulse simulation. Includes drop growth, diffusion, uncompensated resistance, adsorption of both reactant and product with linear isotherm or either reactant or product with nonlinear isotherm.

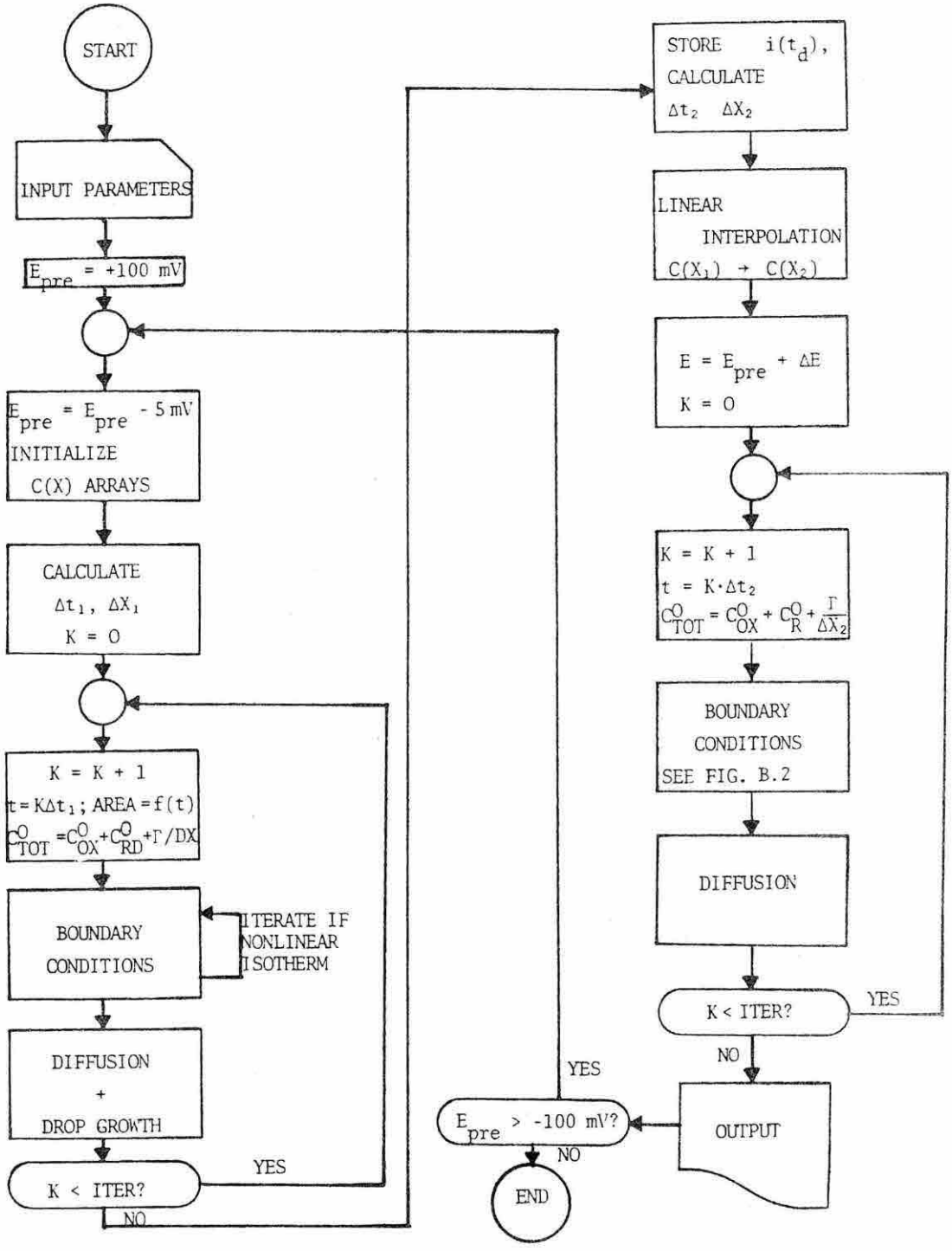
START
INPUT PARAMETERS
E_{pre} = +100 mV
$E_{pre} = E_{pre} - 5$ mV
INITIALIZE
C(X) ARRAYS
CALCULATE
Δt_1, ΔX_1
K = 0
K = K + 1
$t = K\Delta t_1$; AREA = f(t)
$C^O_{TOT} = C^O_{OX} + C^O_{RD} + \Gamma/DX$
BOUNDARY
CONDITIONS
ITERATE IF
NONLINEAR
ISOTHERM
DIFFUSION
+
DROP GROWTH
K < ITER?
YES
NO
STORE $i(t_d)$,
CALCULATE
Δt_2 ΔX_2
LINEAR
INTERPOLATION
$C(X_1) \rightarrow C(X_2)$
$E = E_{pre} + \Delta E$
K = 0
K = K + 1
$t = K \cdot \Delta t_2$
$C^O_{TOT} = C^O_{OX} + C^O_R + \frac{\Gamma}{\Delta X_2}$
BOUNDARY
CONDITIONS
SEE FIG. B.2
DIFFUSION
K < ITER?
YES
NO
OUTPUT
E_{pre} > -100 mV?
YES
NO
END

FIGURE B.1

FIGURE B.2

Boundary condition calculation for $t > t_d$. Illustrates how current and potential are calculated self-consistantly in the presence of adsorption and uncompensated resistance.

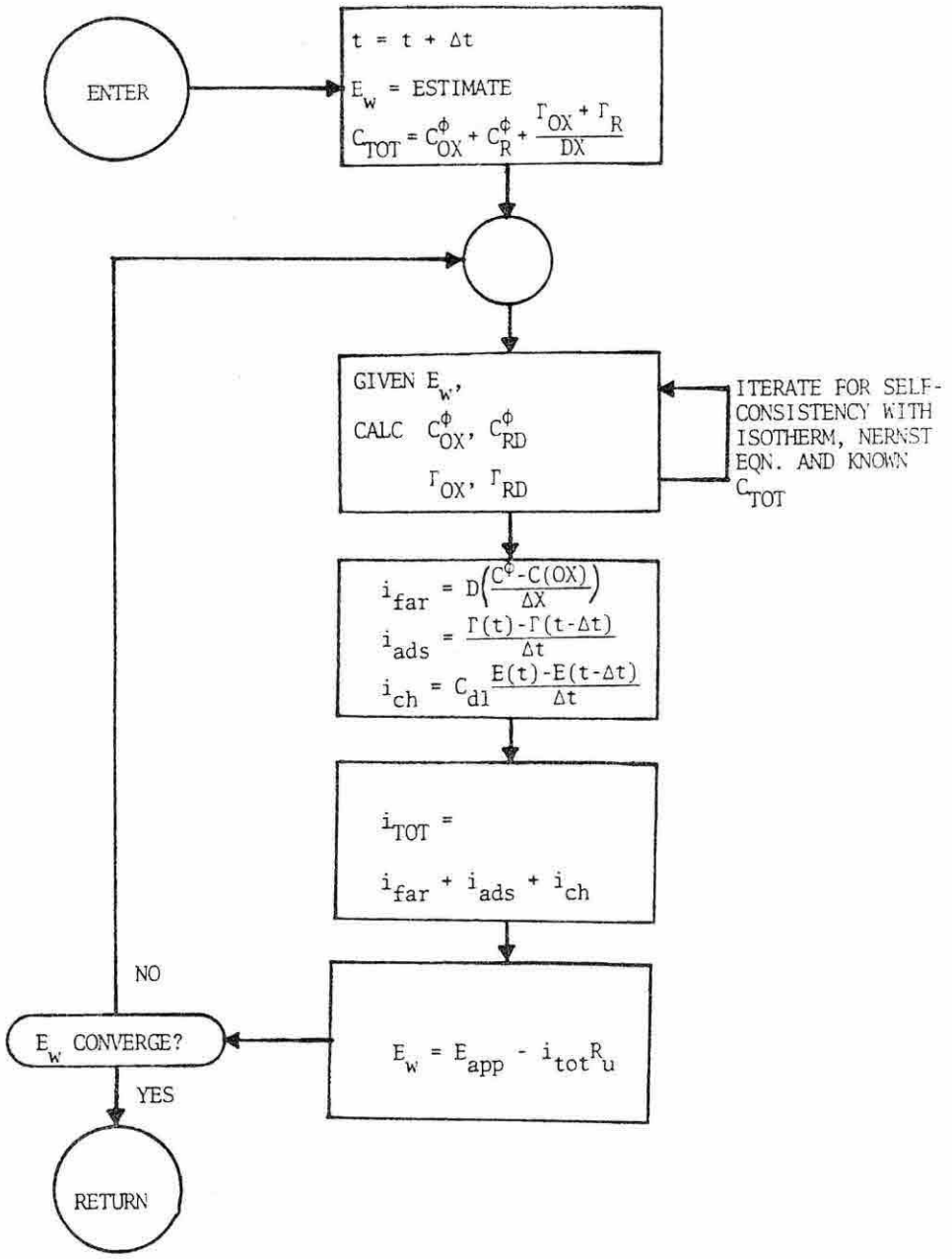
ENTER
$t = t + \Delta t$
E_w = ESTIMATE
$C_{TOT} = C^{\phi}_{OX} + C^{\phi}_{R} + \frac{\Gamma_{OX} + \Gamma_R}{DX}$
GIVEN E_w,
CALC C^{ϕ}_{OX}, C^{ϕ}_{RD}
Γ_{OX}, Γ_{RD}
ITERATE FOR SELF-CONSISTENCY WITH ISOTHERM, NERNST EQN. AND KNOWN C_{TOT}
$i_{far} = D\left(\frac{C^{\phi} - C(OX)}{\Delta X}\right)$
$i_{ads} = \frac{\Gamma(t) - \Gamma(t-\Delta t)}{\Delta t}$
$i_{ch} = C_{dl}\frac{E(t) - E(t-\Delta t)}{\Delta t}$
$i_{TOT} =$
$i_{far} + i_{ads} + i_{ch}$
$E_w = E_{app} - i_{tot}R_u$
E_w CONVERGE?
NO
YES
RETURN

FIGURE B.2

```
C       DPPFMK.FTN
C       DIFFERENTIAL PULSE POLAROGRAPHY SIMULATION
C       INCLUDING ADSORPTIVE DEPLETION OF REACTANT,
C       DROP GROWTH,
C       CHOICE OF LINEAR, LANGMUIR, OR FRUMKIN ISOTHERM
C       UNCOMPENSATED RESISTANCE INCLUDING AREA DEPENDENT
C               SOLUTION RESISTANCE COMPONENT
C       CHARGING OF DOUBLE LAYER THROUGH RU.
C
C       ALL CALCULATIONS ARE DONE IN CGS UNITS
C
C
C
C       STATEMENT FUNCTIONS:
        AREA(HGR,T)= .0085086*(HGR*T)** .6666666
        DIFN(DM,CJM,CJ,CJP)=CJ+DM*(CJM+CJP-2.*CJ)
        OXISO(C0)=FMKISO(C0,GOXMX,XKO1,AOX,DGODC)
        RDISO(C0)=FMKISO(C0,GRDMX,XKR1,ARD,DGRDC)
C
C
C
        DIMENSION TDS(10)
        DIMENSION COXES(10),CAPRES(10)
        DIMENSION COX(200),CRD(200),CNEW(200)
C
C       INPUT SIMULATION PARAMETERS
        CALL VARIN(FITER,'ITER= ',6,2.1,1600.)
        ITER=FITER
        CALL VARIN (DOX,'DOX= ',5,1.E-7,1.E-3)
        CALL VARIN (DRED,'DRED= ',6,1.E-7,1.E-3)
        CALL VARIN (CDL,'CDL, UFD/CMSQ= ',15,0.,0.)
C       CONVERT TO FD/CMSQ
        CDL=CDL*1.E-6
        CALL VARIN (XN,'N ELECTRONS= ',13,.9,9.)
1       CALL VARIN (TS,'SAMPLE TIME, MS= ',17,1.,1000.)
C       CONVERT TO SEC
        TS=TS*1.E-3
        CALL VARIN (DE,'PULSE HEIGHT, MV= ',17,1.,1000.)
C       CONVERT TO V
        DE=DE*1.E-3
C       SIG IS SCAN DIRECTION, -1=CATHODIC SCAN
        SIG=-1.
        ISIG=INT(SIG)
        DE=ABS(DE)*ISIG
C       RCOEF IS SOLN RESISTANCE COEFF:
C               RU=R(CAPILL)+RCOEF*(DROPAREA)**1/2
C       THIS IS USEFUL IN CASES OF VERY LOW SOLUTION
C       CONDUCTIVITY, IN WHICH UNCOMPENSATED RESISTANCE
C       CHANGES GREATLY WITH DROP AREA
        CALL VARIN (RCOEF,'R COEF, OHM-CM= ',16,0.,0.)
        CALL VARIN (CRN,'# CAP R= ',9,.9,10.1)
```

```
      NCAPR=CRN
      DO 60000 JCAPR=1,NCAPR
60000 CALL VARIN (CAPRES(JCAPR),'CAPIL  R, OHMS= ',16,0.,0.)
      CALL VARIN(COXN,'# COX= ',7,1.,10.)

V06.13                  00:00:00    11-AUG-76   PAGE    2

      NCOX=COXN
      DO 30001 JCOX=1,NCOX
30001 CALL VARIN(COXES(JCOX),'COX= ',5,1.E-20,1.)
      CALL VARIN (HGR,'HG FLOW RATE= ',14, .01,10.)
      CALL VARIN (TIMES,'# DROP TIMES= ',14,0.,10.)
      NTIMES=TIMES
      DO 40000 JTIMES=1,NTIMES
      CALL VARIN (TDS(JTIMES),'DROP TIME= ',11,.01,1000.)
40000 CONTINUE
C     INPUT ISOTHERM PARAMETERS
C     XKO1,XKR1--HENRY'S LAW COEFFICIENTS
C     GOXMX,GRDMX--GAMMA MAX'S
C     AOX,ARD--FRUMKIN INTERACTION PARAMETERS
20000 CALL VARIN(XKO1,'K OX= ',6,0.,0.)
      CALL VARIN (XKR1,'K RED= ',7,0.,0.)
      CALL VARIN(GOXMX,'GOXMAX= ',8,0.,0.)
      CALL VARIN(GRDMX,'GRDMAX= ',8,0.,0.)
      CALL VARIN(AOX,'INTERACTION PAR, OX=',20,-5.,5.)
      CALL VARIN(ARD,'INTERACTION PAR, RD=',20,-5.,5.)
C     DEFAULT VALUE FOR GAMMA MAX'S IS VERY LARGE, SO THAT
C     A LINEAR ISOTHERM IS ASSUMED
      IF (GOXMX.EQ.0.) GOXMX=1.
      IF (GRDMX.EQ.0.) GRDMX=1.
C     END INPUT SECTION
C
C
C
C     EPS IS CONVERGENCE CRITERION FOR WORKING ELECTRODE POTL
      EPS=5.E-7
      DO 10002 JCOX=1,NCOX
C     INITIAL CONC OF RED IS SET TO ZERO
      CIR=0.
C     INITIAL CONCENTRATION OF OX IS TAKEN FROM ARRAY
C     OF INITIAL CONCENTRATIONS AND CONVERTED TO MOLES/CMSQ
      CIO=COXES(JCOX)/1000.
      DO 10002 JTIMES=1,NTIMES
C     DROP TIME TAKEN FROM ARRAY
      TD=TDS(JTIMES)
      DO 10002 JCAPR=1,NCAPR
C     CONSTANT PART OF UNCOMPENSATED RESISTANCE IS CHOSEN
C
C     PRINT HEADINGS
      WRITE (6,10003) CIO,TD,CAPRES(JCAPR)
      WRITE (6,10004)
10003 FORMAT (//,' COX= ',1PE12.2,5X,' DROP TIME = ',0PF5.1,
     1      5X,'CAPRES= ',F7.1)
10004 FORMAT (//'   EPRE',4X,'RU*CURR',7X,'C1 ',8X,'CUROX',5X,
     1      'DIFF CURR',5X,'I/CR')
```

```
C       INITIALIZE POTENTIAL SCAN VARIABLE
        IEPRE=0
C       INCREMENT POTENTIAL SCAN VARIABLE
10000   IEPRE=IEPRE+1
10005   EPRE=FLOAT(IEPRE-21)/200.*SIG
C       MAXJ IS MAXIMUM NUMBER OF SPACE INCREMENTS TO BE
C       USED IN CONCENTERATION PROFILE
        MAXJ=4.5*SQRT(FLOAT(ITER))+5.

        DT=TD/ITER
C       CALCULATE FIRST DX TO SATISFY STABILITY CRITERION
C       (SEE WRITEUP)
        DX=SQRT(AMAX1(DOX,DRED)*DT/DM)
C       CALCULATE DIMENSIONLESS DIFFN COEFFICIENTS FOR EACH
        DMO=DOX*DT/DX/DX
        DMR=DRED*DT/DX/DX
C       INITIALIZE CONCENTRATION ARRAYS
        DO 9 J=1,200
        COX(J)=CIO
9       CRD(J)=CIR
        C0OX=CIO
        C0RD=CIR
C       INITIALIZE SOME NUMERICAL CONSTANTS
        XK1=DOX*96400.*XN/DX
        XK2=38.92*XN
C       INITIALIZE GOX AND GRD, THE GAMMA'S TO ZERO
        GOX=0.
        GRD=0.
        GOXTOT=0.
        GRDTOT=0.
C       INITIAL ESTIMATE OF WORKING ELECTRODE POTL IS EPRE,
C       APPLIED POTENTIAL.
        E=EPRE
C
C       BEGIN TIME ITERATIONS
C
        DO 100 K=1,ITER
C       UPDATE AREA
        DAREA=AREA(HGR,DT*K)
C       CALCULATE UNCOMPENSATED RESISTANCE (SEE WRITEUP)
        RU=CAPRES(JCAPR)+RCOEF/SQRT(DAREA)
C       CONSERVATION OF MASS IN SURFACE
C       VOLUME ELEMENT
        CTOT=C0OX+C0RD+(GOXTOT+GRDTOT)/DX/DAREA
C       TAKE INTO ACCOUNT DROP GROWTH ON SURFACE COVERAGES
        GOX1=GOXTOT/DAREA
        GRD1=GRDTOT/DAREA
C
C       BEGIN BOUNDARY CONDITION LOOP FOR WORKING POTL.
C
8       EL=E
        THETA=EXP(XK2*EL)
```

```
C
C       BEGIN BOUNDARY CONDITION LOOP FOR SURFACE CONCENTRATIONS
C
300     C0OXL=C0OX
        C0RD=C0OX/THETA
C       C0NUM IS NUMERATOR IN NEWTON-RAPHSON CALCULATION
C       FOR NEW C0OX
C                C0OX'=C0OX-C0NUM/C0DEN
        C0NUM=C0OX*(1 +1 /THETA)+(OXISO(C0OX)+RDISO(C0RD))/DX-CTOT
        C0DEN=1 +1 /THETA+DGODC/DX+DGRDC/DX/THETA
        C0OX=C0OXL-C0NUM/C0DEN
C       TEST AND CORRECT IN CASE NEWTON-RAPHSON CORRECTION
C       CAUSES AN OVERSHOOT OUTSIDE PERMITTED RANGE OF
C       CONCENTRATIONS.  THIS TEST IS VERY IMPORTANT.
        IF (C0OX LT 0 ) C0OX=C0OXL/2.
        IF (C0OX GT CTOT) C0OX=(C0OXL+CTOT)/2.
C       TEST FOR CONVERGENCE TO CONSTANT VALUE
        IF (ABS(C0OXL-C0OX) GT .0001*CTOT) GO TO 300
C       END OF NEWTON-RAPHSON CONCENTRATION CALCULATION
C       CONTINUING WORKING POTENTIAL ITERATION
        C0RD=C0OX/THETA
        GOX=OXISO(C0OX)
        GRD=RDISO(C0RD)
        GOXTOT=GOX*DAREA
        GRDTOT=GRD*DAREA
C       CALCULATE CURRENT FLOWING
        CUROX=XK1*(COX(1)-C0OX)*DAREA
        CUROX=CUROX+96400 *XN*(GOX1-GOX)/DT*DAREA
C       CALCULATE DERIVATIVES FOR
C       CHAIN-RULE CALCULATION OF D(CURRENT)/D(POTL)
        DTHDE=XK2*THETA
        DCDTH=1 +DGRDC/DX
        DCDTH=DCDTH*C0OX/THETA/THETA
        DCDTH=DCDTH/(1 +DGODC/DX+(1 +DGRDC/DX)/THETA)
        DCOXDE=DCDTH*DTHDE
        DIDE=(-DOX/DX*DCOXDE-DGODC*DCDTH*DTHDE/DT)
        DIDE=DIDE*96400. *XN*DAREA
        DENOM=RU*DIDE-1.
C       NEWTON-RAPHSON CORRECTION FORMULA FOR WORKING POTL
        E=EL-(EPRE+CUROX*RU-EL)/DENOM
C       TEST FOR CONVERGENCE
        IF (ABS(E-EL) LT EPS) GO TO 80
        GO TO 8
C       END OF WORKING POTL LOOP
80      CONTINUE
C
C       DIFFUSION CALCULATION
C
```

```
C
C       DROP GROWTH
C               CALCULATED AS A HYDRODYNAMIC FLOW OF
C               MATERIAL TOWARD THE SURFACE AS A RESULT
C               OF STRETCHING OF THE SURFACE LAYER
C               WITH DROP GROWTH   THE APPROACH AND TERMINOLOGY
C               ARE NOT EXACTLY THE SAME AS FELDBERG'S.
        CNEW(1)=DIFN(DMO,C0OX,COX(1),COX(2))
        C0OX=(COX(1)-C0OX)*DMO+C0OX
C       JMAX IS MAXIMUM CONCENTRATION INDEX THIS ITERATION
        JMAX=4.5*SQRT(FLOAT(K))+4.
        DO 10 J=2,JMAX
10      CNEW(J)=DIFN(DMO,COX(J-1),COX(J),COX(J+1))
        DO 11 J=1,JMAX
11      COX(J)=CNEW(J)
        CNEW(1)=DIFN(DMR,C0RD,CRD(1),CRD(2))
        C0RD=(CRD(1)-C0RD)*DMR+C0RD
        DO 12 J=2,JMAX
12      CNEW(J)=DIFN(DMR,CRD(J-1),CRD(J),CRD(J+1))
        DO 13 J=1,JMAX
13      CRD(J)=CNEW(J)
C
        RATA=AREA(HGR,DT*(K+1))/DAREA
        DO 20 J=1,JMAX
        FJ=J
        FJOLD=FJ*RATA
        JOMIN=INT(FJOLD)
        JOMAX=JOMIN+1
        IF(JOMIN.GE.JMAX) GO TO 21
        FR=FJOLD-FLOAT(JOMIN)
        COX(J)=(1.-FR)*COX(JOMIN)+FR*COX(JOMAX)
        CRD(J)=(1.-FR)*CRD(JOMIN)+FR*CRD(JOMAX)
20      CONTINUE
        GO TO 100
21      COX(J)=CIO
        CRD(J)=CIR
        GO TO 20
C       END DROP GROWTH SECTION
C
C       LABEL 100 IS END OF PREPOTENTIAL SECTION (0<T<TD)
100     CONTINUE
C
C       BEGIN POTENTIAL STEP SECTION (TD<T<TD+TS)
C
C       SAVE CURRENT AT END OF PREELECTROLYSIS STAGE
        C1=CUROX
        E1=E
C       CALCULATE NEW DT AND DX AND DIMENSIONLESS DIFFN COEFS
```

```
      DT=TS/ITER
      DXOLD=DX
      DX=SQRT(AMAX1(DOX,DRED)*DT/DM)
      DXRAT=DX/DXOLD
      DMO=DOX*DT/DX/DX
      DMR=DRED*DT/DX/DX
C
C     CALCULATE NEW CONCENTRATION PROFILE BY LINEAR INTERP
C
      DO 19 J=1,MAXJ
      FJOLD=DXRAT*J
      JOLD=FJOLD
      FR=FJOLD-JOLD
      IF (JOLD.EQ.0) GO TO 419
      CNEW(J)=(1.-FR)*COX(JOLD)+FR*COX(JOLD+1)
19    CONTINUE
      DO 119 J=1,MAXJ
119   COX(J)=CNEW(J)
      DO 219 J=1,MAXJ
      FJOLD=DXRAT*J
      JOLD=FJOLD
      FR=FJOLD-JOLD
      IF (JOLD.EQ.0) GO TO 519
      CNEW(J)=(1.-FR)*CRD(JOLD)+FR*CRD(JOLD+1)
219   CONTINUE
      DO 319 J=1,MAXJ
319   CRD(J)=CNEW(J)
      GO TO 619
419   CNEW(J)=(1.-FR)*C0OX+FR*COX(1)

      GO TO 19
519   CNEW(J)=(1.-FR)*C0RD+FR*CRD(1)
      GO TO 219
619   CONTINUE
C     END LINEAR INTERPOLATION
C
C     CALC SOME NUMERICAL CONSTANTS
      XK1=DOX*96400.*XN/DX
      XK2=38.92*XN
C     ESTIMATE A STARTING VALUE FOR ELECTRODE POTL
      E=E+DE
C     BECAUSE THE CONCENTRATION PROFILE IS PERTURBED,
C     IT IS NECESSARY TO CALCULATE DIFFUSION TO THE LIMIT
C     EACH TIME
      JMAX=MAXJ-1
C
C     BEGIN TIME ITERATIONS FOR SECOND PHASE
      DO 200 K=1,ITER
```

```
C
C       BEGIN BOUNDARY CONDITION CALCULATION AS ABOVE
        CTOT=C0OX+C0RD+GOX/DX+GRD/DX
        GOX1=GOX
        GRD1=GRD
18      EL=E
        THETA=EXP(XK2*EL)
301     C0OXL=C0OX
        C0RD=C0OX/THETA
        C0NUM=C0OX*(1.+1./THETA)+(OX1SO(C0OX)+RD1SO(C0RD))/DX-CTOT
        C0DEN=1.+1./THETA+DGODC/DX+DGRDC/DX/THETA
        C0OX=C0OXL-C0NUM/C0DEN
        IF (C0OX.LT.0.) C0OX=C0OXL/2.
        IF (C0OX.GT.CTOT) C0OX=(C0OXL+CTOT)/2.
        IF (ABS(C0OXL-C0OX).GT..00001*CTOT) GO TO 301
        C0RD=C0OX/THETA
        GOX=OX1SO(C0OX)
        GRD=RD1SO(C0RD)
        CUROX=XK1*(COX(1)-C0OX)*DAREA-DAREA*CDL*(EL-E1)/DT
        CUROX=CUROX+96400.*XN*(GOX1-GOX)/DT*DAREA
        DTHDE=XK2*THETA
        DCDTH=1.+DGRDC/DX
        DCDTH=DCDTH*C0OX/THETA/THETA
        DCDTH=DCDTH/(1.+DGODC/DX+(1.+DGRDC/DX)/THETA)
        DCOXDE=DCDTH*DTHDE
        DIDE=(-DOX/DX*DCOXDE-DGODC*DCDTH*DTHDE/DT)
        DIDE=DIDE*96400.*XN*DAREA
        DIDE=DIDE-DAREA*CDL/DT
        DENOM=RU*DIDE-1.
        E=EL-(EPRE+DE+CUROX*RU-EL)/DENOM
        IF (ABS(E).GT.0.2) E=(EL*99.+E)/100.
        IF (ABS(E-EL).LT.EPS) GO TO 180
        GO TO 18
C       END BOUNDARY CONDITION CALCULATION
180     CONTINUE
        E1=E
C
C       DIFFUSION CALCULATION

        CNEW(1)=DIFN(DMO,C0OX,COX(1),COX(2))
        C0OX=C0OX+DMO*(COX(1)-C0OX)
        DO 110 J=2,JMAX
110     CNEW(J)=DIFN(DMO,COX(J-1),COX(J),COX(J+1))
        DO 111 J=1,JMAX
111     COX(J)=CNEW(J)
        CNEW(1)=DIFN(DMR,C0RD,CRD(1),CRD(2))
        C0RD=C0RD+DMR*(CRD(1)-C0RD)
        DO 112 J=2,JMAX
112     CNEW(J)=DIFN(DMR,CRD(J-1),CRD(J),CRD(J+1))
        DO 113 J=1,JMAX
113     CRD(J)=CNEW(J)
```

```
C       LABEL 200 ENDS TIME ITERATIONS IN SECOND PHASE OF
C       THE DROP LIFE (TD<T<TD+TS)
200     CONTINUE
C       CALCULATE DIFFERENCE CURRENT
        CURDIF=CUROX-C1
C       CALCULATE UNCOMPENSATED RESISTANCE POTENTIAL DROP
C       THIS VALUE SHOULD EQUAL CURRENT*RU.
        RI=E-EPRE-DE
C       CALCULATE I/CA, NORMALIZED CURRENT DENSITY
        CURDCA=CURDIF/CID/DAREA
        WRITE (6,10001) EPRE,RI,C1,CUROX,CURDIF,CURDCA
10001   FORMAT (F7.3,5E12.4)
        IF (IEPRE.GT.30) GO TO 10002
C       IF SCAN NOT COMPLETE, GO TO STATEMENT # 10000 AND
C       INCREMENT POTENTIAL
        GO TO 10000
C       STATEMENT #10002 IS TERMINATION OF LOOPS IN CONCENTRATION,
C       DROP TIME, AND RU.
10002   CONTINUE
C       STATEMENT # 20000 ASKS FOR NEW ISOTHERM PARAMETERS
        GO TO 20000
        END


ROUTINES CALLED:
FMKISO, VARIN , INT   , ABS   , FLOAT , SQRT  , AMAX1
EXP
```

```
      FUNCTION FMKISO(C0,GM,XK,A,DGDC)
      IF (XK.LT. 0000001) GO TO 40
      CK=C0*XK
      CKOGM=CK/GM
      IF (ABS(A).LT..00001) GO TO 30
C             LANGMUIR SOLUTION TO START
      G=CK/(1.+CKOGM)
C             BEGIN NEWTON-RAPHSON ITERATIONS
10    TH=G/GM
      EXATH=EXP(A*TH)
      X=G/(1.-TH)*EXATH-CK
      Y=EXATH/(1.-TH)*(1.+G/(GM-G)+A*TH)
      GN=G-X/Y
      IF (ABS(G-GN).LT.1.E-16) GO TO 20
      IF (GN.GT.GM) GN=(G+GM)/2.
      IF (GN.LT.0.) GN=ABS(9.*G+GN)/10.
      G=GN
      GO TO 10
C
C     RETURN WITH CONVERGED VALUE
C
20    FMKISO=GN
      DGDC=XK/Y
      RETURN
C
C     LANGMUIR ISOTHERM CALC & RETURN
C
30    FMKISO=CK/(1.+CKOGM)
      DGDC=XK/(1.+CKOGM)**2
      RETURN
C
C     ZERO RETURN IF K=0
C
40    FMKISO=0.
      DGDC=0.
      RETURN
      END
```

APPENDIX C

Digital Simulation of D.C. Polarography with Adsorbed Reactants

INTRODUCTION

The computer program given in this Appendix is logically similar to the differential pulse program outlined in flowcharts B.1 and B.2, for the part of the simulation before the step ($t \leqslant t_d$). Subroutine FMKISO.FTN and VARIN.FTN are also required.

```
C       DCPOL.FTN
C       DC POLAROGRAPHY PROGRAM
C       INCLUDING ADSORPTIVE DEPLETION OF REACTANT,
C       DROP GROWTH,
C       CHOICE OF LINEAR, LANGMUIR, OR FRUMKIN ISOTHERM
C       UNCOMPENSATED RESISTANCE INCLUDING AREA DEPENDENT
C               SOLUTION RESISTANCE COMPONENT
C
C       ALL CALCULATIONS ARE DONE IN CGS UNITS
C
C
C
C       STATEMENT FUNCTIONS:
        AREA(HGR,T)=.0085086*(HGR*T)**.6666666
        DIFN(DM,CJM,CJ,CJP)=CJ+DM*(CJM+CJP-2.*CJ)
        OXISO(C0)=FMKISO(C0,GOXMX,XKO1,AOX,DGODC)
        RDISO(C0)=FMKISO(C0,GRDMX,XKR1,ARD,DGRDC)
C
C
C
        DIMENSION TDS(10)
        DIMENSION COXES(10),CAPRES(10)
        DIMENSION COX(200),CRD(200),CNEW(200)
C
C       INPUT SIMULATION PARAMETERS
        CALL VARIN(FITER,'ITER= ',6,2.1,1600.)
        ITER=FITER
        CALL VARIN (DOX,'DOX= ',5,1.E-7,1.E-3)
        CALL VARIN (DRED,'DRED= ',6,1.E-7,1.E-3)
        CALL VARIN (XN,'N ELECTRONS= ',13,.9,9.)
C       RCOEF IS SOLN RESISTANCE COEFF:
C               RU=R(CAPILL)+RCOEF*(DROPAREA)**1/2
C       THIS IS USEFUL IN CASES OF VERY LOW SOLUTION
C       CONDUCTIVITY, IN WHICH UNCOMPENSATED RESISTANCE
C       CHANGES GREATLY WITH DROP AREA
        CALL VARIN (RCOEF,'R COEF, OHM-CM= ',16,0.,0.)
        CALL VARIN (CRN,'# CAP R= ',9,.9,10.1)
        NCAPR=CRN
        DO 60000 JCAPR=1,NCAPR
60000   CALL VARIN (CAPRES(JCAPR),'CAPIL. R, OHMS= ',16,0.,0.)
        CALL VARIN(COXN,'# COX= ',7,1.,10.)
        NCOX=COXN
        DO 30001 JCOX=1,NCOX
30001   CALL VARIN(COXES(JCOX),'COX= ',5,1.E-20,1.)
        CALL VARIN (HGR,'HG FLOW RATE= ',14,.01,10.)
        CALL VARIN (TIMES,'# DROP TIMES= ',14,0.,10.)
        NTIMES=TIMES
        DO 40000 JTIMES=1,NTIMES
        CALL VARIN (TDS(JTIMES),'DROP TIME= ',11,.01,1000.)
40000   CONTINUE
C       INPUT ISOTHERM PARAMETERS
C       XKO1,XKR1--HENRY'S LAW COEFFICIENTS
C       COXMX,GRDMX--GAMMA MAX'S
C       AOX,ARD--FRUMKIN INTERACTION PARAMETERS
20000   CALL VARIN(XKO1,'K OX= ',6,0.,0.)
        CALL VARIN (XKR1,'K RED= ',7,0.,0.)
        CALL VARIN(GOXMX,'GOXMAX= ',8,0.,0.)
        CALL VARIN(GRDMX,'GRDMAX= ',8,0.,0.)
        CALL VARIN(AOX,'INTERACTION PAR, OX=',20,-5.,5.)
        CALL VARIN(ARD,'INTERACTION PAR, RD=',20,-5.,5.)
```

```
C       DEFAULT VALUE FOR GAMMA MAX'S IS VERY LARGE, SO THAT
C       A LINEAR ISOTHERM IS ASSUMED
        IF (GOXMX.EQ.0.) GOXMX=1.
        IF (GRDMX.EQ.0.) GRDMX=1.
C       END INPUT SECTION
C
C
C
C       EPS IS CONVERGENCE CRITERION FOR WORKING ELECTRODE POTL
        EPS=5.E-7
        DO 10002 JCOX=1,NCOX
C       INITIAL CONC OF RED IS SET TO ZERO
        CIR=0.
C       INITIAL CONCENTRATION OF OX IS TAKEN FROM ARRAY
C       OF INITIAL CONCENTRATIONS AND CONVERTED TO MOLES/CMSQ
        CIO=COXES(JCOX)/1000.
        DO 10002 JTIMES=1,NTIMES
C       DROP TIME TAKEN FROM ARRAY
        TD=TDS(JTIMES)
        DO 10002 JCAPR=1,NCAPR
C       CONSTANT PART OF UNCOMPENSATED RESISTANCE IS CHOSEN
C
C       PRINT HEADINGS
C       INITIALIZE POTENTIAL SCAN VARIABLE
        IEPRE=0
C       INCREMENT POTENTIAL SCAN VARIABLE
        WRITE (6,10003) CIO,TD,CAPRES(JCAPR)
10003   FORMAT (//,' COX= ',1PE12.2,5X,' DROP TIME = ',0PF5.1,
        1      5X,'CAPRES= ',F7.1)
10000   IEPRE=IEPRE+1
10005   EPRE=-(IEPRE-11)/100.
        WRITE (6,10004) EPRE
10004   FORMAT (' EPRE=',E12.4)
C       MAXJ IS MAXIMUM NUMBER OF SPACE INCREMENTS TO BE
C       USED IN CONCENTERATION PROFILE
        MAXJ=4.5*SQRT(FLOAT(ITER))+5.
        DT=TD/ITER
C       CALCULATE FIRST DX TO SATISFY STABILITY CRITERION
        DX=SQRT(AMAX1(DOX,DRED))*DT/.45)
C       CALCULATE DIMENSIONLESS DIFFN COEFFICIENTS FOR EACH SPECIES
        DMO=DOX*DT/DX/DX
        DMR=DRED*DT/DX/DX
C       INITIALIZE CONCENTRATION ARRAYS
        DO 9 J=1,200
        COX(J)=CIO
9       CRD(J)=CIR
        C0OX=CIO
        C0RD=CIR
C       INITIALIZE SOME NUMERICAL CONSTANTS
        XK1=DOX*96400.*XN/DX
        XK2=38.92*XN
C       INITIALIZE GOX AND GRD, THE GAMMA'S TO ZERO
        GOX=0.
        GRD=0.
        GOXTOT=0.
        GRDTOT=0.
C       INITIAL ESTIMATE OF WORKING ELECTRODE POTL IS EPRE, THE
C       APPLIED POTENTIAL.
        E=EPRE
```

```
C
C       BEGIN TIME ITERATIONS
C
        DO 100 K=1,ITER
C       UPDATE AREA
        DAREA=AREA(HGR,DT*K)
C       CALCULATE UNCOMPENSATED RESISTANCE (SEE WRITEUP)
        RU=CAPRES(JCAPR)+RCOEF/SQRT(DAREA)
C       CONSERVATION OF MASS IN SURFACE
C       VOLUME ELEMENT
        CTOT=C0OX+C0RD+(GOXTOT+GRDTOT)/DX/DAREA
C       TAKE INTO ACCOUNT DROP GROWTH ON SURFACE COVERAGES
        GOX1=GOXTOT/DAREA
        GRD1=GRDTOT/DAREA
C
C       BEGIN BOUNDARY CONDITION LOOP FOR WORKING POTL.
C
6       EL=E
        THETA=EXP(XK2*EL)
C
C       BEGIN BOUNDARY CONDITION LOOP FOR SURFACE CONCENTRATIONS
C
300     C0OXL=C0OX
        C0RD=C0OX/THETA
C       C0NUM IS NUMERATOR IN NEWTON-RAPHSON CALCULATION
C       FOR NEW C0OX
C                C0OX'=C0OX-C0NUM/C0DEN
        C0NUM=C0OX*(1.+1./THETA)+(OXISO(C0OX)+RDISO(C0RD))/DX-CTOT
        C0DEN=1.+1./THETA+DGODC/DX+DGRDC/DX/THETA
        C0OX=C0OXL-C0NUM/C0DEN
C       TEST AND CORRECT IN CASE NEWTON-RAPHSON CORRECTION
C       CAUSES AN OVERSHOOT OUTSIDE PERMITTED RANGE OF
C       CONCENTRATIONS.  THIS TEST IS VERY IMPORTANT.
        IF (C0OX.LT.0.) C0OX=C0OXL/2.
        IF (C0OX.GT.CTOT) C0OX=(C0OXL+CTOT)/2.
C       TEST FOR CONVERGENCE TO CONSTANT VALUE
        IF (ABS(C0OXL-C0OX).GT..00001*CTOT) GO TO 300
C       END OF NEWTON-RAPHSON CONCENTRATION CALCULATION
C       CONTINUING WORKING POTENTIAL ITERATION
        C0RD=C0OX/THETA
        GOX=OXISO(C0OX)
        GRD=RDISO(C0RD)
        GOXTOT=GOX*DAREA
        GRDTOT=GRD*DAREA
C       CALCULATE CURRENT FLOWING
        CUROX=XK1*(COX(1)-C0OX)*DAREA
        CUROX=CUROX+96400.*XN*(GOX1-GOX)/DT*DAREA
C       CALCULATE DERIVATIVES FOR
C       CHAIN-RULE CALCULATION OF D(CURRENT)/D(POTL)
        DTHDE=XK2*THETA
        DCDTH=1.+DGRDC/DX
        DCDTH=DCDTH*C0OX/THETA/THETA
        DCDTH=DCDTH/(1.+DGODC/DX+(1.+DGRDC/DX)/THETA)
        DCOXDE=DCDTH*DTHDE
        DIDE=(-DOX/DX*DCOXDE-DGODC*DCDTH*DTHDE/DT)
        DIDE=DIDE*96400.*XN*DAREA
        DENOM=RU*DIDE-1.
C       NEWTON-RAPHSON CORRECTION FORMULA FOR WORKING POTL
        E=EL-(EPRE+CUROX*RU-EL)/DENOM
```

```
C       TEST FOR CONVERGENCE
        IF (ABS(E-EL).LT.EPS) GO TO 80
        GO TO 8
C       END OF WORKING POTL LOOP
80      CONTINUE
C
        TIME=K*DT
        IF (10*(K/10).EQ.K) WRITE (6,200) K,TIME,CURDX
200     FORMAT (I5,2E12.4)
C       DIFFUSION CALCULATION
C
        CNEW(1)=DIFN(DMO,C0OX,COX(1),COX(2))
        C0OX=(COX(1)-C0OX)*DMO+C0OX
C       JMAX IS MAXIMUM CONCENTRATION INDEX THIS ITERATION
        JMAX=4.5*SQRT(FLOAT(K))+4.
        DO 10 J=2,JMAX
10      CNEW(J)=DIFN(DMO,COX(J-1),COX(J),COX(J+1))
        DO 11 J=1,JMAX
11      COX(J)=CNEW(J)
        CNEW(1)=DIFN(DMR,C0RD,CRD(1),CRD(2))
        C0RD=(CRD(1)-C0RD)*DMR+C0RD
        DO 12 J=2,JMAX
12      CNEW(J)=DIFN(DMR,CRD(J-1),CRD(J),CRD(J+1))
        DO 13 J=1,JMAX
13      CRD(J)=CNEW(J)
C
C       DROP GROWTH
C               CALCULATED AS A HYDRODYNAMIC FLOW OF
C               MATERIAL TOWARD THE SURFACE AS A RESULT
C               OF STRETCHING OF THE SURFACE LAYER
C               WITH DROP GROWTH.  THE APPROACH AND TERMINOLOGY
C               ARE NOT EXACTLY THE SAME AS FELDBERG'S.
C
        RATA=AREA(HGR,DT*(K+1))/DAREA
        DO 20 J=1,JMAX
        FJ=J
        FJOLD=FJ*RATA
        JOMIN=INT(FJOLD)
        JOMAX=JOMIN+1
        IF(JOMIN.GE.JMAX) GO TO 21
        FR=FJOLD-FLOAT(JOMIN)
        COX(J)=(1.-FR)*COX(JOMIN)+FR*COX(JOMAX)
        CRD(J)=(1.-FR)*CRD(JOMIN)+FR*CRD(JOMAX)
20      CONTINUE
        GO TO 100
21      COX(J)=CIO
        CRD(J)=CIR
        GO TO 20
100     CONTINUE
C
        IF (IEPRE.GT.20) GO TO 10002
C       IF SCAN NOT COMPLETE, GO TO STATEMENT # 10000 AND
C       INCREMENT POTENTIAL
        GO TO 10000
C       STATEMENT #10002 IS TERMINATION OF LOOPS IN CONCENTRATION,
C       DROP TIME, AND RU.
10002   CONTINUE
C       STATEMENT # 20000 ASKS FOR NEW ISOTHERM PARAMETERS
        GO TO 20000
        END
```

```
      AREA(HGR,T)=.0085086*(HGR*T)**.6666666
      DIFN(DM,CJM,CJ,CJP)=CJ+DM*(CJM+CJP-2.*CJ)
      OXISO(C0)=FMKISO(C0,GOXMX,XKO,AOX,DGODC)
      RDISO(C0)=FMKISO(C0,GRDMX,XKR,ARD,DGRDC)
      DIMENSION TDS(10)
      DIMENSION COXES(10)
      DIMENSION COX(200),CRD(200),CNEW(200)
C     CALL SETERR(4,-1)
C     CALL SETERR(3,-1)
      DM=.45
      CALL VARIN (SIG,'SCAN DIR: 1=FOR; -1=REV: ',25,-1.1,1.1)
      IF (SIG.NE.-1.) SIG=1.
      CALL VARIN (DOX,'DOX= ',5,1.E-7,1.E-3)
      CALL VARIN (DRED,'DRED= ',6,1.E-7,1.E-3)
      CALL VARIN (XN,'N ELECTRONS= ',13,.9,9.)
1     CALL VARIN (TS,'SAMPLE TIME, MS= ',17,1.,1000.)
      TS=TS*1.E-3
      CALL VARIN(COXN,'# COX= ',7,1.,10.)
      NCOX=COXN
      DO 30001 JCOX=1,NCOX
30001 CALL VARIN(COXES(JCOX),'COX= ',5,1.E-20,1.)
      CALL VARIN (HGR,'HG FLOW RATE= ',14,.01,10.)
      CALL VARIN (TIMES,'# DROP TIMES= ',14,0.,10.)
      NTIMES=TIMES
      DO 40000 JTIMES=1,NTIMES
      CALL VARIN (TDS(JTIMES),'DROP TIME= ',11,.01,1000.)
40000 CONTINUE
      WRITE (6,20010)
20010 FORMAT (///'      INITIAL POTL ISOTHERM:')
      CALL VARIN(XKO1,'K OX= ',6,0.,0.)
      CALL VARIN (XKR1,'K RED= ',7,0.,0.)
      CALL VARIN(GOXMX,'GOXMAX= ',8,0.,0.)
      CALL VARIN(GRDMX,'GRDMAX= ',8,0.,0.)
      CALL VARIN(AOX,'A OX= ',6,-5.,5.)
      CALL VARIN(ARD,'A RD= ',6,-5.,5.)
      IF (GOXMX.EQ.0.) GOXMX=1.
      IF (GRDMX.EQ.0.) GRDMX=1.
      WRITE (6,20020)
20020 FORMAT (///,'      AFTER STEP ISOTHERM:')
      CALL VARIN(XKO2,'K OX= ',6,0.,0.)
      CALL VARIN (XKR2,'K RED= ',7,0.,0.)
      CALL VARIN(DM,'DM= ',4,0.,.5)
      CALL VARIN(FITER,'ITER= ',6,2.1,1600.)
      ITER=FITER
      DO 10002 JCOX=1,NCOX
      CIR=0.
      CIO=COXES(JCOX)/1000.
      DO 10002 JTIMES=1,NTIMES
      TD=TDS(JTIMES)
      WRITE (6,10003) CIO,TD
      WRITE (6,10004)
10003 FORMAT (//,' COX= ',1PE12.2,5X,' DROP TIME = ',0PF5.1//)
10004 FORMAT (/'   E',7X,'C1 ',8X,'CUROX',5X,
     1     'DIFF CURR',5X,'I/CA')
      CURLST=0.
      IEPRE=0
      CALL SSWTCH(0,IBIT0)
      IF (IBIT0.EQ.1) IEPRE=34
```

```
10000    IEPRE=IEPRE+1
10005    EPRE=.15*SIG
         DE=-FLOAT(IEPRE)*.01*SIG
         MAXJ=4.5*SQRT(FLOAT(ITER))+5.
         DT=TD/ITER
         DX=SQRT(AMAX1(DOX,DRED)*DT/DM)
         DMO=DOX*DT/DX/DX
         DMR=DRED*DT/DX/DX
         XKO=XKO1
         XKR=XKR1
         DO 9 J=1,200
         COX(J)=CIO
9        CRD(J)=CIR
         C0OX=CIO
         C0RD=CIR
         XK1=DOX*96400.*XN/DX
         XK2=38.92*XN
         GOX=0.
         GRD=0.
         GOXTOT=0.
         GRDTOT=0.
         E=EPRE
         DO 100 K=1,ITER
         DAREA=AREA(HGR,DT*K)
         CTOT=C0OX+C0RD+(GOXTOT+GRDTOT)/DX/DAREA
         GOX1=GOXTOT/DAREA
         GRD1=GRDTOT/DAREA
8        EL=E
         THETA=EXP(XK2*EL)
300      C0OXL=C0OX
         C0RD=C0OX/THETA
         C0NUM=C0OX*(1.+1./THETA)+(OXISO(C0OX)+RDISO(C0RD))/DX-CTOT
         C0DEN=1.+1./THETA+DGODC/DX+DGRDC/DX/THETA
         C0OX=C0OXL-C0NUM/C0DEN
         IF (C0OX.LT.0.) C0OX=ABS(C0OXL/2.)
         IF (C0OX.GT.CTOT) C0OX=(C0OXL+CTOT)/2.
         IF (ABS(C0OXL-C0OX).GT..00001*CTOT) GO TO 300
         C0RD=C0OX/THETA
         GOX=OXISO(C0OX)
         GRD=RDISO(C0RD)
         GOXTOT=GOX*DAREA
         GRDTOT=GRD*DAREA
         CUROX=XK1*(2.*COX(1)-1.5*C0OX-.5*COX(2))*DAREA
         CUROX=CUROX+96400.*XN*(GOX1-GOX)/DT*DAREA
80       CONTINUE
         CNEW(1)=DIFN(DMO,C0OX,COX(1),COX(2))
         C0OX=(COX(1)-C0OX)*DMO+C0OX
         JMAX=4.5*SQRT(FLOAT(K))+4.
         DO 10 J=2,JMAX
10       CNEW(J)=DIFN(DMO,COX(J-1),COX(J),COX(J+1))
         DO 11 J=1,JMAX
11       COX(J)=CNEW(J)
         CNEW(1)=DIFN(DMR,C0RD,CRD(1),CRD(2))
         C0RD=(CRD(1)-C0RD)*DMR+C0RD
         DO 12 J=2,JMAX
12       CNEW(J)=DIFN(DMR,CRD(J-1),CRD(J),CRD(J+1))
         DO 13 J=1,JMAX
13       CRD(J)=CNEW(J)
         RATA=AREA(HGR,DT*(K+1))/DAREA
```

```
      DO 20 J=1,JMAX
      FJ=J
      FJOLD=FJ*RATA
      JOMIN=INT(FJOLD)
      JOMAX=JOMIN+1
      IF(JOMIN.GE.JMAX) GO TO 21
      FR=FJOLD-FLOAT(JOMIN)
      COX(J)=(1.-FR)*COX(JOMIN)+FR*COX(JOMAX)
      CRD(J)=(1.-FR)*CRD(JOMIN)+FR*CRD(JOMAX)
20    CONTINUE
      GO TO 100
21    COX(J)=CIO
      CRD(J)=CIR
      GO TO 20
100   CONTINUE
      C1=CUROX
      E1=E
      DT=TS/ITER
      DXOLD=DX
      DX=SQRT(AMAX1(DOX,DRED)*DT/DM)
      DXRAT=DX/DXOLD
      DMO=DOX*DT/DX/DX
      DMR=DRED*DT/DX/DX
      XKO=XKO2
      XKR=XKR2
      DO 19 J=1,MAXJ
      FJOLD=DXRAT*J
      JOLD=FJOLD
      FR=FJOLD-JOLD
      IF (JOLD.EQ.0) GO TO 419
      CNEW(J)=(1.-FR)*COX(JOLD)+FR*COX(JOLD+1)
19    CONTINUE
      DO 119 J=1,MAXJ
119   COX(J)=CNEW(J)
      DO 219 J=1,MAXJ
      FJOLD=DXRAT*J
      JOLD=FJOLD
      FR=FJOLD-JOLD
      IF (JOLD.EQ.0) GO TO 519
      CNEW(J)=(1.-FR)*CRD(JOLD)+FR*CRD(JOLD+1)
219   CONTINUE
      DO 319 J=1,MAXJ
319   CRD(J)=CNEW(J)
      GO TO 619
419   CNEW(J)=(1.-FR)*C0OX+FR*COX(1)
      GO TO 19
519   CNEW(J)=(1.-FR)*C0RD+FR*CRD(1)
      GO TO 219
619   CONTINUE
      XK1=DOX*96400.*XN/DX
      XK2=38.92*XN
      E=E+DE
      JMAX=MAXJ-1
      DO 200 K=1,ITER
      CTOT=C0OX+C0RD+GOX/DX+GRD/DX
      GOX1=GOX
      GRD1=GRD
18    EL=E
      THETA=EXP(XK2*EL)
```

```
301     C0OXL=C0OX
        C0RD=C0OX/THETA
        C0NUM=C0OX*(1. +1. /THETA)+(OXISO(C0OX)+RDISO(C0RD))/DX-CTOT
        C0DEN=1. +1. /THETA+DGODC/DX+DGRDC/DX/THETA
        C0OX=C0OXL-C0NUM/C0DEN
        IF (C0OX. LT. 0. ) C0OX=ABS(C0OXL/2. )
        IF (C0OX. GT. CTOT) C0OX=(C0OXL+CTOT)/2.
        IF (ABS(C0OXL-C0OX). GT. .00001*CTOT) GO TO 301
        C0RD=C0OX/THETA
        GOX=OXISO(C0OX)
        GRD=RDISO(C0RD)
        CUROX=XK1*(2. *COX(1)-1. 5*C0OX-. 5*COX(2))*DAREA
        CUROX=CUROX+96400. *XN*(GOX1-GOX)/DT*DAREA
180     CONTINUE
        E1=E
        CNEW(1)=DIFN(DMO, C0OX, COX(1), COX(2))
        C0OX=C0OX+DMO*(COX(1)-C0OX)
        DO 110 J=2, JMAX
110     CNEW(J)=DIFN(DMO, COX(J-1), COX(J), COX(J+1))
        DO 111 J=1, JMAX
111     COX(J)=CNEW(J)
        CNEW(1)=DIFN(DMR, C0RD, CRD(1), CRD(2))
        C0RD=C0RD+DMR*(CRD(1)-C0RD)
        DO 112 J=2, JMAX
112     CNEW(J)=DIFN(DMR, CRD(J-1), CRD(J), CRD(J+1))
        DO 113 J=1, JMAX
113     CRD(J)=CNEW(J)
200     CONTINUE
        CURDIF=CUROX-C1
        EPLUS=EPRE+DE
        CUROCA=CURDIF/CIO/DAREA
        WRITE (6, 10001) EPLUS, C1, CUROX, CURDIF, CUROCA
10001   FORMAT (F7. 3, 4E12. 4)
        CALL SSWTCH(0, IBIT0)
        IF (IBIT0. EQ. 1)GO TO 10002
        IF (IEPRE. LT. 40) GO TO 10000
10002   CONTINUE
        GO TO 20000
        END
```

APPENDIX D

Digital Simulation Program for Normal Pulse Polarography with Adsorbed Reactants

INTRODUCTION

Program NPPFMK.FTN is the main program for the digital simulation of normal pulse polarography with uncompensated resistance, drop growth and nonlinear adsorption isotherms for either reactant. The logical flow of this program is similar to that given for differential pulse in Appendix B, Figs. B.1 and B.2. Subroutines FMKISO.FTN and VARIN.FTN, discussed in Appendices A and B are also required.

```
C       NPP2 FTN
C
C       AUG 27,1976
C
C       DEPLETION, DROP GROWTH, FRUMKIN ISOTHERM
C
        AREA(HGR,T)= 0085086*(HGR*T)** 6666666
        DIFN(DM,CJM,CJ,CJP)=CJ+DM*(CJM+CJP-2 *CJ)
        OXISO(C0)=FMKISO(C0,GOXMX,XKO1,AOX,DGODC)
        RDISO(C0)=FMKISO(C0,GRDMX,XKR1,ARD,DGRDC)
        DIMENSION TDS(10)
        DIMENSION COXES(10)
        DIMENSION COX(200),CRD(200),CNEW(200)
C       CALL SETERR(4,-1)
C       CALL SETERR(3,-1)
        DM= 45
        CALL VARIN (SIG,'SCAN DIR: 1=FOR; -1=REV: ',25,-1 1,1.1)
        IF (SIG NE -1.) SIG=1.
        CALL VARIN (DOX,'DOX= ',5,1.E-7,1.E-3)
        CALL VARIN (DRED,'DRED= ',6,1.E-7,1.E-3)
        CALL VARIN (XN,'N ELECTRONS= ',13,.9,9.)
1       CALL VARIN (TS,'SAMPLE TIME, MS= ',17,1 ,1000 )
        TS=TS*1.E-3
        CALL VARIN(COXN,'# COX= ',7,1.,10.)
        NCOX=COXN
        DO 30001 JCOX=1,NCOX
30001   CALL VARIN(COXES(JCOX),'COX= ',5,1 E-20,1.)
        CALL VARIN (HGR,'HG FLOW RATE= ',14, 01,10.)
        CALL VARIN (TIMES,'# DROP TIMES= ',14,0.,10.)
        NTIMES=TIMES
        DO 40000 JTIMES=1,NTIMES
        CALL VARIN (TDS(JTIMES),'DROP TIME= ',11, 01,1000.)
40000   CONTINUE
20000   CALL VARIN(XKO1,'K OX= ',6,0.,0.)
        CALL VARIN (XKR1,'K RED= ',7,0.,0.)
        CALL VARIN(GOXMX,'GOXMAX= ',8,0.,0.)
        CALL VARIN(GRDMX,'GRDMAX= ',8,0.,0.)
        CALL VARIN(AOX,'A OX= ',6,-5.,5.)
        CALL VARIN(ARD,'A RD= ',6,-5.,5.)
        IF (GOXMX EQ 0.) GOXMX=1.
        IF (GRDMX EQ 0.) GRDMX=1.
        CALL VARIN(DM,'DM= ',4,0.,.5)
        CALL VARIN(FITER,'ITER= ',6,2 1,1600.)
        ITER=FITER
        DO 10002 JCOX=1,NCOX
        CIR=0.
        CIO=COXES(JCOX)/1000.
        DO 10002 JTIMES=1,NTIMES
        TD=TDS(JTIMES)
        WRITE (6,10003) CIO,TD
        WRITE (6,10004)
10003   FORMAT (//,' COX= ',1PE12.2,5X,' DROP TIME = ',0PF5.1//)
10004   FORMAT (/'    E',7X,'C1 ',8X,'CURDX',5X,
        1     'DIFF CURR',5X,'I/CR')
        CURLST=0.
        IEPRE=0
        CALL SSWTCH(0,IBIT0)
        IF (IBIT0.EQ.1) IEPRE=34
10000   IEPRE=IEPRE+1
10005   EPRE= 15*SIG
```

```
      DE=-FLOAT(IEPRE)*.01*SIG
      MAXJ=4.5*SQRT(FLOAT(ITER))+5
      DT=TD/ITER
      DX=SQRT(AMAX1(DOX,DRED)*DT/DM)
      DMO=DOX*DT/DX/DX
      DMR=DRED*DT/DX/DX
      DO 9 J=1,200
      COX(J)=CID
9     CRD(J)=CIR
      C0OX=CID
      C0RD=CIR
      XK1=DOX*96400.*XN/DX
      XK2=38.92*XN
      GOX=0.
      GRD=0.
      GOXTOT=0.
      GRDTOT=0.
      E=EPRE
      DO 100 K=1,ITER
      DAREA=AREA(HGR,DT*K)
      CTOT=C0OX+C0RD+(GOXTOT+GRDTOT)/DX/DAREA
      GOX1=GOXTOT/DAREA
      GRD1=GRDTOT/DAREA
8     EL=E
      THETA=EXP(XK2*EL)
300   C0OXL=C0OX
      C0RD=C0OX/THETA
      C0NUM=C0OX*(1.+1./THETA)+(OXISO(C0OX)+RDISO(C0RD))/DX-CTOT
      C0DEN=1.+1./THETA+DGODC/DX+DGRDC/DX/THETA
      C0OX=C0OXL-C0NUM/C0DEN
      IF (C0OX.LT.0.) C0OX=ABS(C0OXL/2.)
      IF (C0OX.GT.CTOT) C0OX=(C0OXL+CTOT)/2.
      IF (ABS(C0OXL-C0OX).GT..00001*CTOT) GO TO 300
      C0RD=C0OX/THETA
      GOX=OXISO(C0OX)
      GRD=RDISO(C0RD)
      GOXTOT=GOX*DAREA
      GRDTOT=GRD*DAREA
      CUROX=XK1*(2.*COX(1)-1.5*C0OX-.5*COX(2))*DAREA
      CUROX=CUROX+96400.*XN*(GOX1-GOX)/DT*DAREA
80    CONTINUE
      CNEW(1)=DIFN(DMO,C0OX,COX(1),COX(2))
      C0OX=(COX(1)-C0OX)*DMO+C0OX
      JMAX=4.5*SQRT(FLOAT(K))+4.
      DO 10 J=2,JMAX
10    CNEW(J)=DIFN(DMO,COX(J-1),COX(J),COX(J+1))
      DO 11 J=1,JMAX
11    COX(J)=CNEW(J)
      CNEW(1)=DIFN(DMR,C0RD,CRD(1),CRD(2))
      C0RD=(CRD(1)-C0RD)*DMR+C0RD
      DO 12 J=2,JMAX
12    CNEW(J)=DIFN(DMR,CRD(J-1),CRD(J),CRD(J+1))
      DO 13 J=1,JMAX
13    CRD(J)=CNEW(J)
      RATA=AREA(HGR,DT*(K+1))/DAREA
      DO 20 J=1,JMAX
      FJ=J
      FJOLD=FJ*RATA
      JOMIN=INT(FJOLD)
      JOMAX=JOMIN+1
      IF(JOMIN.GE.JMAX) GO TO 21
      FR=FJOLD-FLOAT(JOMIN)
      COX(J)=(1.-FR)*COX(JOMIN)+FR*COX(JOMAX)
      CRD(J)=(1.-FR)*CRD(JOMIN)+FR*CRD(JOMAX)
20    CONTINUE
```

```
      GO TO 100
21    COX(J)=CIO
      CRD(J)=CIR
      GO TO 20
100   CONTINUE
      C1=CUROX
      E1=E
      DT=TS/ITER
      DXOLD=DX
      DX=SQRT(AMAX1(DOX,DRED)*DT/DM)
      DXRAT=DX/DXOLD
      DMO=DOX*DT/DX/DX
      DMR=DRED*DT/DX/DX
      DO 19 J=1,MAXJ
      FJOLD=DXRAT*J
      JOLD=FJOLD
      FR=FJOLD-JOLD
      IF (JOLD EQ 0) GO TO 419
      CNEW(J)=(1.-FR)*COX(JOLD)+FR*COX(JOLD+1)
19    CONTINUE
      DO 119 J=1,MAXJ
119   COX(J)=CNEW(J)
      DO 219 J=1,MAXJ
      FJOLD=DXRAT*J
      JOLD=FJOLD
      FR=FJOLD-JOLD
      IF (JOLD.EQ.0) GO TO 519
      CNEW(J)=(1.-FR)*CRD(JOLD)+FR*CRD(JOLD+1)
219   CONTINUE
      DO 319 J=1,MAXJ
319   CRD(J)=CNEW(J)
      GO TO 619
419   CNEW(J)=(1.-FR)*C0OX+FR*COX(1)
      GO TO 19
519   CNEW(J)=(1.-FR)*C0RD+FR*CRD(1)
      GO TO 219
619   CONTINUE
      XK1=DOX*96400.*XN/DX
      XK2=38.92*XN
      E=E+DE
      JMAX=MAXJ-1
      DO 200 K=1,ITER
      CTOT=C0OX+C0RD+GOX/DX+GRD/DX
      GOX1=GOX
      GRD1=GRD
18    EL=E
      THETA=EXP(XK2*EL)
301   C0OXL=C0OX
      C0RD=C0OX/THETA
      C0NUM=C0OX*(1.+1./THETA)+(OXISO(C0OX)+RDISO(C0RD))/DX-CTOT
      C0DEN=1.+1./THETA+DGODC/DX+DGRDC/DX/THETA
      C0OX=C0OXL-C0NUM/C0DEN
      IF (C0OX.LT.0.) C0OX=ABS(C0OXL/2.)
      IF (C0OX.GT.CTOT) C0OX=(C0OXL+CTOT)/2.
      IF (ABS(C0OXL-C0OX).GT..00001*CTOT) GO TO 301
      C0RD=C0OX/THETA
      GOX=OXISO(C0OX)
      GRD=RDISO(C0RD)
      CUROX=XK1*(2.*COX(1)-1.5*C0OX-.5*COX(2))*DAREA
      CUROX=CUROX+96400.*XN*(GOX1-GOX)/DT*DAREA
180   CONTINUE
```

```
      E1=E
      CNEW(1)=DIFN(DMD,C0DX,COX(1),COX(2))
      C0DX=C0DX+DMD*(COX(1)-C0DX)
      DO 110 J=2,JMAX
110   CNEW(J)=DIFN(DMD,COX(J-1),COX(J),COX(J+1))
      DO 111 J=1,JMAX
111   COX(J)=CNEW(J)
      CNEW(1)=DIFN(DMR,C0RD,CRD(1),CRD(2))
      C0RD=C0RD+DMR*(CRD(1)-C0RD)
      DO 112 J=2,JMAX
112   CNEW(J)=DIFN(DMR,CRD(J-1),CRD(J),CRD(J+1))
      DO 113 J=1,JMAX
113   CRD(J)=CNEW(J)
200   CONTINUE
      CURDIF=CUROX-C1
      EPLUS=EPRE+DE
      CURDCR=CURDIF/CID/DAREA
      WRITE (6,10001) EPLUS,C1,CUROX,CURDIF,CURDCR
10001 FORMAT (F7.3,4E12.4)
      CALL SSWTCH(8,IBIT8)
      IF (IBIT8 EQ 1)GO TO 10002
      IF (IEPRE LT 40) GO TO 10000
10002 CONTINUE
      GO TO 20000
      END
```